AD-A045 332 CALIFORNIA UNIV BERKELEY OFFICE OF RESEARCH SERVICES F/G 13/2
ANALYSIS OF CONSOLIDATION OF EARTH AND ROCKFILL DAMS. VOLUME I.--ETC(U)
SEP 77 C S CHANG, J M DUNCAN DACW39-74-C-0027
UNCLASSIFIED TE-77-3-VOL-1 WES-CR-S-77-4-VOL-1 NL

1 OF 2
AD
A045332

(2)

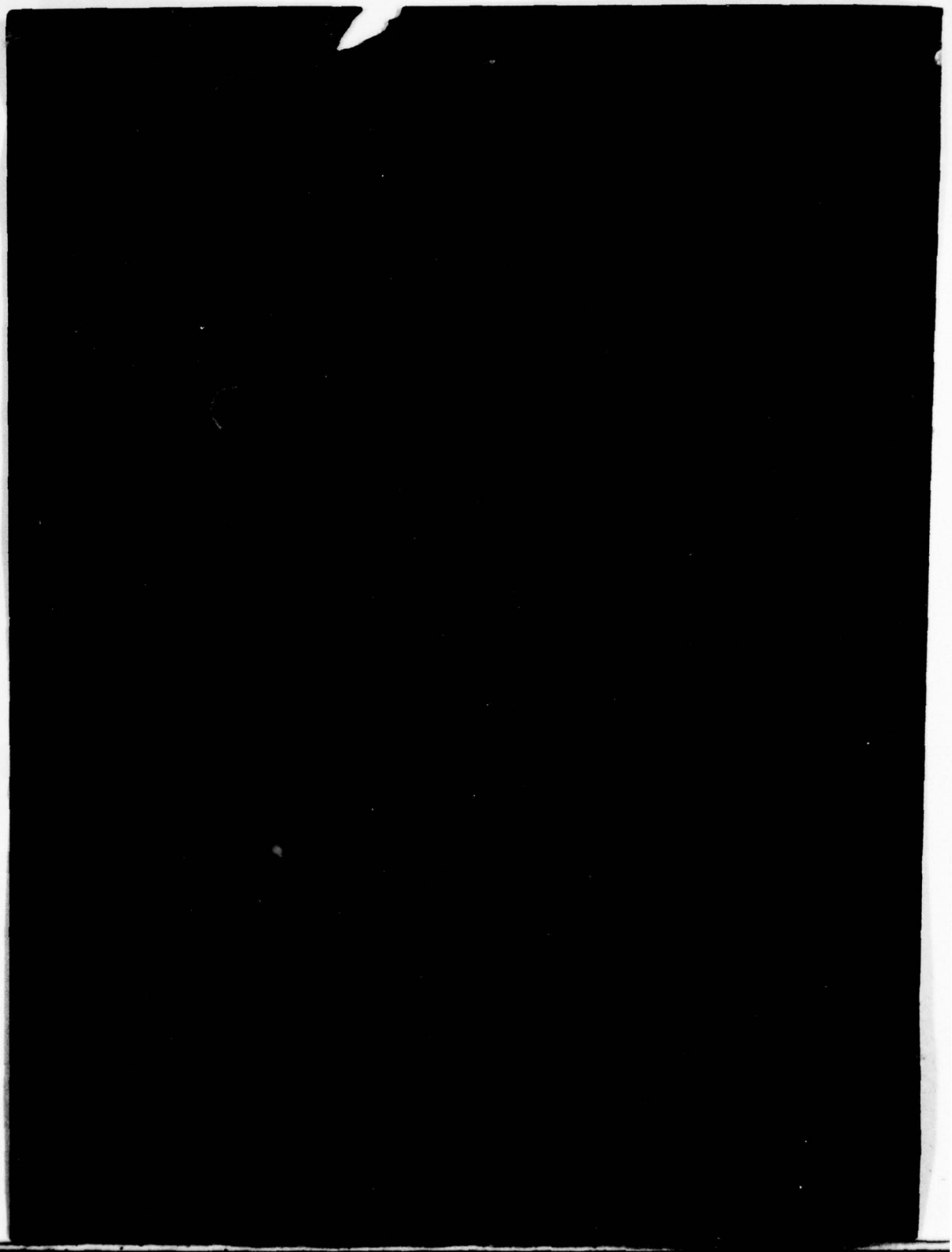

Unclassified

SECURITY CLASSIFICATION OF THIS PAGE (When Data Entered)

REPORT DOCUMENTATION PAGE

READ INSTRUCTIONS BEFORE COMPLETING FORM

1. REPORT NUMBER: Contract Report S-77-4, Volume I
2. GOVT ACCESSION NO.
3. RECIPIENT'S CATALOG NUMBER

4. TITLE (and Subtitle): ANALYSIS OF CONSOLIDATION OF EARTH AND ROCKFILL DAMS; MAIN TEXT AND APPENDICES A AND B. Volume I
5. TYPE OF REPORT & PERIOD COVERED: Final report
6. PERFORMING ORG. REPORT NUMBER: Report No. TE-77-3, Volume 1

7. AUTHOR(s): Ching S. Chang; James M. Duncan
8. CONTRACT OR GRANT NUMBER(s): DACW39-74-C-0027

9. PERFORMING ORGANIZATION NAME AND ADDRESS: College of Engineering, Office of Research Services, University of California, Berkeley, Calif. 94720
10. PROGRAM ELEMENT, PROJECT, TASK AREA & WORK UNIT NUMBERS: CWIS 31173

11. CONTROLLING OFFICE NAME AND ADDRESS: Office, Chief of Engineers, U. S. Army, Washington, D. C. 20314
12. REPORT DATE: September 1977
13. NUMBER OF PAGES: 141 (12) 146 p.

14. MONITORING AGENCY NAME & ADDRESS (if different from Controlling Office): U. S. Army Engineer Waterways Experiment Station, Soils and Pavements Laboratory, P. O. Box 631, Vicksburg, Miss. 39180
15. SECURITY CLASS. (of this report): Unclassified
15a. DECLASSIFICATION/DOWNGRADING SCHEDULE

16. DISTRIBUTION STATEMENT (of this Report): Approved for public release; distribution unlimited.
(18) WES
(19) CR-S-77-4-Vol-1

17. DISTRIBUTION STATEMENT (of the abstract entered in Block 20, if different from Report)

18. SUPPLEMENTARY NOTES

400 370

19. KEY WORDS (Continue on reverse side if necessary and identify by block number)

Clay soils
Consolidation (soils)
Dam instrumentation
Earth dams
Finite element method
Rockfill dams
Saturated soils
Stress-strain relations (soils)

20. ABSTRACT (Continue on reverse side if necessary and identify by block number)

This study was undertaken to develop the theory for analyzing the consolidation of partly saturated clay soils, and subsequently to develop a practical procedure for performing finite element analyses of the behavior of dams during construction, during reservoir filling, and during the development of long-term seepage. The theory developed couples the effects of both stress and flow. It takes account of the varying permeability and compressibility of the pore fluid, and the nonlinear stress-strain behavior of the soil. A number of

(Continued)

DD FORM 1 JAN 73 1473 EDITION OF 1 NOV 65 IS OBSOLETE

Unclassified

SECURITY CLASSIFICATION OF THIS PAGE (When Data Entered)

20. ABSTRACT (Continued).

elastic-plastic, stress-strain relationships are reviewed with respect to their capabilities for modeling the stress-strain behavior of compacted clays. It is shown that if the Cam Clay Model is revised by introducing a cohesion intercept and a nonlinear e - log σ_m' curve, it can be used to model the stress-strain behavior of compacted clay quite accurately. This model provides an incremental stress-strain relationship which can be used for analyses of drained, undrained, and partly drained conditions.

Available data are reviewed to show how the permeability of compacted clays varies with degree of saturation and void ratio, and an empirical relationship is developed which expresses the dependence of permeability on these factors for a wide variety of compacted clays. A concept of homogenized pore fluid is proposed to simulate the air-water mixture in the pores of partly saturated clays so that the three-phase partly saturated clay can be treated phenomenologically as a two-phase material. Compressibility of the homogenized pore fluid is then derived using Boyle's Law and Henry's Law and taking account of the effect of surface tension. Biot's theory of consolidation is reviewed, and a finite element formulation for the consolidation of saturated soils is derived. The computer program based on this formulation is verified by comparing results derived from the program with known solutions for several problems.

The theory of consolidation for partly saturated soil is derived and a computer program is developed. To check the utility and effectiveness of the theory and the computer program developed, two examples of one-dimensional consolidation with compressible pore fluid and varying permeability are analyzed. Finite element analyses performed using this program are shown to agree well with closed-form solutions for the consolidation of both saturated and unsaturated soils. A finite element analysis is performed to study the stresses and movements in New Melones Dam, which is now under construction. The results of this analysis indicate that the behavior of the dam during consolidation is closely related to the stiffness and degree of saturation of the core. The results of this study indicate that the finite element procedure developed is a potentially useful tool. It seems likely that its greatest value in application will be in connection with interpretation of instrumentation studies for zoned earth and rockfill dams.

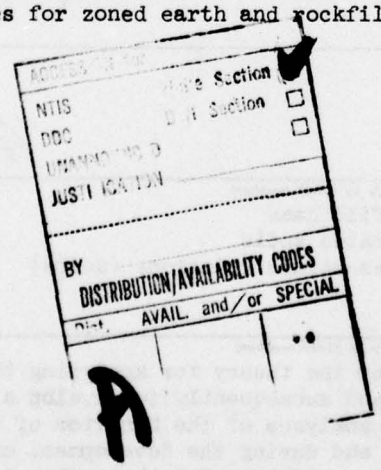

FOREWORD

The work described in this report was performed under Contract No. DACW39-74-C-0027, "Behavior of Zoned Embankments on Soft Foundations," between the U. S. Army Engineer Waterways Experiment Station and the University of California. This is the eighth report on investigations performed under this contract. The first report, "Finite Element Analyses of Stresses and Movements in Embankments During Construction," by F. H. Kulhawy, J. M. Duncan and H. Bolton Seed, was published in November, 1969. The second report, "Three-Dimensional Finite Element Analyses of Dams," by Guy Lefebvre and J. M. Duncan, was published in May, 1971. The third report, "Effect of Reservoir Filling on Stresses and Movements in Earth and Rockfill Dams," by E. S. Nobari and J. M. Duncan, was published in January, 1972. The fourth report, "Hydraulic Fracturing in Zoned Earth and Rockfill Dams," by E. S. Nobari, K. L. Lee and J. M. Duncan, was published in January, 1973. The fifth report, "Finite Element Analyses of Transverse Cracking in Low Embankment Dams," by Guy Lefebvre and J. M. Duncan, was published in October, 1974. The sixth report, "Finite Element Analyses of Stresses and Movements in Birch Dam," by Antonio Soriano, J. M. Duncan, Kai Wong and Jean-Michel Simon, was published in April, 1976. The seventh report, "The Role of Fill Strength in the Stability of Embankments on Soft Clay Foundations," by Suphon Chirapuntu and J. M. Duncan, was published in June, 1976. The research was sponsored by The Office, Chief of Engineers, under the Civil Works Program CWIS No. 31173, Special Studies for Civil Works Soils Problems, Task 2.

The general objective of this research, which was begun in June, 1968, is to develop methods for analysis of stresses and movements in embankments. Work on this project is conducted under the supervision of J. M. Duncan, Professor of Civil Engineering. The project is administered by the Office of Research Services of the College of Engineering. The phase of the investigation described in this report was conducted, and the report was prepared by C. S. Chang and J. M. Duncan.

The contract was monitored by Mr. C. L. McAnear, Chief, Soil Mechanics Division, under the general supervision of Mr. J. P. Sale, Chief, Soils and Pavements Laboratory. Contracting Officer was Col. John L. Cannon, Director of the U. S. Army Waterways Experiment Station.

TABLE OF CONTENTS

		Page No.
CHAPTER 1	INTRODUCTION	1
CHAPTER 2	EFFECTIVE STRESS-STRAIN RELATIONSHIP OF CLAY	4
	INTRODUCTION	4
	CAM CLAY MODELS	6
	Basic Assumptions on Soil Properties	6
	Elastic Behavior	7
	Plastic Behavior	10
	STRESS-STRAIN BEHAVIOR OF COMPACTED CLAY COMPARED WITH THAT PREDICTED BY THE CAM CLAY MODELS	11
	A MODIFICATION OF THE CAM CLAY MODEL	19
	Elastic Behavior	19
	Plastic Behavior	20
	Parameters Required	20
	STRESS-STRAIN BEHAVIOR OF CANYON DAM CLAY PREDICTED USING THE EXTENDED CAM CLAY MODEL	20
	MODIFICATIONS TO THE SHAPE OF THE GAP	23
	Curved Failure Envelope for Granular Soils	23
	Composite Cap	25
CHAPTER 3	THE PERMEABILITY OF PARTLY SATURATED SOILS	28
	INTRODUCTION	28
	THEORETICAL PERMEABILITY EQUATIONS	28
	PROPOSED PERMEABILITY EQUATIONS	29
	Determination of k_s	30
	Determination of G_e	30
	Determination of H_s	34
	SUMMARY	36

		Page No.
CHAPTER 4	EFFECTIVE STRESS EQUATION FOR PARTLY SATURATED SOILS	37
	INTRODUCTION	37
	CONCEPT OF HOMOGENIZED PORE FLUID	40
	THE HOMOGENIZED PORE FLUID PRESSURE	40
	ANALYSIS OF CONSOLIDATION OF PARTLY SATURATED SOILS	41
	THE COMPRESSIBILITY OF THE HOMOGENIZED PORE FLUID OF PARTLY SATURATED SOIL	42
	ASSUMPTIONS FOR DERIVATION OF THE COMPRESSIBILITY OF THE HOMOGENIZED PORE FLUID	43
	DERIVATION OF THE COMPRESSIBILITY OF A MIXTURE OF AIR AND WATER	46
	COMPARISON BETWEEN THEORIES AND TEST DATA	47
	FLOW BEHAVIOR OF HOMOGENIZED FLUID	49
CHAPTER 5	FINITE ELEMENT ANALYSIS OF CONSOLIDATION OF SATURATED CLAY	52
	INTRODUCTION	52
	FIELD EQUATIONS	53
	FINITE ELEMENT DISCRETIZATION	57
	NUMERICAL INTEGRATION	59
	Formulation for an Incremental Effective Stress-Strain Law	60
	Iteration Scheme	61
	EXAMPLES	61
CHAPTER 6	FINITE ELEMENT ANALYSIS OF CONSOLIDATION OF PARTLY SATURATED CLAY	71
	INTRODUCTION	71
	FIELD EQUATION	71
	FINITE ELEMENT FORMULATION	72
	EXAMPLES	73

		Page No.
CHAPTER 7	NEW MELONES DAM	81
	INTRODUCTION	81
	DESCRIPTION OF NEW MELONES DAM	82
	ANALYSIS PROCEDURE	82
	PROPERTIES OF THE MATERIALS IN NEW MELONES DAM	86
	ANALYSIS	88
	Construction Stage	89
	Reservoir Filling Stage	89
	Long Term Seepage Stage	91
	Settlement	91
	Horizontal Movement	96
	Effective Stresses	96
	Pore Pressures	105
	SUMMARY	111
CHAPTER 8	CONCLUSION	114
REFERENCES		117
APPENDIX A	DERIVATIONS OF STRESS-STRAIN RELATIONSHIP FOR AN ELASTIC PLASTIC MATERIAL	123
APPENDIX B	ANALYTICAL SOLUTION FOR MATERIAL WITH COMPRESSIBLE PORE FLUID IN A ONE-DIMENSIONAL CONSOLIDATION CASE	126

LIST OF FIGURES

Figure No.		Page No.
2.1	Cap Model in Principal Stress Space	5
2.2	A Failure Envelope in the σ_m' - q Plane	8
2.3	Simplified e - ln σ_m' Curve	9
2.4	Yield Loci for Cam Clay Models	12
2.5	Stress-Strain Curves from Drained Triaxial Tests on Canyon Dam Compacted Clay (After Casagrande, 1962)	14
2.6	One-Dimensional Consolidation Curve for Canyon Dam Compacted Clay (After Casagrande, 1962)	15
2.7	Failure Lines for Canyon Dam Compacted Clay	16
2.8	Comparisons of Measured and Calculated Stress-Strain Curves	18
2.9	Isotropic Compression Curve for Canyon Dam Clay	21
2.10	Comparison of Measured Stress-Strain Curves with those Calculated Using the Extended Dam Clay Model	24
2.11	The Extended Cam Clay Model	26
3.1	Permeability Behavior of Jamaica Sandy Clay (After Lambe, 1958)	31
3.2	Variation of Permeability with Void Ratio from Permeability Tests on Sand (After Lambe and Whitman, 1969)	32
3.3	Permeability Test Data (After Lambe and Whitman, 1969)	33
3.4	Variations of Permeability with Degree of Saturation for Compacted Clay (Data from Mitchell, et al., 1965)	35
4.1	Variations of χ with Degree of Saturation	41

Figure No.		Page No.
4.2	Doubly Curved Interface between Air and Water	45
4.3	Calculated and Measured Variations of Degree of Saturation with Back Pressure (Data from Mitchell, et al., 1965)	48
4.4	Comparison between Measured Variation of Degree of Saturation and that Calculated Assuming $R_c = R_{cs}\ (S - S_f)/(1 - S_f)$ (Data from Mitchell, et al., 1965)	50
5.1	Analyses of One-Dimensional Consolidation	63
5.2	Calculated Pore Pressure Isochrones for Contiguous Layers with Different Permeabilities	64
5.3	Finite Element Mesh for a Strip Footing on a Finite Layer	65
5.4	Surface Displacement of a Strip Footing on a Layer of Finite Thickness	67
5.5	One-Dimensional Deposition of a Soil Layer	68
5.6	Pore Distributions for Deposition of an Impermeable Base	69
5.7	Pore Pressure Distribution for Deposition on a Permeable Base	70
6.1	Variation of Degree of Consolidation with Time for One-Dimensional Consolidation of an Idealized Elastic Material	75
6.2	Pore Pressure Dissipation with Time for One-Dimensional Consolidation of an Idealized Elastic Material	76
6.3	Time Settlement Curve for the New Melones Dam Core Material	79
7.1	Project Location Map	83
7.2	Plan View and Longitudinal Section of Dam and Abutments	84
7.3	Maximum Dam Section	85

Figure No.		Page No.
7.4	Finite Element Mesh for New Melones Dam	87
7.5	Changes in Load Due to Reservoir Filling	90
7.6	Settlement Along Elev. 803 in New Melones Dam (Stiff Core)	92
7.7	Settlement Along Elev. 803 in New Melones Dam (Soft Core)	93
7.8	Settlement Along Line B - B' in New Melones Dam (Stiff Core)	94
7.9	Settlement Along B - B' in New Melones Dam (Soft Core)	95
7.10	Horizontal Movement Along Section AA' in New Melones Dam (Stiff Core)	97
7.11	Horizontal Movement Along Section AA' in New Melones Dam (Soft Core)	98
7.12	Horizontal Movement Along Section CC' in New Melones Dam (Stiff Core)	99
7.13	Horizontal Movements Along Section CC' in New Melones Dam (Soft Core)	100
7.14	Maximum Effective Principal Stresses at Elev. 860 in New Melones Dam (Stiff Core)	101
7.15	Minimum Effective Principal Stresses at Elev. 860 in New Melones Dam (Stiff Core)	102
7.16	Maximum Effective Principal Stresses at Elev. 860 in New Melones Dam (Soft Core)	103
7.17	Minimum Effective Principal Stresses at Elev. 860 in New Melones Dam (Soft Core)	104
7.18	Pore Pressure Distributions in the Core of New Melones Dam (Soft Core)	106
7.19	Pore Pressure Distributions in the Core of New Melones Dam (Stiff Core)	107
7.20	Pore Pressure Variation at Point A in the Core of New Melones Dam	108

Figure No.		Page No.
7.21	Pore Pressure Variation at Point B in the Core of New Melones Dam	109
7.22	Pore Pressures Distributions in the Core of the Cofferdam (Stiff Core)	110
7.23	Comparison of Long Term Stress Calculated Using Hyperbolic Stress-Strain Relationship with Slow Construction and Cam Clay Stress-Strain Relationship with Consolidation	113

LIST OF TABLES

Table No.		Page No.
2.1	Summary of the Parameters for Cam Clay Models (1963 & 1968)	17
2.2	Summary of the Parameters for the Extended Cam Clay Model	22
6.1	Summary of Elastic Plastic Cam Clay Parameters for Stiff Core in New Melones Dam	77

LIST OF SYMBOLS

English Letters

A	effective soil-particle contact area per unit area
A_s	wetted area
B	elastic bulk modulus
b	the slope of rebound curve in σ_m' - e plane
c	cohesion intercept
c_v	coefficient of consolidation
D_f	diffusion coefficient
D'	constrained modulus
E'	Young's modulus
e	void ratio
e_a	air void ratio
e_0	initial void ratio
e_s	dissolved air void ratio
e_{a0}	initial air void ratio
f_b	body force
G	shear modulus
G_e	void ratio function
H	Henry's coefficient of solubility or thickness
H_s	degree of saturation function
h, h_1, h_2	hardening parameters
K_0	coefficient of lateral earth pressure at rest
k	permeability
k_s	saturated permeability

k_{vs}	vertical principal saturated permeability
k_{ij}	permeability tensor
k_{hs}	horizontal principal saturated permeability
M	slope of failure envelope in $\sigma_m' - q$ plane
p_a	atmospheric pressure
p_0	initial isotropic pressure
Q	inverse of the compressibility of pore fluid
q	deviatoric stress invariant
q_0	stress parameter
R_c	capillary radius
R_{cs}	saturated capillary radius
R_0	initial radius of air bubbles
r	radius of spherical air bubble
r_1, r_2	principal radii of curvature of air bubble
S	degree of saturation
S_D	portion of the boundary surface subjected to applied displacement
S_f	threshold degree of saturation
S_p	portion of boundary surface subjected to applied pore pressure
S_q	portion of boundary surface subjected to applied flow
S_T	portion of the boundary surface subjected to applied tractions
T	time factor
T_c	surface tension
T_f	tractions
t	time
t_0	time 0

t_1	time 1
u	pore fluid pressure
u_a	pore air pressure
u_c	capillary pressure
u_m	homogenized pore fluid pressure
u_w	pore water pressure
V_d	volume of gas dissolved in the water
V_s	volume of solid
V_w	volume of water
v	superficial velocity
v_x, v_y, v_z	superficial velocities in x, y and z directions
w_0	initial settlement
w_x, w_y, w_z	displacement in x, y, and z directions
w_∞	total settlement at infinite time
z	elevation

Greek Letters

α	shear strain parameter
β	the slope of e - log k_s line
β_s	shape coefficient
γ	density or unit weight
γ_d	dry density of compacted soil
γ_ω	unit weight of water
$\gamma_{xy}\ \gamma_{yz}\ \gamma_{zx}$	shear strains on xy, yz or zx plane
$\bar{\varepsilon}$	deviatoric strain invarient
$\bar{\varepsilon}^p$	plastic deviatoric strain invariant
ε_v	volumetric strain

ε_v^p	plastic volumetric strain
$\varepsilon_x, \varepsilon_y, \varepsilon_z$	strains in x, y, z directions
η	deviatoric stress ratio
$\bar{\eta}$	compressibility ratio
θ	scalar parameter
κ	the slope of isotropic rebound curve
λ	Lame constant
λ	the slope of isotropic compression virgin curve
$\lambda, \lambda_1, \lambda_2$	parameters in flow rule
μ	viscosity
ν'	Poisson's ratio
ξ	effective stress parameter
σ	stress, total stress
σ'	effective stress
σ_m'	mean effective stress
σ_{mp}'	value of mean effective stress for which ε_v^p is zero
$\sigma_1' \sigma_2' \sigma_3'$	effective principal stresses
$\sigma_x \sigma_y \sigma_z$	stresses in x, y, z directions
$\tau_{xy} \tau_{yz} \tau_{zx}$	shear stresses on xy, yz or zx plane
ϕ'	angle of friction
ϕ_0'	initial angle of friction
$\Delta\phi'$	coefficient of decrease of the angle of friction
χ	effective stress parameter
ψ	effective stress parameter
Ω	effective stress parameter

Matrix Notation

$[C]$	stress-strain matrix
$[C^E]$	elastic stress-strain matrix
$[C^{Ep}]$	elastic plastic stress-strain matrix
$[C_t]$	tangential stress-strain matrix
$[E]$	compressibility matrix
$\{F\}$	force vector
$\{F_b\}$	body force vector
$[H]$	transmissibility matrix
$[K]$	stiffness matrix
$[K^t]$	tangent stiffness matrix
$[k]$	permeability matrix
$[L]$, $[G]^T$	geometry matrices
$\{N_u\}$	vector of shape functions for pore pressure
$\{N_w\}$	vector of shape functions for displacement
$\{n\}$	normal vector
$\{w\}$	displacement vector
$\{\Gamma\}$	vector of boundary flows
$\{\varepsilon\}$, $\{\dot{\varepsilon}\}$	strain vector, rate of strain vector
$\{\sigma\}$, $\{\dot{\sigma}\}$	stress vector, rate of stress vector

CHAPTER 1

INTRODUCTION

INTRODUCTION

The theory of consolidation was first developed by Terzaghi (1924). In one-dimensional cases, such as those considered by Terzaghi, the consolidation process is governed by the diffusion equation. In two- or three-dimensional cases it is often assumed that the consolidation process is governed by a two- or three-dimensional diffusion equation, as, for example, in the work done by Rendulic (1936).

For problems with simple geometries and simple boundary conditions it is often possible to find an analytic solution to the diffusion equation. Solutions of this type have been developed by Carrilo (1942), Carslaw and Jaegar (1959), and Scott (1963), Subrahmanyam (1971). For more complicated problems, it is necessary to resort to numerical methods; the use of the finite difference solution for the diffusion form of the equations of consolidation was pioneered by Gibson and Lumb (1953).

The diffusion approach is only an approximation to the actual process of consolidation, because it neglects the changes in bulk stress which occur during consolidation. A more correct formulation for a soil with an elastic skeleton was developed by Biot (1941a, b, 1956a, b).

Analytical solutions of Biot's equations have been obtained by Biot (1955)(1956), Josselin De Jong (1957)(1963), McNamee and Gibson (1960a, b), and Gibson, Schiffman and Pu (1970) for particular boundary conditions. However such solutions are limited to problems with extremely simple geometry and boundary conditions. For more complicated problems it is necessary to find solutions by numerical techniques. Finite element methods have been developed for this purpose by Sandhu and Wilson (1969), Yokoo, Yamagata and Nagaota (1971), Christian and Boehmer (1970) and Hwang et al. (1971).

The previous theories and analyses assume that the soil skeleton behaves as a linear elastic porous medium. Under many loading conditions, however, soils do not behave elastically. Zienkiewicz and Naylor (1972), Small, Booker and Davis (1976) have developed formulations and finite element solution techniques for the consolidation of soils with elasto-plastic stress-strain behavior of the soil skeleton.

For analyses of consolidation in earth dams, it is important to be able to predict the pore pressures and the rate at which the pore pressures dissipate during construction, for the following reasons:

(1) Considerable movement, both vertical and horizontal, may occur due to pore pressure dissipation and may cause the loss of freeboard.

(2) Pore pressure generation and dissipation leads to stress changes during consolidation which may influence the likelihood of hydraulic fracturing after the reservoir is filled.

(3) It is useful to be able to predict movements and pore pressures in dams in order to understand the significance of measurements made during and after construction.

(4) In order to perform effective stress analyses of stability, it is essential that the pore pressures within the dam be known.

Previously developed procedures for analysis of consolidation are only applicable to saturated clays. Because dams generally consist of unsaturated materials, it is therefore important to develop a means of describing and analyzing the consolidation of unsaturated clay soils.

This study shows that the air-water mixture in the pores of a clay compacted wet of optimum water content can be treated as a homogenized compressible fluid. Biot's theory can be used to analyze this condition if the following factors are taken into account:

(1) the effective stress-strain behavior of the clay,

(2) the compressibility of the pore fluid, and

(3) the permeability of the unsaturated clay.

These factors are discussed in detail in this study and are used to formulate a theory of consolidation applicable to the behavior of unsaturated clays.

The final part of this study is concerned with the development of a numerical technique based on the finite element method, and the use of this technique to analyze the behavior of New Melones Dam.

CHAPTER 2

EFFECTIVE STRESS-STRAIN RELATIONSHIP OF CLAY

INTRODUCTION

It is well known that the effective stress controls the failure and deformation behavior of soil, and so it is important to investigate the relation between effective stress, strains, and failure.

The first attempt to describe the effective stress-strain relationship assumed linear elastic behavior. Although this approach is sometimes applicable, it cannot duplicate the irrecovable deformation observed in real soils, nor can it predict the possibility of failure.

More realistic behavior can be simulated by using a non-linear elastic model with a varying Young's modulus and Poisson's ratio. This type of model predicts real soil behavior more accurately for some conditions. However such models assume that the principal directions of the incremental stress and incremental strains coincide, which is generally incorrect near failure.

One way to overcome these limitations is to use the theory of plasticity. A first attempt would be to assume that the soil is an elastic-perfectly plastic material. Such a model, however, does not predict the early irrecovable deformation which is observed in practice. Drucker, Gibson and Henkel (1957) recognized that in order to obtain a more realistic soil behavior it was necessary to propose an elastic-plastic work hardening model.

The concept of soil as an elastic-plastic work hardening material has been studied exhaustively by Roscoe and his co-workers in Cambridge. The Cam Clay Model was developed by Roscoe and Schofield (1963) and Roscoe, Schofield and Thurairajah (1963). It is assumed that a conical failure surface is capped by a yield surface, as shown in Fig. 2.1, and that the cap yield surface expands according to a work hardening law. This

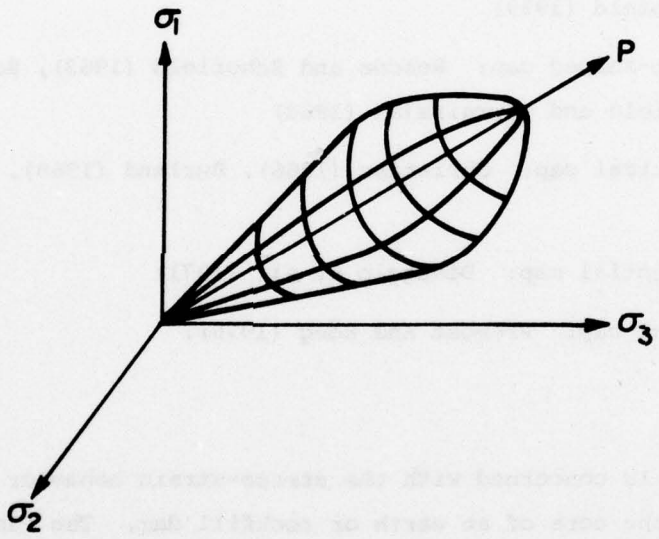

FIG. 2.1 CAP MODEL IN PRINCIPAL STRESS SPACE

assumption models volume changes due to changes in both shear and normal stress. The plastic incremental strain is assumed to be governed by an associated flow rule. The shape of the cap yield surface was later modified and revised by Roscoe and Burland (1968). Similar models have been investigated by Jenike and Shield (1959), Christian (1966), DiMaggio and Sandler (1971), and Prevost and Höeg (1975).

The main differences between these models is the shape of the caps. The different caps which have been used are summarized below:

(1) Spherical cap: Drucker, Gibson and Henkel (1958), Jenike and Shield (1959)

(2) Bullet-shaped cap: Roscoe and Schofield (1963), Roscoe, Schofield and Thurairajah (1963)

(3) Elliptical cap: Christian (1966), Burland (1968), Hagmamn (1971)

(4) Exponential cap: DiMaggio et al. (1971)

(5) Conical cap: Prevost and Höeg (1975).

CAM CLAY MODELS

This study is concerned with the stress-strain behavior of compacted clays in the core of an earth or rockfill dam. The Cam Clay Models were developed for remolded clays and have been used successfully to predict their stress-strain behavior. In general, the properties of compacted clays are similar to those of remolded clays, and it thus seems reasonable to adopt the concepts of the Cam Clay Models to describe the behavior of compacted clays. These concepts are outlined briefly in the following section.

Basic Assumptions on Soil Properties

The Cam Clay Model assumes that the failure surface can be expressed by a linear relation between σ_m' and q:

$$\sigma_m' = Mq \tag{2.1}$$

where $$\sigma_m' = (\sigma_1 + \sigma_2 + \sigma_3)/3 \tag{2.2}$$

and $$q = \sqrt{\frac{1}{2}\left[(\sigma_1 - \sigma_2)^2 + (\sigma_2 - \sigma_3)^2 + (\sigma_3 - \sigma_1)^2\right]} \tag{2.3}$$

The failure criterion represented by Eq. 2.1 is shown in Fig. 2.2.

In describing the volume change characteristics, it is assumed that the isotropic compression curve (the $e - \ln \sigma_m'$ curve) can be represented by two lines with different slopes, λ and κ, as shown in Fig. 2.3.

Elastic Behavior

An elastic-plastic model behaves elastically during unloading. Therefore the rebound curve of an isotropic compression curve can be used to determine the elastic volume change behavior.

The relationship between an incremental change in void ratio (de) and the corresponding increment of volumetric strain ($d\varepsilon_v$) is:

$$d\varepsilon_v = \frac{-de}{1 + e_0} \tag{2.4}$$

where e_0 is the initial void ratio.

Bulk modulus is defined as:

$$B = \frac{d\sigma_m'}{d\varepsilon_v} \tag{2.5}$$

With the aid of Eq. 2.4, the bulk modulus can be expressed as:

$$B = -\frac{d\sigma_m}{de}(1 + e_0) \tag{2.6}$$

As shown in Fig. 2.3, κ is the slope of the rebound curve in the $e - \ln \sigma_m'$ plot. That is:

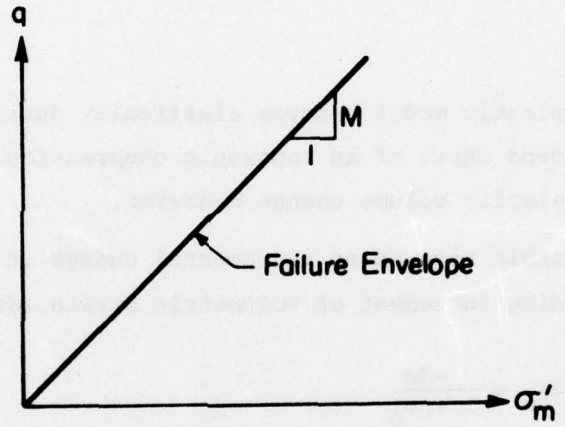

FIG. 2.2 A FAILURE ENVELOPE IN THE σ_m' - q PLANE

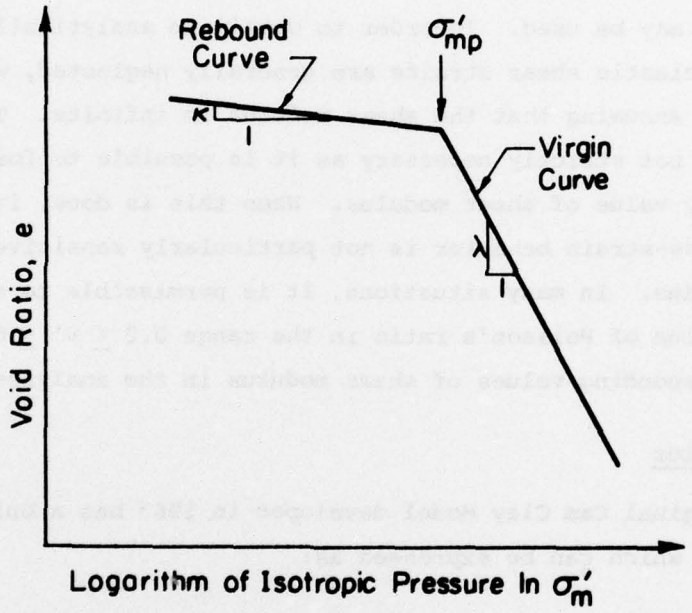

FIG. 2.3 SIMPLIFIED e - ln σ_m' CURVE

$$\frac{1}{\kappa} = -\frac{d\sigma_m'}{de} \cdot \frac{1}{\sigma_m'} \tag{2.7}$$

Substituting Eq. 2.7 into Eq. 2.6, the bulk modulus can be calculated for different values of mean effective stress σ_m' as follows:

$$B = \frac{\sigma_m'}{\kappa}(1 + e_0) \tag{2.8}$$

In order to determine the elastic behavior, it is necessary to determine two elastic parameters. For example, the bulk modulus and the shear modulus may be used. In order to obtain an analytically simple formulation, elastic shear strains are generally neglected, which is equivalent to assuming that the shear modulus is infinite. This assumption is not strictly necessary as it is possible to formulate the theory for any value of shear modulus. When this is done, it is observed that the stress-strain behavior is not particularly sensitive to the value of shear modulus. In many situations, it is permissible to select a reasonable value of Poisson's ratio in the range $0.2 \leq \nu' \leq 0.45$, and to use the corresponding values of shear modulus in the analyses.

Plastic Behavior

The original Cam Clay Model developed in 1963 has a bullet-shaped yield surface which can be expressed as:

$$\sigma_m' \, \text{Exp}\left(\frac{\eta}{M}\right) - p_0\left(\varepsilon_v^p\right) = 0 \tag{2.9}$$

where
$$\eta = \frac{q}{\sigma_m'} \tag{2.10}$$

$p_0\left(\varepsilon_v^p\right)$ = the hydrostatic pressure necessary to produce a plastic volumetric strain of magnitude ε_v^p.

The yield surface expressed in Eq. 2.9 expands according to the work hardening parameter $p_0\left(\varepsilon_v^p\right)$, which can be obtained by deducting the elastic volumetric strain from the total volumetric strain. Thus the plastic volumetric strain can be expressed as

$$\varepsilon_v^p = (\lambda - \kappa) \ln \frac{\sigma_m'}{\sigma_{mp}'}, \quad (\sigma_m' > \sigma_{mp}') \tag{2.11}$$

where σ_{mp}' is the value of mean effective stress for which ε_v^p is zero, as shown in Fig. 2.3.

In the Cambridge theory it is assumed that the plastic strain increment is given by an associated flow rule. Thus the vector of plastic strain increment can be determined by the shape of the yield cap. For some soils, Roscoe and Burland (1968) suggested that an elliptical yield surface may be more appropriate than the bullet shape yield surface in Eq. 2.9. The elliptical yield surface can be expressed as

$$\frac{M^2 + \eta^2}{M^2} \cdot \sigma_m' - p_0 (\varepsilon_v^p) = 0 \tag{2.12}$$

The modified Cam Clay theory can be obtained by replacing Eq. 2.9 by this equation. Both yield surfaces are shown schematically in Fig. 2.4.

STRESS-STRAIN BEHAVIOR OF COMPACTED CLAY COMPARED WITH THAT PREDICTED BY THE CAM CLAY MODELS

This study is concerned with the pore pressure dissipation and the stress-strain behavior of compacted clay in the core of earth and rock-fill dams. Therefore it is interesting to see how well the Cam Clay Models can predict the observed stress-strain behavior of compacted clays. In order to do this, the results of predictions made using both Cam Clay Models are compared with the observed behavior of compacted Canyon Dam clay which was tested by Casagrande (1962).

Canyon Dam clay is a silty clay with PI = 19 and LL = 34. The maximum dry density as determined by the Harvard compaction test is 112.8 lb/ft^3 and the optimum water content is 16.7%. Test samples of this clay were compacted 2% wet of optimum water content with an average water content 17.4%, and an average dry density 111.3 lb/ft^3.

The tests available for parameters evaluation were:

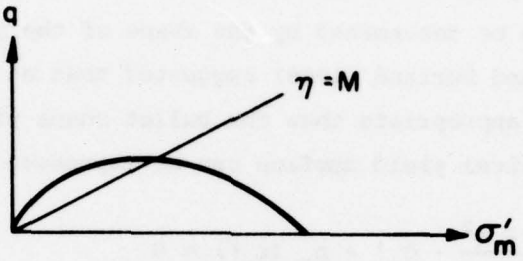

Yield locus of the 1963 Cam Clay Model

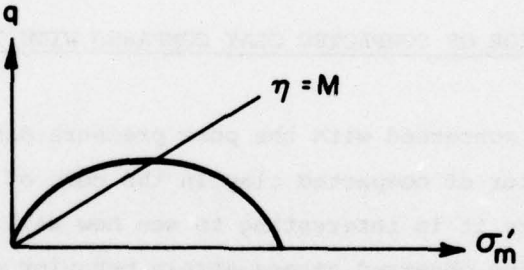

Yield locus of the 1968 Modified Cam Clay Model

FIG. 2.4 YIELD LOCI FOR CAM CLAY MODELS

(1) Drained triaxial tests, and

(2) One-dimensional compression tests.

The results of these tests are shown in Fig. 2.5 and Fig. 2.6.

The value of the parameter M can be determined from the drained triaxial tests. The failure line from the drained triaxial tests is plotted in Fig. 2.7.

It is noted that the most appropriate failure line for this clay does not pass through the origin as postulated in the Cam Clay Models.

It is most desirable to determine λ and κ from an isotropic compression curve. Unfortunately, this type of test was not available for Canyon Dam clay. However, the results of a one-dimensional compression curve were available. Therefore, the assumption that K_0 remained constant through the test was made so that the slopes λ and κ measured from the one-dimensional compression test could be assumed to be the same as those measured from isotropic consolidation tests. Values of Poisson's ratio could be determined if the results of drained triaxial tests on overconsolidated specimens were available. Such tests had not been conducted for Canyon Dam clay, but, as observed before, the stress-strain behavior is not sensitive to the value of Poisson's ratio. Thus a value of 0.3 was chosen for ν' and was used in the calculations.

By using the parameters summarized in Table 2.1, the stress-strain curves for the drained triaxial tests can be predicted. Comparisons between the predicted and the experimental stress-strain curves are shown in Fig. 2.8. It may be seen that the stress-strain behavior predicted by the elliptical cap (Roscoe and Burland, 1968) is somewhat better than that predicted by the bullet shaped cap (Roscoe and Schofield, 1963). However, the comparison shows the stress-strain behavior predicted by these theories is not altogether satisfactory.

The predicted stress-strain behavior is deficient in two ways: the strength is not predicted accurately, and the calculated values of shear strain ε are too large.

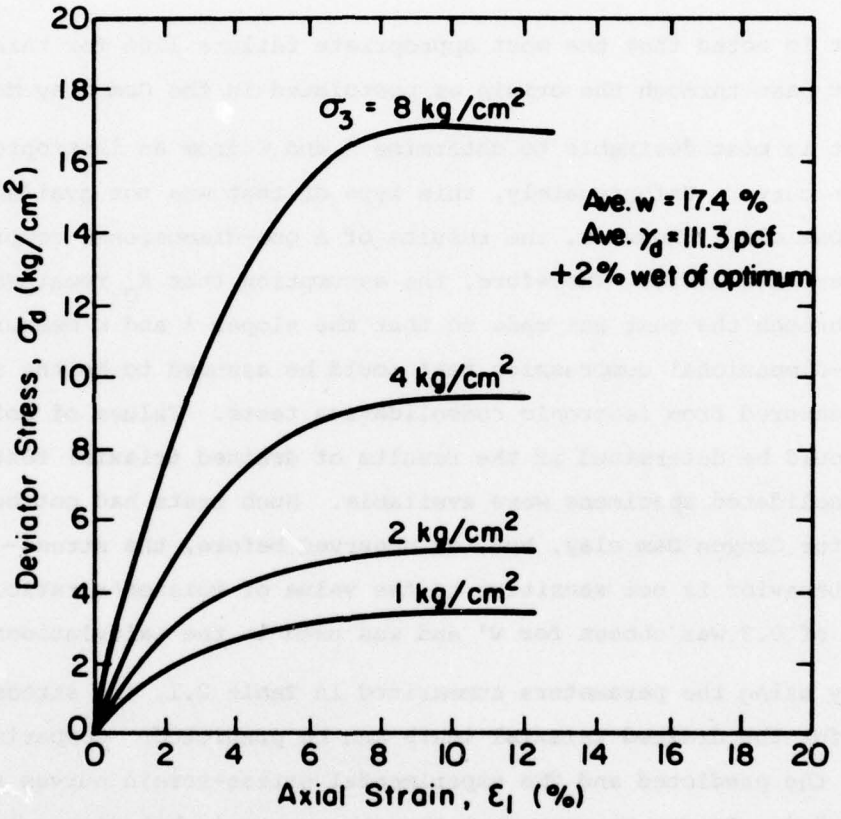

FIG. 2.5 STRESS-STRAIN CURVES FROM DRAINED TRIAXIAL TESTS ON CANYON DAM COMPACTED CLAY

(After Casagrande, 1962)

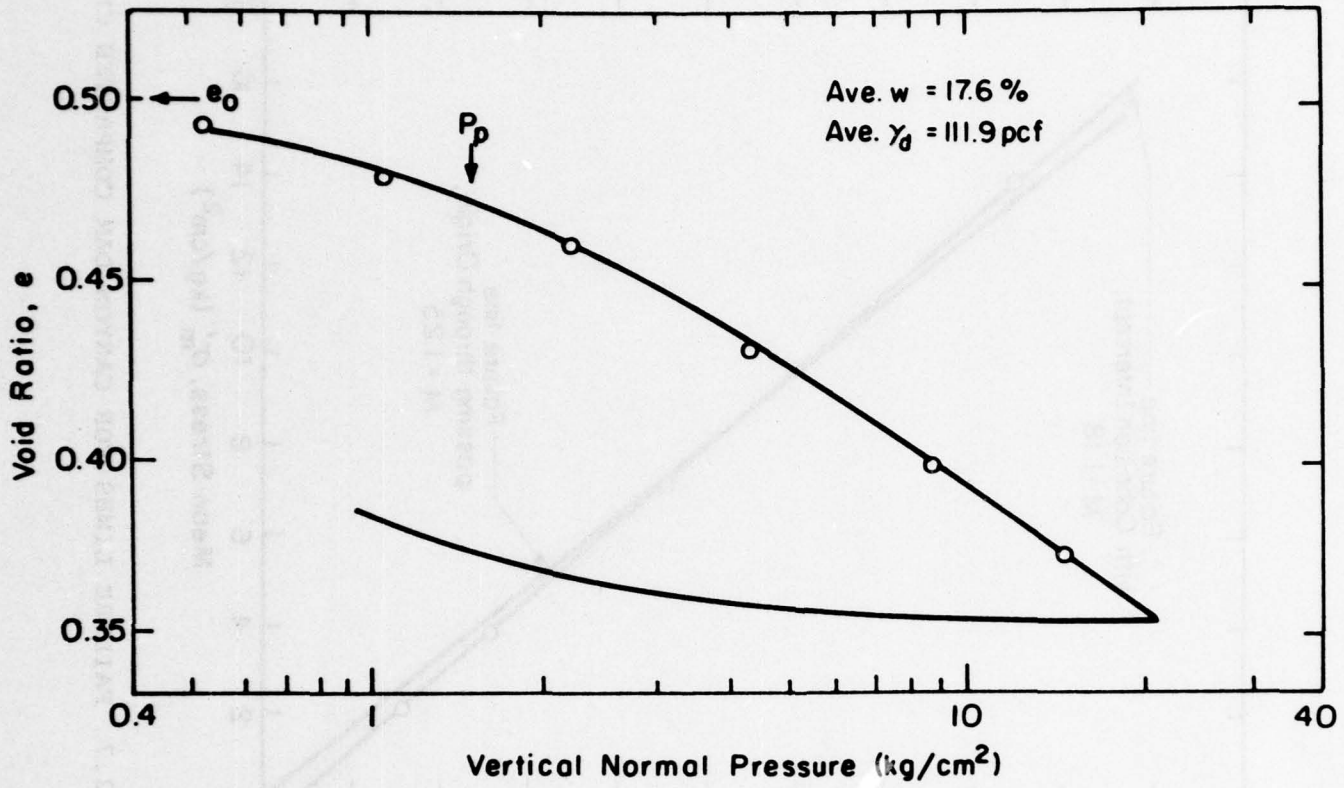

FIG. 2.6 ONE DIMENSIONAL CONSOLIDATION CURVE FOR CANYON DAM COMPACTED CLAY
(After Casagrande, 1962)

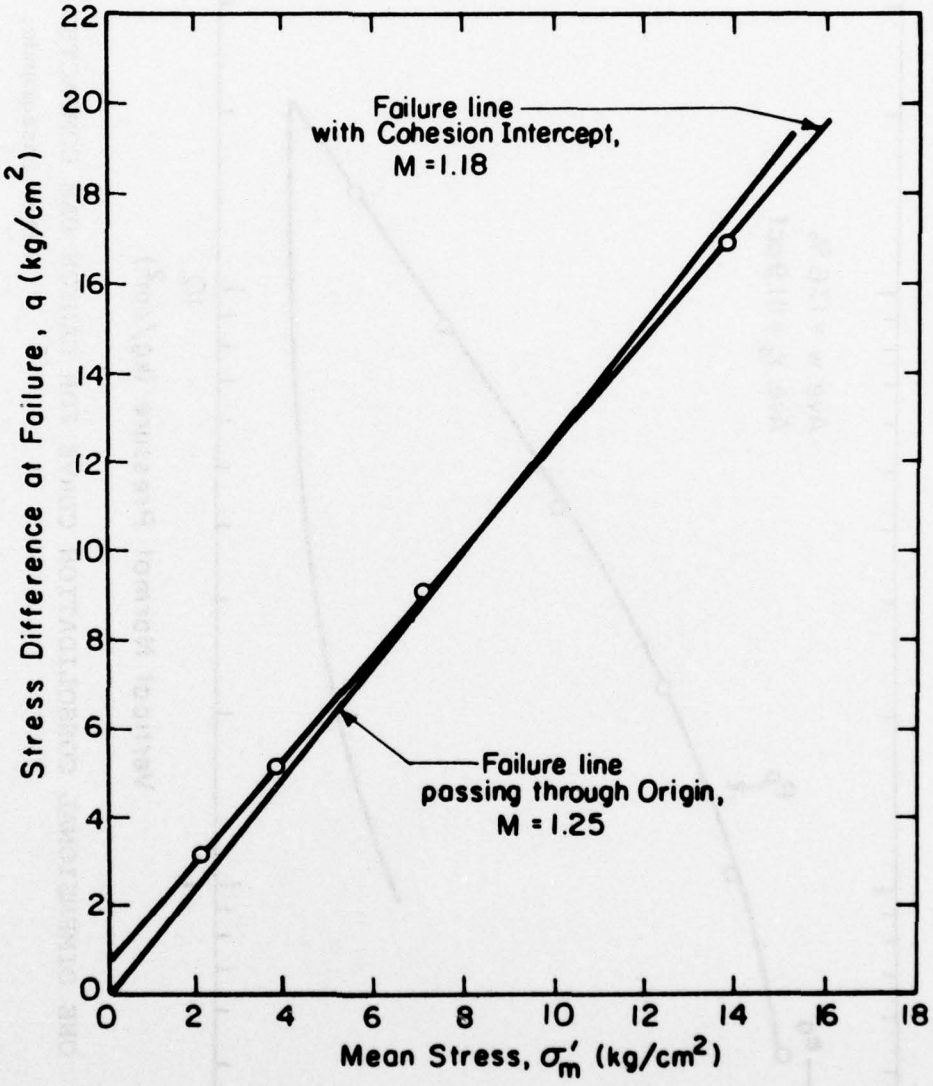

FIG. 2.7 FAILURE LINES FOR CANYON DAM COMPACTED CLAY

Table 2.1 Summary of the Parameters for Cam Clay Models (1963 & 1968)

Parameters	Cam Clay (1963)	Cam Clay (1968)
λ	0.05	0.05
κ	0.004	0.004
M	1.25	1.25
ν'	0.3	0.3

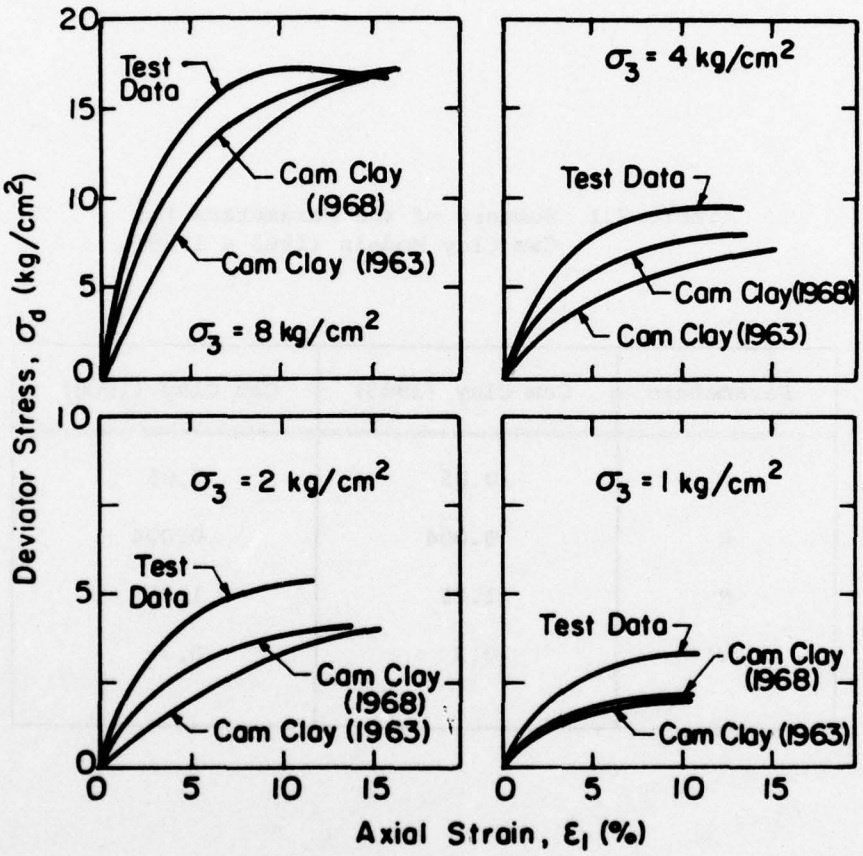

FIG. 2.8 COMPARISONS OF MEASURED AND CALCULATED STRESS-STRAIN CURVES

The possible reasons for this are:

(1) The strength of Canyon Dam clay is not well represented by a failure line passing through origin, as shown in Fig. 2.7.

(2) The use of two straight lines to simulate the measured $e - \ln \sigma_m'$ curve may not be sufficiently accurate.

The following section describes a modification of the Cam Clay Model intended to overcome these defects.

A MODIFICATION OF THE CAM CLAY MODEL

In order to be able to predict more realistic stress-strain behavior for compacted clays, the following modifications were made to the Cam Clay Model.

(1) It was assumed that the failure line had a cohesion intercept so that the strength of the soil could be represented more accurately. The failure line in the $\sigma_m' - q$ plane may be expressed as

$$q = q_0 + \sigma_m' M \tag{2.13}$$

where q_0 is the intercept on the q axis of the $q - \sigma_m'$ diagram.

(2) The measured $e - \ln \sigma_m'$ curve is used instead of a straight line approximation. The $e - \ln \sigma_m'$ relationship was represented by a table of pairs of values of e and σ_m', and intermediate values were determined by interpolation.

Elastic Behavior

With a rebound curve represented by pairs of values of e and σ_m', the tangent value of bulk modulus can be expressed as

$$B = (1 + e_0)/b \tag{2.14}$$

where b is the tangent value of the slope of the rebound $e - \sigma_m'$ curve. For Canyon Dam compacted clay the value of B is very nearly constant

over a range of values of σ_m' as shown in Fig. 2.9. The value of Poisson's ratio was assumed to be 0.3, as discussed previously.

Plastic Behavior

With a failure line which does not pass through the origin, the elliptical yield cap can be expressed as

$$\left(\frac{M^2 + \eta^2}{M^2}\right)\left(\sigma_m + p_r\right) - p_r = p_0\left(\varepsilon_v^p\right) \tag{2.15}$$

where $$p_r = q_0/M \tag{2.16}$$

$p_0\left(\varepsilon_v^p\right)$ can be obtained from a σ_m' - e curve by deducting the elastic volumetric strain from the total volumetric strain. The plastic strain increments are calculated using an associated flow rule.

Parameters Required

The parameters required to implement the theory are B, ν', M, c and the pairs of values of e and σ_m' which represent the isotropic compression curve. Values of these parameters for Canyon Dam clay are evaluated in the following section.

STRESS-STRAIN BEHAVIOR OF CANYON DAM CLAY PREDICTED USING THE EXTENDED CAM CLAY MODEL

The values of the parameters M and q_0 can be determined from Fig. 2.7. The isotropic compression curve was not available, and therefore, as before, the σ_m' - e curve was calculated using the one-dimensional compression curve shown in Fig. 2.6. In calculating values of e and σ_m' for the curve shown in Fig. 2.9, it was assumed that K_0 was equal to 0.5.

The evaluation of the slope of the rebound curve (b) is shown in Fig. 2.9.

Using the parameters summarized in Table 2.2, the Extended Cam Clay Model was used to predict the stress-strain curves for Canyon Dam clay.

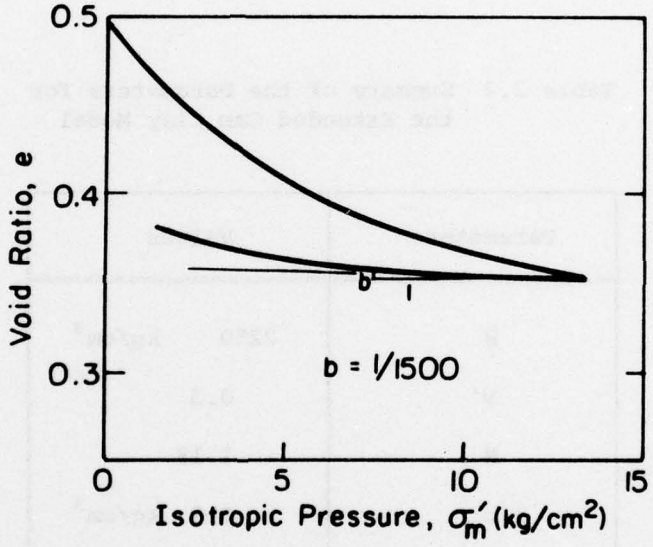

FIG. 2.9 ISOTROPIC COMPRESSION CURVE FOR CANYON DAM CLAY

Table 2.2 Summary of the Parameters for the Extended Cam Clay Model

Parameters	Values
B	2250 kg/cm^3
ν'	0.3
M	1.18
c	0.9 kg/cm^3
$p_0(e)$	in Fig. 2.9

As shown in Fig. 2.10, the Extended Model provides significant improvement in the prediction of both strength and the shape of the stress-strain curves.

MODIFICATIONS TO THE SHAPE OF THE CAP

The plastic strain increments are determined by the shape of the cap. For some soils, the stress-strain behavior cannot be described sufficiently well by the models described previously. Therefore, some further modifications were considered to extend the range of applicability of the elastic-plastic work hardening model.

Curved Failure Envelope for Granular Soils

For some granular materials, it is found that the failure envelope is curved due to particle crushing at high confining pressures. The corresponding reductions in the values of ϕ' with increasing pressure may be represented by the equation proposed by Wong and Duncan (1974):

$$\phi' = \phi_0' - \Delta\phi' \log_{10} \frac{\sigma_3'}{p_a} \tag{2.17}$$

where p_a is the atmospheric pressure, ϕ_0' is the value of ϕ' for σ_3' equal to p_a, and $\Delta\phi'$ is the reduction in ϕ' for a ten-fold increase in σ_3'. Eq. 2.17 can be used to evaluate the angle of internal friction appropriate to any confining pressure within the range of pressures encompassed by the test results. The slope of failure line in $\sigma_m' - q$ plane, M, can be related to ϕ' by the equation:

$$M = \frac{6 \sin \phi'}{3 - \sin \phi'} \tag{2.18}$$

Therefore the cap is a function of M, and the value of M varies with confining pressure σ_3'.

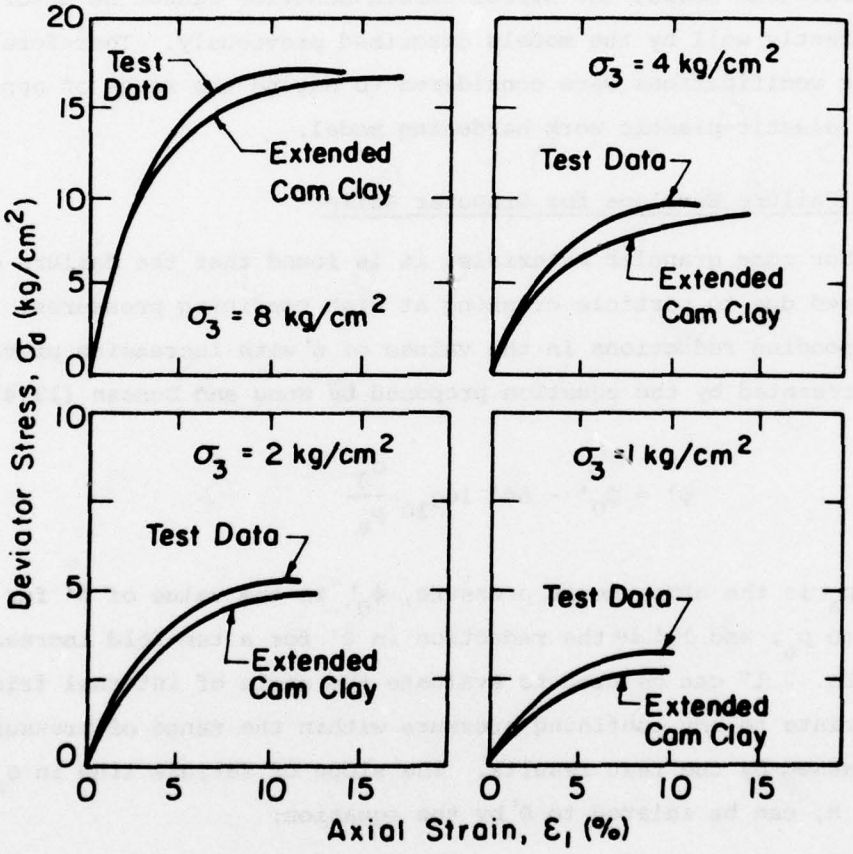

FIG. 2.10 COMPARISON OF MEASURED STRESS-STRAIN CURVES WITH THOSE CALCULATED USING THE EXTENDED CAM CLAY MODEL

Composite Cap

For some soils the observed shear strain is larger than that predicted by the Cam Clay Models discussed previously. This limitation can be overcome by a proposed revision of the cap suggested by Roscoe and Burland (1968).

According to the concept proposed by Roscoe and Burland, it is assumed that the yield surface consists of two parts, AB and BC, as shown in Fig. 2.11. The portion AB is elliptical, and BC is a straight line. The elliptical part can be expressed by Eq. 2.12. Another hardening parameter $\bar{\varepsilon}^p$ is chosen to describe the straight line yield surface. $\bar{\varepsilon}^p$ is the octahedral plastic shear strain, which is given by the following equation:

$$\bar{\varepsilon}^p = \frac{1}{3}\sqrt{2\left[(\varepsilon_1^p - \varepsilon_2^p)^2 + (\varepsilon_2^p - \varepsilon_3^p)^2 + (\varepsilon_3^p - \varepsilon_1^p)^2\right]} \qquad (2.19)$$

Experimental results suggest that the yield function of the straight line part of the cap surface can be expressed as:

$$\alpha \frac{q^2}{(Mp)^2} - \bar{\varepsilon}^p = 0 \qquad (2.20)$$

where α is a constant.

It is assumed that an associated flow rule can be used for both parts of the cap yield surface for the determination of the plastic strain increment. On the portion BC, only plastic shear strain occurs, without any plastic volume strain.

At the corner B, where the two parts of the yield surface intersect, it is assumed that the plastic strain increment can be obtained by superimposing plastic strains derived from the two yield surfaces AB and BC (Koiter, 1953). The plastic strain increments can be expressed as:

$$d\varepsilon_v^p = d\varepsilon_{v_{AB}}^p \qquad (2.21)$$

$$d\bar{\varepsilon}^p = d\bar{\varepsilon}^p_{AB} + d\bar{\varepsilon}^p_{BC} \qquad (2.22)$$

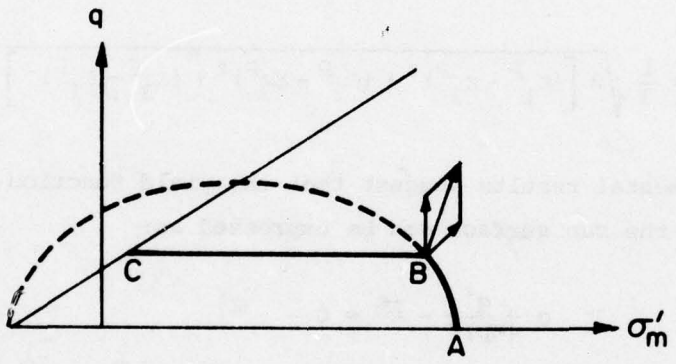

FIG. 2.11 THE EXTENDED CAM CLAY MODEL

in which the $d\varepsilon_{v_{AB}}^{p}$ and $d\bar{\varepsilon}^{p}_{AB}$ are determined from the elliptical yield surface AB , and $d\bar{\varepsilon}^{p}_{BC}$ is determined from the yield surface BC.

The parameter α governs the magnitude of $d\bar{\varepsilon}^{p}_{BC}$. One possible way of determining the parameter α is to determine values of $d\bar{\varepsilon}^{p}_{BC}$ by subtracting the corresponding values of $d\bar{\varepsilon}^{p}_{AB}$ and the elastic strain increments from the total strains. Then the appropriate α could be calculated using Eq. 2.20. This procedure is not simple, however, because the values of $d\bar{\varepsilon}^{p}_{AB}$ are difficult to calculate.

Perhaps the most straight-forward way of determining α for practical purposes is by curve fitting. If all the other parameters are known, the stress-strain curves for a series of drained triaxial tests can be calculated for different values of α, and a value of α which best fits the tests can be chosen. A computer program for determining the stress-strain curves for triaxial tests is provided in Appendix C. An example is shown in Appendix D.

CHAPTER 3

THE PERMEABILITY OF PARTLY SATURATED SOILS

INTRODUCTION

The permeability of the compacted clay core of an earth dam depends on a number of factors, including the type of soil, the compaction conditions, the void ratio or density, and the degree of saturation. The coefficient of permeability may be measured in laboratory tests on samples compacted under the same conditions as those in the field. However, the permeability will change as the degree of saturation changes during seepage, and it will also change as the clay is compressed under the weight of overlying fill. In an analysis of the consolidation of the core of a dam, it is important to take into account the variations of permeability with void ratio and degree of saturation.

In this chapter, an empirical equation is proposed for describing the changes in permeability of partly saturated compacted clays which result from changes in degree of saturation and void ratio.

THEORETICAL PERMEABILITY EQUATIONS

There have been many attempts at establishing relationships between soil permeability and other soil properties. Poiseiulle developed a formula for the permeability of a porous medium with irregular pores. He found that

$$k = \left(\frac{\gamma_\omega}{\mu}\right)\left(\frac{\beta_s V_s^2}{A_s^2}\right)\left(\frac{e^3}{1+e}\right) S^3 \qquad (3.1)$$

where k is the coefficient of permeability, μ is the viscosity of fluid, γ_ω is the unit weight of water (these are both functions of temperature), V_s is the volume of solid, A_s is the wetted area, e is the void ratio, S is the degree of saturation and β_s is a shape coefficient whose value depends on the degree of irregularity of the pore spaces.

Formulae similar to Poiseiulle's equation have been also developed by Kozney (1927), Taylor (1948), and Carman (1956). All of these theoretical equations are based on the assumptions that the particles are approximately equidimensional, that they are of a uniform size larger than 1 μm, and that the flow is laminar. The equations have been observed to hold fairly well in sandy and silty soils. However, considerable discrepancies between these theoretical expressions and experimental results have been found for clays. It seems well established that the major cause of these discrepancies is that the pores of clay soils are not of a uniform size. Olsen (1961) has discussed these discrepancies in detail.

PROPOSED PERMEABILITY EQUATION

Because the theoretical permeability equations are not applicable to clays, it is preferrable to adopt an experimental or empirical approach.

Soil permeability is influenced by many factors including particle size distribution, particle shape, structure, void ratio and degree of saturation. The effects of each of these is hard to isolate from the others because these characteristics are closely interrelated -- e.g., structure depends on particle size, void ratio, method of compaction, and compaction water content.

In the study described in this report no attempt has been made to formulate the effects of particle size distribution, particle shape and structure on permeability, because these factors are nearly constant for a particular clay, a particular method of compaction and a given compaction water content, and their effects are accounted for when laboratory tests are performed on specimens compacted under the same conditions as the soil in the field.

Two major factors which change the permeability of compacted core material after compaction are changes in the degree of saturation and the void ratio. It seems reasonable to postulate that their effects can be accounted for by using an empirical equation of the form:

$$k = k_s G_e H_s \tag{3.2}$$

in which k is the permeability of the partly saturated clay, k_s is the permeability of the clay when it has been completely saturated using back pressure, G_e is a factor whose value depends on void ratio, and H_s is a factor whose value depends on degree of saturation.

Determination of k_s

The value of k_s is influenced significantly by the water content at compaction because the water content at compaction influences the structural arrangement of soil properties. Therefore k_s must be determined from test specimens compacted using procedures which produce the same structure as does the field compaction procedure. Seed and Chan (1959) found that a flocculated structure (random particle arrangement) tends to be formed for clays compacted dry of optimum, while a dispersed structure (more parallel particle arrangement) tends to be formed for clays compacted wet of optimum by kneading compaction. As shown in Fig. 3.1, the permeability of a soil with a flocculated structure is far higher than the permeability of the same soil with a dispersed structure.

Determination of G_e

The variation of the factor G_e with void ratio can be determined experimentally by testing saturated specimens which have been consolidated under different pressures, and therefore have different void ratios.

Data from a number of tests on a sand are shown in Fig. 3.2. For this sand, the variation of k_s with e appears to be fairly accurately approximately by Poiseiulle's equation which corresponds to

$$G_e = \frac{e^3}{1+e} \Big/ \frac{e_0^3}{1+e_0} \tag{3.3}$$

Additional data for a number of sands, silts, and clays are shown in Fig. 3.3 (from Lambe and Whitman, 1969). These data indicate that the log of k_s varies linearly with e. This variation corresponds to

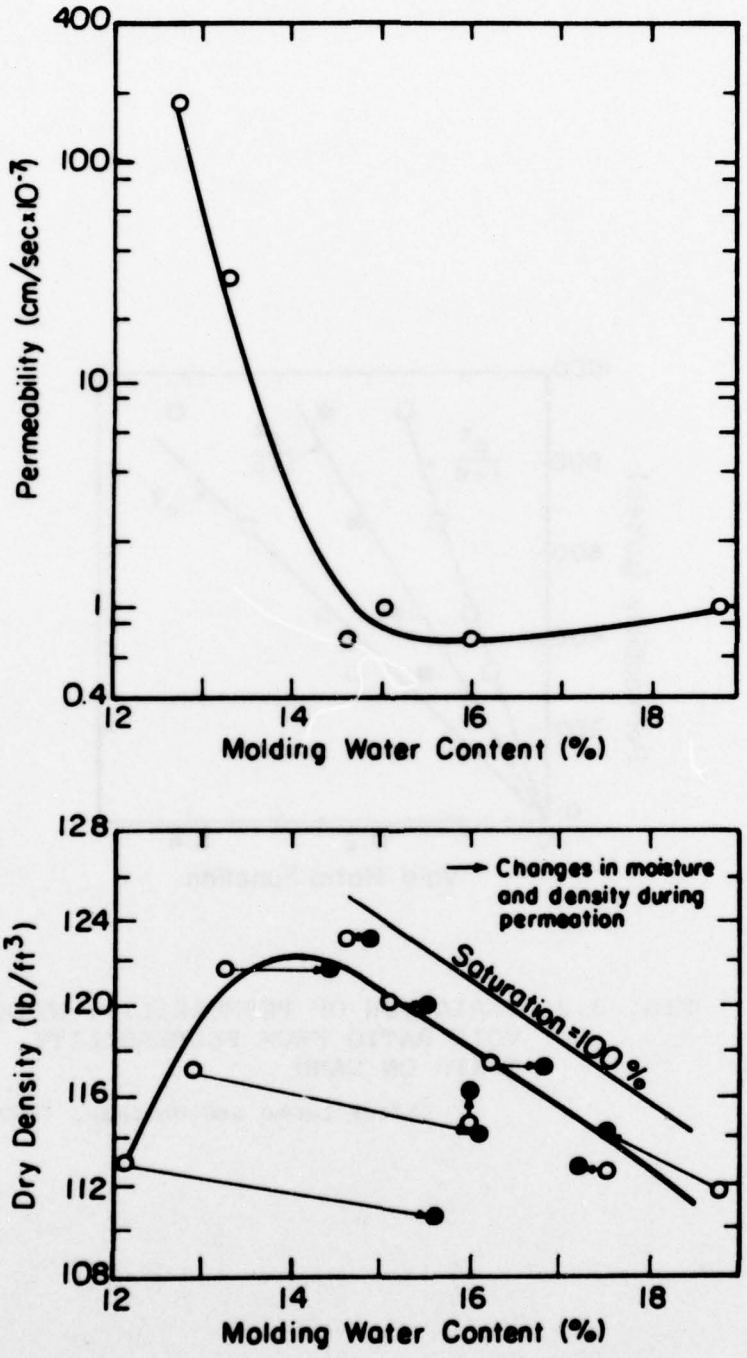

FIG. 3.1 PERMEABILITY BEHAVIOR OF JAMAICA SANDY CLAY
(After Lambe, 1958)

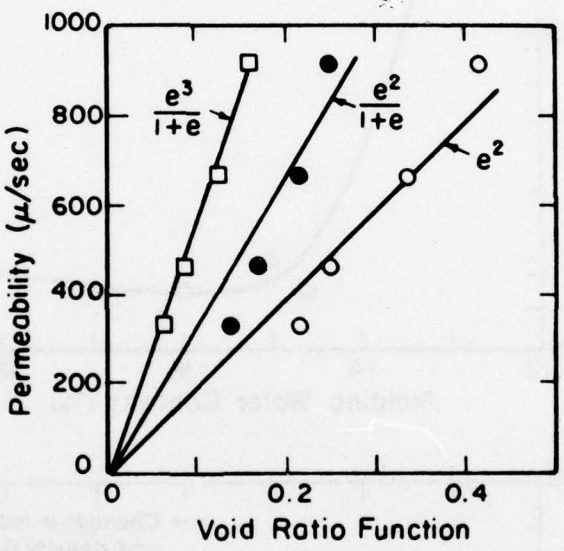

FIG. 3.2 VARIATION OF PERMEABILITY WITH VOID RATIO FROM PERMEABILITY TESTS ON SAND

(After Lambe and Whitman, 1969)

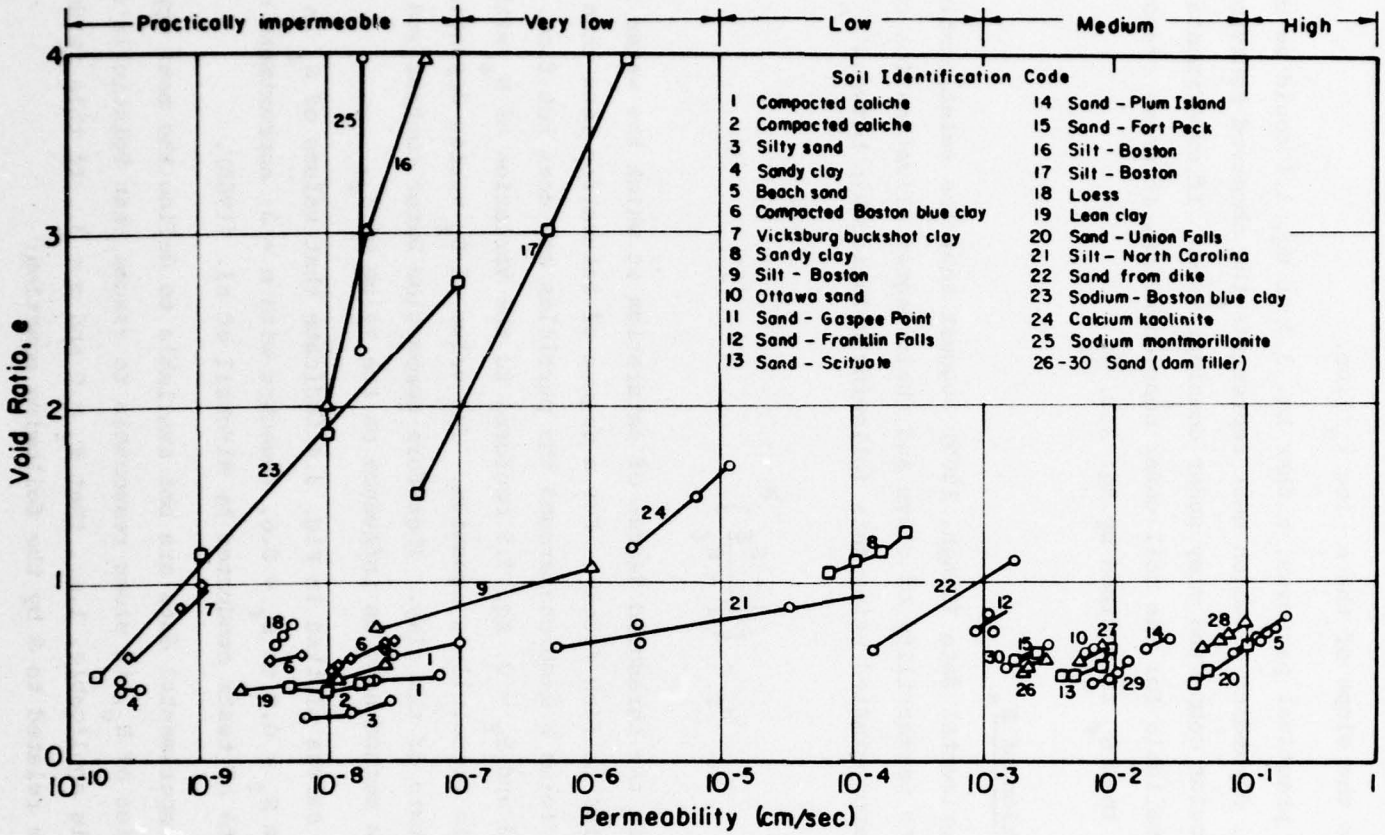

FIG. 3.3 PERMEABILITY TEST DATA (After Lambe and Whitman, 1969)

$$G_e = \text{Exp}\left(\frac{e}{\beta}\right) \Big/ \text{Exp}\left(\frac{e_0}{\beta}\right) \tag{3.4}$$

where β is the slope of the e - log k_s line.

For practical purposes, either Eq. 3.3 or Eq. 3.4 could be used to define G_e, depending on which best represents the observed behavior of the particular compacted clay under consideration. If experimental data are not available for the soil under consideration, it seems reasonable to assume that G_e is defined by Eq. 3.3.

Determination of H_s

Experimental data (Singh, 1965) suggest that the relationship between the permeability of clays and their degree of saturation can often be approximated using this following relationship between H_s and S.

$$H_s = \left(\frac{S - S_f}{1 - S_f}\right)^m \tag{3.5}$$

where S_f is the threshold degree of saturation at which the water in the pores begins to flow freely. For a degree of saturation less than S_f, the water forms a membrane around the particles and does not flow. When m = 3 and S_f = 0, Eq. 3.5 conforms to the variation of H_s with S implicit in Poiseiulle's equation. The value of S_f varies depending on the structure of the clay. Therefore compaction water content and compaction method have an influence on the value of S_f.

The curves plotted in Fig. 3.4 indicate that values of S_f in the range from S_f = 0.0 to S_f = 0.6, together with m = 3, approximate closely the results of tests conducted by Mitchell et al. (1965).

If experimental data are not available to define the most appropriate value of H_s, it seems reasonable to assume that Poiseiulle's equation is applicable, i.e., that S_f = 0 and m = 3. If this is done, H_s will be related to S by the following equation:

$$H_s = S^3 \tag{3.6}$$

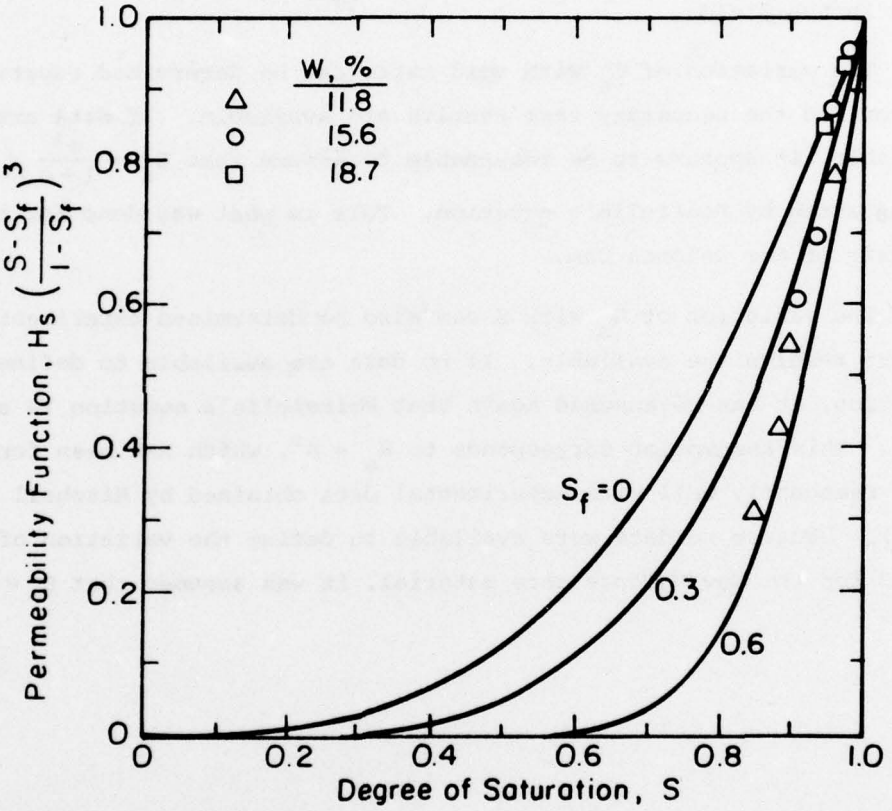

FIG. 3.4 VARIATIONS OF PERMEABILITY WITH DEGREE OF SATURATION FOR COMPACTED CLAY
(Data from Mitchell, et al., 1965)

SUMMARY

The permeability of compacted clay depends on the type of soil, the compaction conditions, the degree of saturation, and the void ratio. The effects of changes in degree of saturation and void ratio can be approximated using Eq. 3.2. The value of saturated permeability, k_s, can be measured using test specimens compacted under the same condition as those in the field.

The variation of G_e with void ratio can be determined experimentally provided the necessary test results are available. If data are not available, it appears to be reasonable to assume that $G_e = \frac{e^3}{1+e} \Big/ \frac{e_0^3}{1+e_0}$, as suggested by Poseiulle's equation. This is what was done for the analysis of New Melones Dam.

The variation of H_s with S can also be determined experimentally if test results are available. If no data are available to define this variation, it can be assumed again that Poiseiulle's equation is applicable. This assumption corresponds to $H_s = S^3$, which has been found to agree reasonably well with experimental data obtained by Mitchell et al., (1965). Because no data were available to define the variation of H_s with S for the New Melones core material, it was assumed that $H_s = S^3$.

CHAPTER 4

EFFECTIVE STRESS EQUATION FOR PARTLY SATURATED SOILS

INTRODUCTION

It is well established that effective stresses govern the deformation and strength of soils. For a saturated soil, the expression for effective stress may be written as:

$$\sigma' = \sigma - u \tag{4.1}$$

where σ is total stress, u is the pore fluid pressure and σ' denotes effective stress.

For an unsaturated soil, the pore fluid consists of air and water. The effective stress equation involves water pressure u_w, air pressure u_a, and surface tension between air and water. Considering equilibrium of force in a microscopic section of soil, the effective stress equation can be expressed as:

The total forces = the interparticle forces
+ the sum of the water pressure forces
+ the sum of the air pressure forces
+ the surface tension forces (4.2)

The effective stress equation is thus quite simply conceptually. However, it is difficult to express quantitatively.

A possible form of the effective stress equation for partly saturated soils had been suggested by Bishop (1959):

$$\sigma' = \sigma - u_a + \chi (u_a - u_w) \tag{4.3}$$

where χ is an empirical parameter representing the portion of the surface tension, $(u_a - u_w)$, that contributes to the effective stress.

χ is a function of degree of saturation. The form of this relation has been derived by Aitchison (1960), who assumed that the soil consists

of uniformly packed spheres. This relation is plotted in Fig. 4.1. However, a number of discrepancies have been found between the theoretical curve and experimental data for clays (Blight, 1965). Also it has been found that the values of χ measured from strength behavior may be significantly different from those measured from volume change behavior (Coleman, 1962; Matyas and Radhakrishna, 1968).

Another possible relationship, suggested by Sparks (1963), is:

$$\sigma' = \sigma - \Omega\, u_a - \xi\, u_w + \psi\, T_c \tag{4.4}$$

where T_c is the surface tension and Ω, ξ and ψ are parameters representing the portions of u_a, u_w, and T_c which contribute to the effective stress.

Sparks employed a model composed of uniform spheres arranged in various packings, and having various contact angles between the water and the soil particles. On the basis of these studies, Sparks concluded that χ may assume values greater than one or less than zero, as shown in Fig. 4.1

Sparks also developed an extensive set of charts to be used to determine the values Ω, ξ and ψ for different packing conditions and contact angles. All of the values proposed by Sparks were calculated on the assumption that the soil consists of uniformly packed spheres. Therefore the values of these parameters are more accurate for sandy and silty soils than for clayey soils.

A frequent special case occurs when the clay is compacted at high water contents, and occluded air bubbles form in the pores. Under this condition, Sparks assumed

$$\sigma' = \sigma - (1 - A)\, u_w \tag{4.5}$$

where A is the effective soil particle contact area per unit area. At high water contents, the area of contact between the solid particles is small compared to the area of contact between the solid particles and the water. Under this condition, the value of A approaches zero. With $A = 0$, Eq. 4.5 becomes

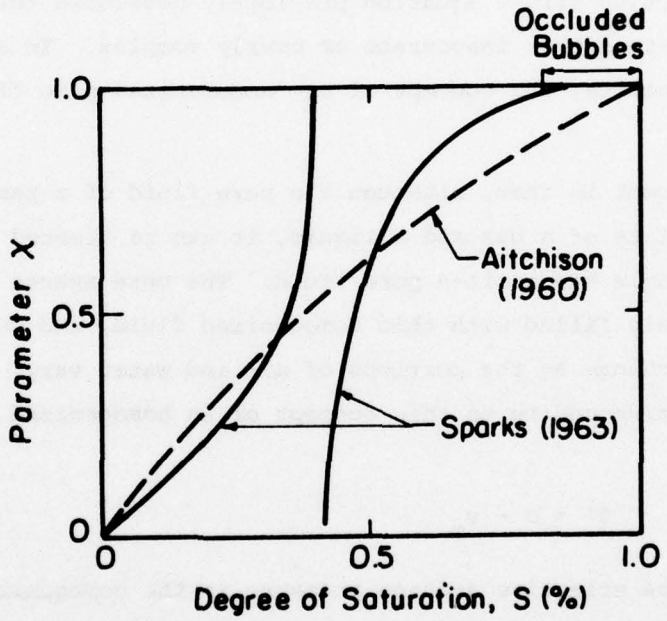

FIG. 4.1 VARIATIONS OF χ WITH DEGREE OF SATURATION

$$\sigma' = \sigma - u_w \tag{4.6}$$

Thus, according to Sparks' studies, the same effective stress equation which applies to saturated soils can also be used for partly saturated conditions where the degree of saturation is high and the air in the voids is in the form of occluded bubbles.

CONCEPT OF HOMOGENIZED PORE FLUID

During the investigation described in this study, it was concluded that the effective stress equation previously developed for partly saturated soils were either inaccurate or overly complex. In an attempt to find an alternative, the concept of an "homogenized pore fluid" was developed.

The concept is that, although the pore fluid of a partly saturated material consists of a gas and a liquid, it can be treated phenomenologically as a single homogenized pore fluid. The pore spaces are viewed as being completely filled with this homogenized fluid, and the properties of the fluid change as the portions of air and water vary. The effective stress law corresponding to this concept of an homogenized pore fluid is expressed as:

$$\sigma' = \sigma - u_m \tag{4.7}$$

where u_m is the effective average pressure in the homogenized pore fluid. For an occluded bubble system, u_m is simply u_w, as shown by Sparks. For clays with lower degrees of saturation, u_m is a function of the air pressure, the water pressure and the surface tension.

THE HOMOGENIZED PORE FLUID PRESSURE

Because the three-phase unsaturated soil is treated as a saturated material with an homogenized pore fluid, the total stress is the sum of effective stress, σ', and pressure in the homogenized pore fluid, u_m, as expressed by Eq. 4.7.

$$\sigma = \sigma' + u_m \tag{4.8}$$

The effective stress equation for partly saturated soil suggested by Bishop (1959) corresponds to the following homogenized pore fluid pressure:

$$u_m = u_a - \chi (u_a - u_w) \tag{4.9}$$

The effective stress equation suggested by Sparks (1963) corresponds to the following homogenized pore fluid pressure:

$$u_m = \Omega u_a + \xi u_w + \psi T_c \tag{4.10}$$

It has been observed previously that neither of these effective stress equations is entirely satisfactory for clays with low degrees of saturation. Fortunately, the clay used as the core material in an earth dam is usually compacted at a water content corresponding to a degree of saturation in the neighborhood of 85%. In this case, the air bubbles are likely to be occluded. Therefore, as observed by Sparks, it can be assumed with a high degree of accuracy that u_m is equal to u_w. This was done in the analysis of the consolidation of the core of New Melones Dam.

ANALYSIS OF CONSOLIDATION OF PARTLY SATURATED SOILS

As a partly saturated soil is loaded, the skeleton is subjected to changes in the effective stress σ' and undergoes deformations. At the same time, the homogenized pore fluid is subjected to changes in pore pressure, and it compresses or expands. Under the influence of the hydraulic gradient induced, the pore fluid will flow.

The homogenized pore fluid model can be used for analyses of consolidation provided the following are known:

(1) The relationship between effective stress and strain for the soil skeleton.

(2) The relationship between permeability and the degree of saturation of the homogenized pore fluid.

(3) The relationship between the compressibility of the homogenized

pore fluid and the proportions of air and water it contains.

The effective stress-strain relationship was discussed in Chapter 2, and the permeability relationship was discussed in Chapter 3. The compressibility relationship will be discussed in the following sections of this chapter.

THE COMPRESSIBILITY OF THE HOMOGENIZED PORE FLUID OF PARTLY SATURATED SOIL

The compressibility of the homogenized pore fluid, $\frac{1}{Q}$, is defined as the volumetric strain induced by a unit change in pore fluid pressure. It can be defined by the following equation:

$$\frac{1}{Q} = - \frac{d\varepsilon_v}{du_m} \tag{4.11}$$

where ε_v is the volumetric strain and u_m is the pore fluid pressure.

As observed previously, the homogenized pore fluid pressure can be expressed as a function of air pressure, water pressure, and surface tension. It may be expressed:

$$u_m = f(u_a, u_w, T_c) \tag{4.12}$$

The compressibility of the homogenized pore fluid therefore can be evaluated using the following equation,

$$Q = -\left(\frac{\partial f}{\partial u_a} \frac{\partial u_a}{\partial \varepsilon_v} + \frac{\partial f}{\partial u_w} \frac{\partial u_w}{\partial \varepsilon_v} + \frac{\partial f}{\partial T_c} \frac{T_c}{\partial \varepsilon_v} \right) \tag{4.13}$$

If the form of Equation 4.13 is known, the compressibility of the homogenized pore fluid can be evaluated by knowing the changes in air pressure, water pressure, and tension due to unit change in volumetric strain. For the case in which the air bubbles are occluded, Eq. 4.13 reduces to:

$$Q = - \frac{\partial u_w}{\partial \varepsilon_v} \tag{4.14}$$

For this important practical case, the compressibility of the homogenized pore fluid can be evaluated using Boyle's and Henry's Law. The details will be given later.

For clays with low degrees of saturation, open channels are likely to be present. The behavior in this case is extremely complicated, and no consideration has been given to it during this study.

ASSUMPTIONS FOR DERIVATION OF THE COMPRESSIBILITY OF THE HOMOGENIZED PORE FLUID

(1) Boyle's Law

Boyle's Law states that the product of pressure and volume of a gas is constant under constant temperature conditions:

(2) Henry's Law

Henry's Law states that at a constant temperature, the weight of gas which can be dissolved in a given volume of liquid is directly proportional to the gas pressure.

Let V_d be the volume that would be occupied by the dissolved gas if it was extracted from the liquid and compressed to the pressure acting on the fluid. According to Boyle's and Henry's Law this volume will be constant and thus independent of the pressure. V_d is only dependent on the volume of water and can be calculated as follows:

$$V_d = H\, V_w \tag{4.15}$$

where V_w is the volume of water, H is the coefficient of solubility. At 20°C, H = 0.02.

According to Dalton's division law, the saturated water vapor pressure in the free air does not obey Boyle's Law. However, the saturated water vapor pressure is usually very small (Schuurman, 1966) and the influence can be disregarded.

According to Henry's Law, the volume of air dissolved in the water is proportional to the volume of water. The rate at which the air dissolves in the water depends on the air pressure. The time t necessary to dissolve the air for a unit change in pressure was shown by Beek (1963) to be

$$t = \frac{r^2}{D_f} \tag{4.16}$$

where D_f is the diffusion coefficient and r is the radius of the bubble. At 20°C, D_f is equal to 10^{-5} cm^2/sec. For small air bubbles, the time necessary to dissolve the air is very small. Therefore it can be assumed that the air dissolves in the water instantaneously and that the water is always saturated with dissolved air.

As a result of the surface tension, T_c, the air pressure and the water pressure of an air-water mixture are not the same. The value of u_w and u_a are related by

$$u_w = u_a - u_c \tag{4.17}$$

where u_c is the capillary pressure due to surface tension. u_c is usually expressed in terms of the meniscus radii, r_1, r_2, as shown in Fig. 4.2.

$$u_c = \frac{T_c}{r_1} + \frac{T_c}{r_2} \tag{4.18}$$

In a mixture of air and water, the bubbles do not necessarily all have the same shape and size. Therefore, it is assumed that:

$$u_c = 2\,\frac{T_c}{R_c} \tag{4.19}$$

where R_c is the average capillary radius for the mixture of air and water. Generally, for soils with high degrees of saturation, the effect of u_c is small.

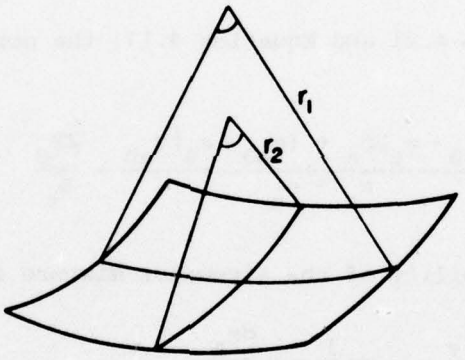

FIG. 4.2 DOUBLY CURVED INTERFACE BETWEEN AIR AND WATER

DERIVATION OF THE COMPRESSIBILITY OF A MIXTURE OF AIR AND WATER

If e_a is the volume of free air and e_s is the volume of dissolved air in the air-water mixture, then it follows from Boyle's and Henry's Law that

$$(e_a + e_s)(p_a + u_a) = (e_{a0} + e_s)(p_a + u_{a0}) \tag{4.20}$$

where p_a is atmospheric pressure, e_{a0} is the initial air volume and u_{a0} is the initial air gauge pressure. Equation 4.20 can also be expressed as:

$$u_a = \frac{(e_{a0} - e_a)p_a + (e_{a0} + e_s)u_{a0}}{e_a + e_s} \tag{4.21}$$

Using Equation 4.21 and Equation 4.17, the pore water pressure may be expressed as:

$$u_w = \frac{(e_{a0} - e_a)p_a + (e_{a0} + e_s)u_{a0}}{e_a + e_s} - \frac{2T_c}{R_c} \tag{4.22}$$

The compressibility of the air-water mixture is

$$\frac{1}{Q} = -\frac{d\varepsilon_v}{du_w} = -\frac{1}{(1 + e_0)}\frac{de_a}{du_w} \tag{4.23}$$

where e_0 is the initial void ratio. From equation 4.22

$$\frac{du_w}{de_a} = -\frac{(e_{a0} + e_s)p_a + (e_{a0} + e_s)u_{a0}}{(e_a + e_s)^2} + \frac{2T_c}{R_c^2}\frac{dR_c}{de_a} \tag{4.24}$$

In terms of degree of saturation S and void ratio e

$$\frac{du_w}{de_a} = -\frac{(e_0 - S_0e_0 + HS_0e_0)(u_{a0} + p_a)}{(e - Se + HSe)^2} +$$

$$+ \frac{2T_c}{R_c^2}\frac{dR_c}{dS}\frac{S}{e} \tag{4.25}$$

Substituting Eq. 4.23 into Eq. 4.25, the compressibility of the homogenized pore fluid can be expressed as:

$$\frac{1}{Q} = \frac{\frac{1}{(1+e_0)}}{\frac{(e_0 - S_0 e_0 + HS_0 e_0)(u_{a0} + p_a)}{(e - Se + HSe)^2} - \frac{2T_c}{R_c^2}\frac{dR_c}{dS}\frac{S}{e}} \tag{4.26}$$

COMPARISON BETWEEN THEORIES AND TEST DATA

The relationships described in the previous sections can be used to predict the change in the degree of saturation of a sample resulting from application of a back pressure.

If the surface tension term in Eq. 4.26 is neglected, the equation reduces to a form similar to that suggested by Hilf (1948) and Skempton and Bishop (1954). The comparison between test data obtained by Mitchell et al, (1965) and the results predicted by Hilf's and Skempton and Bishop's equation is shown in Fig. 4.3.

Schuurman (1966) took surface tension into account by assuning that the air bubbles were all of equal size and spherical in shape. By this assumption, the value of R_c in Eq. 4.19 would be equal to the radius of the air bubbles. Taking the initial radius of air bubbles as R_0, the radius after a change in void ratio can be expressed as

$$R_c = R_0 \left(\frac{e_a}{e_{a0}}\right)^{1/3} \tag{4.27}$$

Substitute this expression into Eq. 4.25, the compressibility of this air-water mixture can be calculated. A comparison between test data obtained by Mitchell et al. (1965) and the results predicted by Schuurman's equation is shown in Fig. 4.3.

It seems likely that the discrepancies between experimental data and the results predicted by Hilf's and Skempton and Bishop's equation are mainly due to the neglecting of the effect of surface tension. The

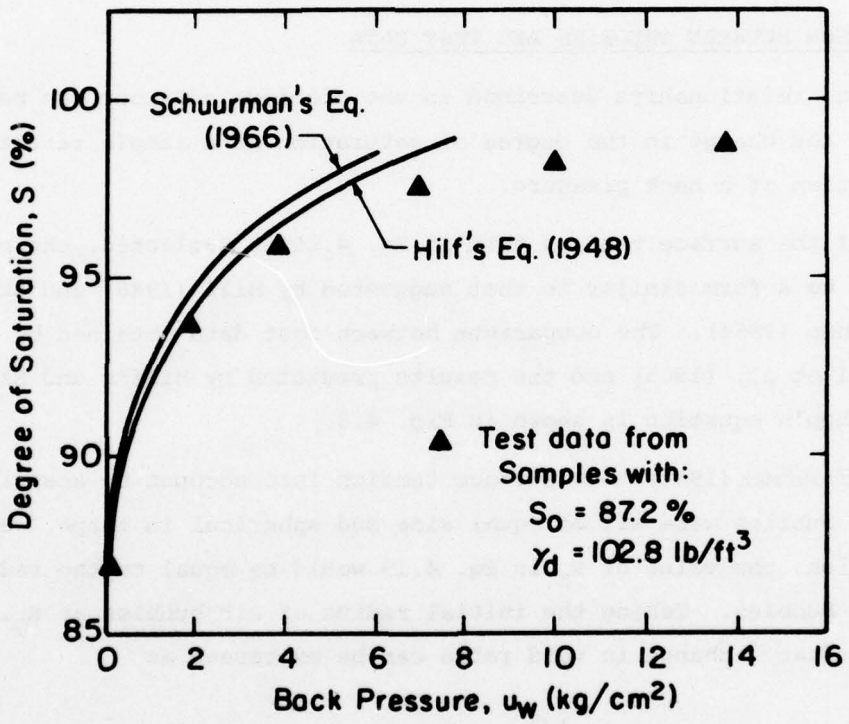

FIG. 4.3 CALCULATED AND MEASURED VARIATIONS OF DEGREE OF SATURATION WITH BACK PRESSURE

(Data from Mitchell, et al., 1965)

discrepancies between the experimental data and the results predicted by Schuurman's equation are probably due to the assumption that all the bubbles are spherical and uniform, and that the total number of bubbles does not change during the compression of the soil.

A further consideration relative to surface tension effects is that the capillary pressure does not necessarily arise only from the bubbles. It can also arise from the other water surfaces exposed to air at the specimen boundaries. Therefore it seems more reasonable to use an empirically determined average capillary radius R_c to simulate capillary effects.

It has been found that the calculated results agree quite well with the test by Mitchell et al. (1965) if it is assumed that the average capillary radius R_c and the degree of saturation are related as follows:

$$R_c = R_{cs}\left(\frac{S - S_f}{1 - S_f}\right) \tag{4.28}$$

where R_{cs} is the capillary radius at saturation. The comparison is shown in Fig. 4.4. S_f is the lowest degree of saturation at which the water begins to flow freely. S_f may be found from permeability tests for samples with different degrees of saturation. For the clay tested by Mitchell et al., S_f was found to be zero. It was also found that the relation between the water pressure and the degree of saturation was approximated best by adopting a value of $2T_c/R_{cs}$ = 5 psi. At 20°C the value of T_c is 74 x 10^{-6} kg/cm. The value of $2T_c/R_{cs}$ = 5 psi corresponds to an effective value of R_{cs} equal to 4.23 x 10^{-4} cm.

In the case of the New Melones Dam core material, sufficient data were not available to determine S_f and $2T_c/R_{cs}$. Therefore, for purposes of approximating the compressibility of pore fluid, it was assumed that both $2T_c/R_{cs}$ and S_f were equal to zero.

FLOW BEHAVIOR OF HOMOGENIZED FLUID

For an isotropic material, Darcy's Law can be expressed as

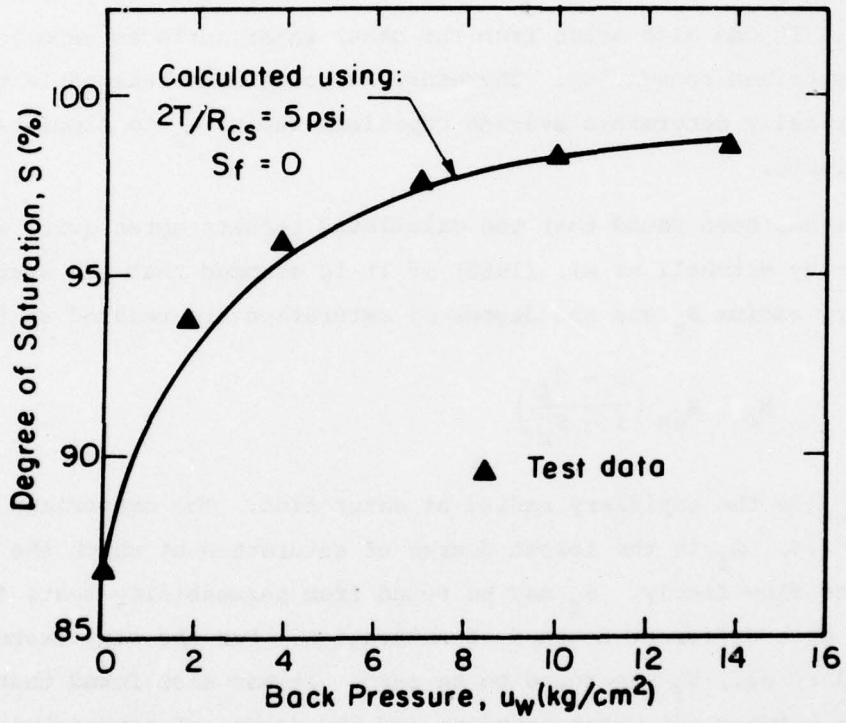

FIG. 4.4 COMPARISON BETWEEN MEASURED VARIATION OF DEGREE OF SATURATION AND THAT CALCULATED ASSUMING

$$R_c = R_{cs} \frac{S - S_f}{1 - S_f}$$

(Data from Mitchell, et al., 1965)

$$v = k \nabla \left(\frac{u_m}{\gamma_\omega} + z \right) \tag{4.29}$$

where z is the elevation and v is the superficial velocity of the pore fluid relative to the soil skeleton.

For the case of clay with occluded bubbles, u_m is equal to u_w, and Darcy's Law may be expressed as

$$v = k \nabla \left(\frac{u_w}{\gamma_\omega} + z \right) \tag{4.30}$$

For the case of clay with a low degree of saturation, it is not known whether Eq. 4.30 is valid. However, such conditions are not likely to arise for compacted clay cores in embankment dams.

CHAPTER 5

FINITE ELEMENT ANALYSIS OF CONSOLIDATION OF SATURATED CLAY

INTRODUCTION

The equations governing the three-dimensional consolidation of elastic media were developed by Biot (1941, 1955, 1956). However, until recently Biot's Theory had only been applied to problems with simple geometry and material properties. The solutions of one-dimensional consolidation problems were achieved by expansion in series, while integral transform techniques were used in the solution of two-dimensional problems by Biot (1941), Gibson et al. (1970), McNamee and Gibson (1960a, b) and Booker (1973).

The development of the finite element method provides a necessary tool for the treatment of general consolidation problems, with no restrictions on geometry, material properties or boundary conditions. Sandhu and Wilson (1969) used Gurtin's variational method (1964) to convert the field equations to a set of integral equations and to formulate a functional for finite element analyses. Later Hwang and Morgenstern (1971) presented a finite element formulation based on the method of weighted residuals. Yokoo et al. (1971a, b, c) investigated the use of discontinuous functions to improve the accuracy of the calculation of initial pore pressures.

During the course of this study, Biot's equations were reviewed, and finite element formulation of these equations were developed using Galerkin's process. An incremental finite element formulation was also developed for analysis of materials with non-linear stress-strain behavior. Several consolidation problems involving linear elastic saturated materials were analyzed and the results were compared with analytic solutions.

FIELD EQUATIONS

The equations governing the consolidation of a saturated soil with an elastic skeleton are

(a) Equilibrium equation. Only changes in stresses and body forces are considered. The geostatic body forces are considered as initial stresses

$$[\partial]\{\sigma\} = \{f_b\} \tag{5.1}$$

where $\{\sigma\}$ is the vector of stress changes,

$$(\sigma_x \quad \sigma_y \quad \sigma_z \quad \tau_{yz} \quad \tau_{xz} \quad \tau_{xy})^T , \tag{5.2}$$

$\{f_b\}$ is the vector of changes in the components of body force, (f_{bx}, f_{by}, f_{bz}), and

$$[\partial] = \begin{bmatrix} \frac{\partial}{\partial x} & 0 & 0 & 0 & \frac{\partial}{\partial z} & \frac{\partial}{\partial y} \\ 0 & \frac{\partial}{\partial y} & 0 & \frac{\partial}{\partial z} & 0 & \frac{\partial}{\partial x} \\ 0 & 0 & \frac{\partial}{\partial z} & \frac{\partial}{\partial y} & \frac{\partial}{\partial x} & 0 \end{bmatrix} \tag{5.3}$$

(b) Continuity equation. For a completely incompressible pore fluid, the amount of volumetric strain of soil equals the amount of water expelled from the soil skeleton. For a compressible pore fluid, the volume decrease of the soil is the sum of the volume expelled, plus the decrease in volume of the fluid within. The continuity equation can therefore be written as

$$-\{\nabla\}^T \{v\} + \{\nabla\}^T \frac{\partial}{\partial t} \{w\} - \frac{1}{Q} \frac{\partial u}{\partial t} = 0 \tag{5.4}$$

$$\text{where } \{\nabla\}^T = \left(\frac{\partial}{\partial x} \frac{\partial}{\partial y} \frac{\partial}{\partial z}\right), \tag{5.5}$$

$\{v\} = (v_x \quad v_y \quad v_z)^T$ is the superficial velocity of the pore

fluid relative to the soil skeleton, $\{w\} = (w_x, w_y, w_z)^T$ is the excess pore pressure, and $1/Q$ is the compressibility of pore fluid.

(c) Total stresses $\{\sigma\}$ are the sum of effective stresses $\{\sigma\}'$ and pore pressure u.

$$\{\sigma\} = \{\sigma\}' + u\{a\} \tag{5.6}$$

where $\{a\} = (1, 1, 1, 0, 0, 0)^T$ (5.7)

(d) The effective stress-strain relationship can be expressed as

$$\{\sigma\}' = [C^E]\{\varepsilon\} \tag{5.8}$$

where $\{\varepsilon\} = (\varepsilon_x \ \varepsilon_y \ \varepsilon_z \ \gamma_{yz} \ \gamma_{zx} \ \gamma_{xy})^T$ is the vector of strain components and the strains $\{\varepsilon\}$ are defined as follows:

$$\{\varepsilon\} = [\partial]^T \{w\} \tag{5.9}$$

where $\{w\}$ is displacement vector, $[\partial]^T$ is the transpose of $[\partial]$ defined by Eq.5.3. $[C^E]$ is the matrix of elastic constants relating effective stress and strain. For an isotropic elastic body, $[C^E]$ has the form

$$[C^E] = \begin{bmatrix} \lambda+2G & \lambda & \lambda & 0 & 0 & 0 \\ \lambda & \lambda+2G & \lambda & 0 & 0 & 0 \\ \lambda & \lambda & \lambda+2G & 0 & 0 & 0 \\ 0 & 0 & 0 & G & 0 & 0 \\ 0 & 0 & 0 & 0 & G & 0 \\ 0 & 0 & 0 & 0 & 0 & G \end{bmatrix} \tag{5.10}$$

where λ is one of Lame's constants, and G is the shear modulus, which may be related to the drained values of Young's modulus E' and Poisson's ratio ν' as follows

$$\lambda = \frac{E'\nu'}{(1+\nu')(1-2\nu')}$$

$$G = \frac{E'}{2(1+\nu')}$$

(f) Darcy's Law. For many soils, it can be assumed that Darcy's Law is valid. The change in superficial velocity $\{v\}$ relative to the soil skeleton can be related to the excess pore pressure by the equation:

$$\{v\} = \frac{1}{\gamma_\omega} [k]\{\nabla\} \cdot u \tag{5.11}$$

where $\{v\}$ and $\{\nabla\}$ are as previously defined, γ_ω is the unit weight of the pore fluid, and [k] is the permeability matrix.

$$[k] = \begin{bmatrix} k_{xx} & k_{xy} & k_{xz} \\ k_{yx} & k_{yy} & k_{yz} \\ k_{zx} & k_{zy} & k_{zz} \end{bmatrix} \tag{5.12}$$

Substituting Eqs. 5.6, 5.8, 5.9 into Eq. 5.1, the equilibrium equation can be written as follows:

$$[\partial][C^E][\partial]^T\{w\} + [\partial]\{a\}u = \{f_b\} \tag{5.13}$$

Substituting Eq. 5.11 into Eq. 5.4, the continuity equation becomes

$$-\frac{1}{\gamma_\omega}\{\nabla\}^T[k]\{\nabla\}u + \{\nabla\}^T\frac{\partial}{\partial t}\{w\} - \frac{1}{Q}\frac{\partial u}{\partial t} = 0 \tag{5.14}$$

To completely define the problem both elastic and flow boundary conditions must be specified. For the elastic boundary conditions, it is assumed that part of the boundary surface (S_T) is subjected to known applied tractions, while the remainder of the surface (S_D) is subjected to specified displacements. For the flow boundary condition, it is assumed that

part of the boundary surface (S_q) is subjected to a specified flow velocity, while the remainder of the surface (S_p) is subjected to known pore pressures. The boundary conditions may be written in the form

$$\left.\begin{aligned} \{w\} &= \{\hat{w}\} \quad \text{on } S_D \text{ for } t \geq 0 \\ [N]\{\sigma\} &= \{\hat{T}_f\} \quad \text{on } S_T \text{ for } t \geq 0 \\ u &= \hat{u} \quad \text{on } S_p \text{ for } t > 0 \\ \{v\}^T\{n\} &= \hat{q} \quad \text{on } S_q \text{ for } t > 0 \end{aligned}\right\} \tag{5.15}$$

where $\{n\}^T = (n_x\ n_y\ n_z)$ is the outward normal to the boundary surface, [N] is defined as follows

$$[N] = \begin{bmatrix} n_x & 0 & 0 & 0 & n_y & n_z \\ 0 & n_y & 0 & n_z & 0 & n_x \\ 0 & 0 & n_z & n_x & n_y & 0 \end{bmatrix} \tag{5.15a}$$

and (^) indicates a prescribed quantity.

To completely describe the problem, the initial conditions must also be defined. When loads are applied, the pore fluid is expelled at a finite rate. Thus the decrease in volume of a soil element must be equal to the decrease in volume of the pore water, so that

$$\varepsilon_v = \frac{1}{Q}\frac{\partial u}{\partial t} \quad \text{at } t = 0^+ \tag{5.16}$$

where $\varepsilon_v = \{a\}^T\{\varepsilon\}$ is the volumetric strain, and $\{a\}$ and $\{\varepsilon\}$ are as previously defined.

For an elastic soil skeleton, the undrained solution can also be obtained by using a bulk modulus equal to the sum of the drained bulk modulus of the soil skeleton and the bulk modulus of the pore fluid, and a shear modulus equal to the drained shear modulus of the skeleton.

FINITE ELEMENT DISCRETIZATION

In Biot's theory of consolidation, the field variables $\{w\}$ and u within an element can be discretized spatially as follows:

$$w_x = (N_w)\{w_x\}^e \tag{5.17}$$

$$w_y = (N_w)\{w_y\}^e \tag{5.18}$$

$$w_z = (N_w)\{w_z\}^e \tag{5.19}$$

$$u = (N_u)\{u\}^e \tag{5.20}$$

where $\{w_x\}^e$, $\{w_y\}^e$, $\{w_z\}^e$ and $\{u\}^e$ are the values of displacements and pore pressure at the nodes of this element, (N_w) is the shape function for displacement, and (N_u) is the shape function for pore pressure.

Eqs. 5.17, 5.18, 5.19 can be combined as:

$$\{w\} = [\phi_w]\{w\}^e \tag{5.21}$$

where

$$\{w\}^e = \begin{Bmatrix} w_x \\ w_y \\ w_x \end{Bmatrix}^e \tag{5.22}$$

and

$$[\phi_w] = \begin{bmatrix} (N_w) \\ (N_w) \\ (N_w) \end{bmatrix} \tag{5.23}$$

By using Galerkin's process, Eqs. 5.13 and 5.14 can be approximated as a set of integral equations.

$$\sum_{n=1}^{N} \int_v [\phi_w]^T [\partial][C^E][\partial]^T \{w\}\, dV + \sum_{n=1}^{N} \int_v [\phi_w]^T [\partial]\{a\}u\, dV =$$

$$\int_s [\phi_w]^T \{\hat{T}_f\}\, dS + \sum_{n=1}^{N} \int_v [\phi_w]^T \{f_b\}\, dV \tag{5.24}$$

$$-\sum_{n=1}^{N} \int_v \frac{1}{\gamma_\omega} (N_u)^T \{\nabla\}^T [k] \{\nabla\} u \; dV + \sum_{n=1}^{N} \int_v (N_u)^T \{\nabla\}^T \frac{\partial}{\partial t} \{w\} \, dV -$$

$$\sum_{n=1}^{N} \int_v \frac{1}{Q} (N_u)^T \frac{\partial u}{\partial t} \, dV = \int_s (N_u)^T \hat{q} \, dS \tag{5.25}$$

where N is the total number of elements. The integrals are evaluated over each element and summed for the entire body. Substituting Eqs. 5.17 - 20 into Eqs. 5.24 and 5.25, the field variables u and {w} for an element can be expressed in terms of the nodal values $\{u\}^e$ and $\{w\}^e$ and Eqs. 5.24, 5.25 yield a set of simultaneous equations (5.26, 5.27) with a finite number of nodal variables $\{u\}^n$ and $\{w\}^n$, where the superscript n indicates the vector of nodal values.

$$[K]\{w\}^n + [L]\{u\}^n = \{F\} + \{F_b\} \tag{5.26}$$

$$-[H]\{u\}^n + [G] \frac{d}{dt} \{w\}^n - [E] \frac{d}{dt} \{u\}^n = \{\Gamma\} \tag{5.27}$$

where

$$[K] = \sum_{n=1}^{N} \int_v [B]^T [C^E] [B] \; dV \tag{5.28}$$

$$[B] = [\partial]^T [\phi_w] \tag{5.29}$$

$$[L] = \sum_{n=1}^{N} \int_v [\phi_w]^T [\partial] \{a\} (N_u) \; dV \tag{5.30}$$

$$[G] = \sum_{n=1}^{N} \int_v (N_u)^T \{\nabla\}^T [\phi_w] \, dV = [L]^T \tag{5.31}$$

$$[H] = \sum_{n=1}^{N} \int_v \frac{1}{\gamma_\omega} (N_u)^T \{\nabla\}^T [k] \{\nabla\} (N_u) \; dV \tag{5.32}$$

$$[E] = \sum_{n=1}^{N} \int_v \frac{1}{Q} (N_u)^T (N_u) \; dV \tag{5.33}$$

$$\{F\} = \int_S [\phi_w]^T \{\hat{T}_f\}\, dS \tag{5.34}$$

$$\{F_b\} = \sum_{n=1}^{N} \int_V [\phi_w]^T \{f_b\}\, dV \tag{5.35}$$

$$\{\Gamma\} = \int_S (N_u)^T \hat{q}\, dS \tag{5.36}$$

NUMERICAL INTEGRATION

Eq. 5.27 contains terms $\frac{d}{dt}\{u\}^n$ and $\frac{d}{dt}\{w\}^n$. Therefore an integration over time is necessary. It is assumed that, to a sufficient degree of approximation:

$$\int_{t_0}^{t_1} \{u\}^n\, dt = \theta\, \Delta t \{u\}^n_{t_1} + (1-\theta)\Delta t\, \{u\}^n_{t_0} \tag{5.37}$$

and

$$\int_{t_0}^{t_1} \{w\}^n\, dt = \theta\, \Delta t \{w\}^n_{t_1} + (1-\theta)\Delta t\, \{w\}^n_{t_0} \tag{5.38}$$

where θ is a factor whose value may vary from 0 to 1. A value of $\theta = \frac{1}{2}$ is equivalent to the assumption of a linear variation in time and thus the central difference approximation (the Crank-Nicholson Method). The approximation $\theta = 0$ leads to the fully explicit method, and the approximation when $\theta = 1$ leads to the fully implicit method. When $\frac{1}{2} \leq \theta \leq 1$, it can be shown that numerical integration is unconditionally stable (Booker and Small, 1974).

Integrating Eq. 5.27 with the aid of Eqs. 5.37, 5.38 leads to

$$-\Delta t[H]\left((1-\theta)\{u\}^n_{t_0} + \theta\{u\}^n_{t_1}\right) + [G]\left(\{w\}^n_{t_1} - \{w\}^n_{t_0}\right) -$$

$$[E]\left(\{u\}^n_{t_1} - \{u\}^n_{t_0}\right) = \Delta t\left((1-\theta)\ \{\Gamma\}^n_{t_0} + \theta\ \{\Gamma\}^n_{t_1}\right) \tag{5.39}$$

or

$$[G]\{w\}^n_{t_1} - \Big([H]\theta\,\Delta t + [E]\Big)\{u\}^n_{t_1} = [G]\{w\}^n_{t_0} +$$

$$\Big([H](1-\theta)\Delta t - [E]\Big)\{u\}^n_{t_0} + \Delta t\Big((1-\theta)\{\Gamma\}^n_{t_0} + \theta\{\Gamma\}^n_{t_1}\Big) \qquad (5.40)$$

Combining Eq. 5.40 and Eq. 5.26 and observing that

$$[G] = [L]^T$$

it is found that

$$\begin{bmatrix}[K] & [L]\\ [L]^T & -[H]\theta\,\Delta t - [E]\end{bmatrix}\begin{Bmatrix}w\\ u\end{Bmatrix}_{t_1} = \begin{Bmatrix}F + F_b\\ \theta\Delta t\Gamma\end{Bmatrix}_{t_1} +$$

$$\begin{Bmatrix}0\\ (1-\theta)\Delta t\,\{\Gamma\}_{t_0} + \Big([H](1-\theta)\Delta t - [E]\Big)\{u\}_{t_0} + [L]^T\{w\}_{t_0}\end{Bmatrix} \qquad (5.41)$$

Eq. 5.41 shows that if the solution is known at t_0, then it can be found at t_1, and the solution can thus be obtained by marching forward.

Formulation for an Incremental Effective Stress-Strain Law

It is often possible to describe the behavior of an inelastic material by an incremental stress-strain law of the form

$$\{\dot{\sigma}\} = [C_t]\{\dot{\epsilon}\} \qquad (5.42)$$

where $\{\dot{\sigma}\} = \frac{\partial\sigma}{\partial t}$ and $\{\dot{\epsilon}\} = \frac{\partial\epsilon}{\partial t}$ are the stress and strain rates, respectively.

$[C_t]$ is a matrix of tangent values which are functions of the current state of stress. In this study, an elasto-plastic hardening material with an associated flow rule was used. The matrix $[C_t]$ is derived in Appendix A.

For such a material it can be shown that Eq. 5.13 must be replaced by

$$[\partial][C_t][\partial]^T\{\dot{w}\} + [\partial]\{a\}\,\dot{u} = \{f_b\} \tag{5.43}$$

Eq. 5.14 remains valid for an increment of displacement and pore pressure, however.

The derivation of the finite element formulation is quite similar to that described previously, and leads to the equations

$$\begin{bmatrix} [K^t] & [L] \\ [L]^T & -[H]\theta\,\Delta t - [E] \end{bmatrix} \begin{Bmatrix} \Delta w \\ u_{t_1} \end{Bmatrix} =$$

$$\begin{Bmatrix} \Delta F + \Delta F_b \\ \theta\Delta t\,\{\Gamma\}_{t_1} + (1-\theta)\Delta t\,\{\Gamma\}_{t_0} \end{Bmatrix} + \begin{Bmatrix} [L]\{u\}_{t_0} \\ \left([H](1-\theta)\Delta t - [E]\right)\{u\}_{t_0} \end{Bmatrix} \tag{5.44}$$

where $[K^t] = \int_V [B]^T[C_t][B]\,dV$ is the average value of the incremental tangent stiffness matrix for this increment.

Eq. 5.44 is a nonlinear equation. An iteration process is necessary in order to obtain an accurate solution.

Iteration Scheme

Embankment construction is simulated using the technique developed by Clough and Woodward (1967). For each increment of loading, the stiffness matrix is recalculated using the current material properties and the current state of stress. For each increment of loading, an initial strain iteration scheme is used to solve the approximating equation (5.44).

EXAMPLES

To demonstrate the accuracy and applicability of the finite element

method presented in this study, a number of problems were analyzed and the results were compared with analytic solutions.

(1) One-dimensional consolidation of a homogeneous layer. Fig. 5.1 shows the isochrones in a single layer with an impervious base. It can be seen that the finite element solution approximates the exact solution of this problem very closely.

(2) One-dimensional consolidation of contiguous layers. The second problem analyzed was that of two contiguous layers with the same compressibility, the upper one being four times as permeable as the lower one. The results obtained by five analyses are shown in Fig. 5.2. They are:

1. Schmidt's graphical procedure (1924)
2. Luscher's analog computer solution (1965)
3. Harr's finite difference solution (1967)
4. Christian's finite element solution (1970)
5. The finite element developed solution developed during this study.

It can be seen that there is considerable spread among these results. Because of the approximations it involved, Luscher expected his result to be too slow. Harr's explicit finite difference procedure does not consider the compressibility of the nearby material at the interface between two materials, and it therefore leads to too rapid consolidation. Christian's finite element solution, Schmidt's graphical procedure, and the finite element solution developed during this study are in good agreement, and are believed to be accurate. However, it should be emphasized that all the solutions to this problem are approximate.

(3) A strip footing on a layer of finite thickness. The finite element mesh used for the analysis is shown in Fig. 5.3. The half width of footing is a. The soil was assumed to be linear and elastic, with a shear modulus, G, and a Poisson's ratio, ν'. The finite element solution is compared with the analytic

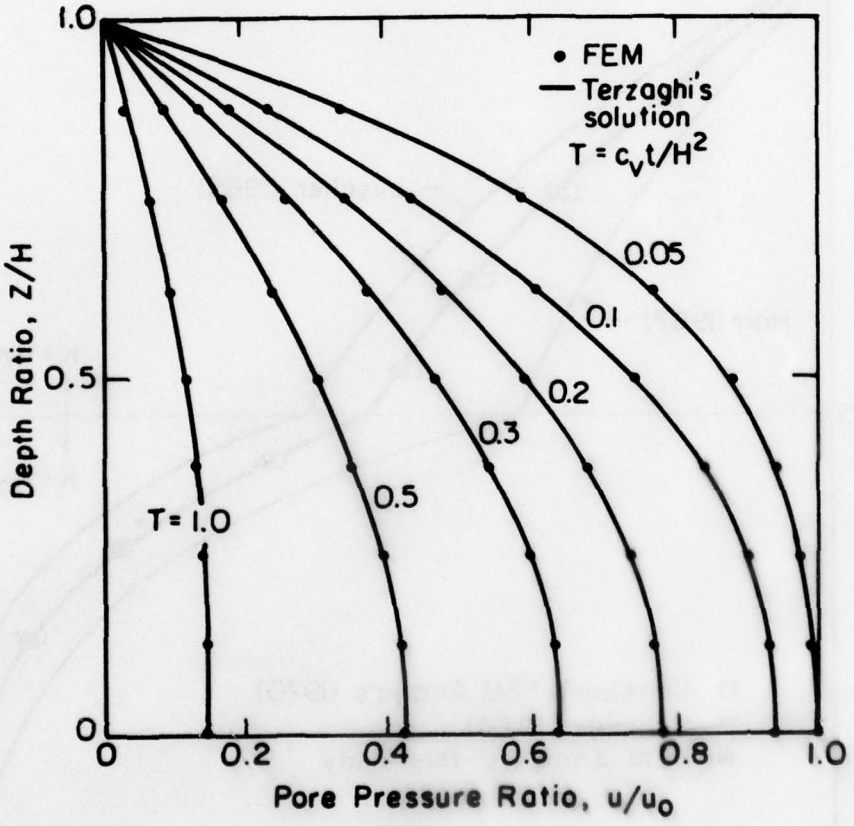

FIG. 5.1 ANALYSES OF ONE-DIMENSIONAL CONSOLIDATION

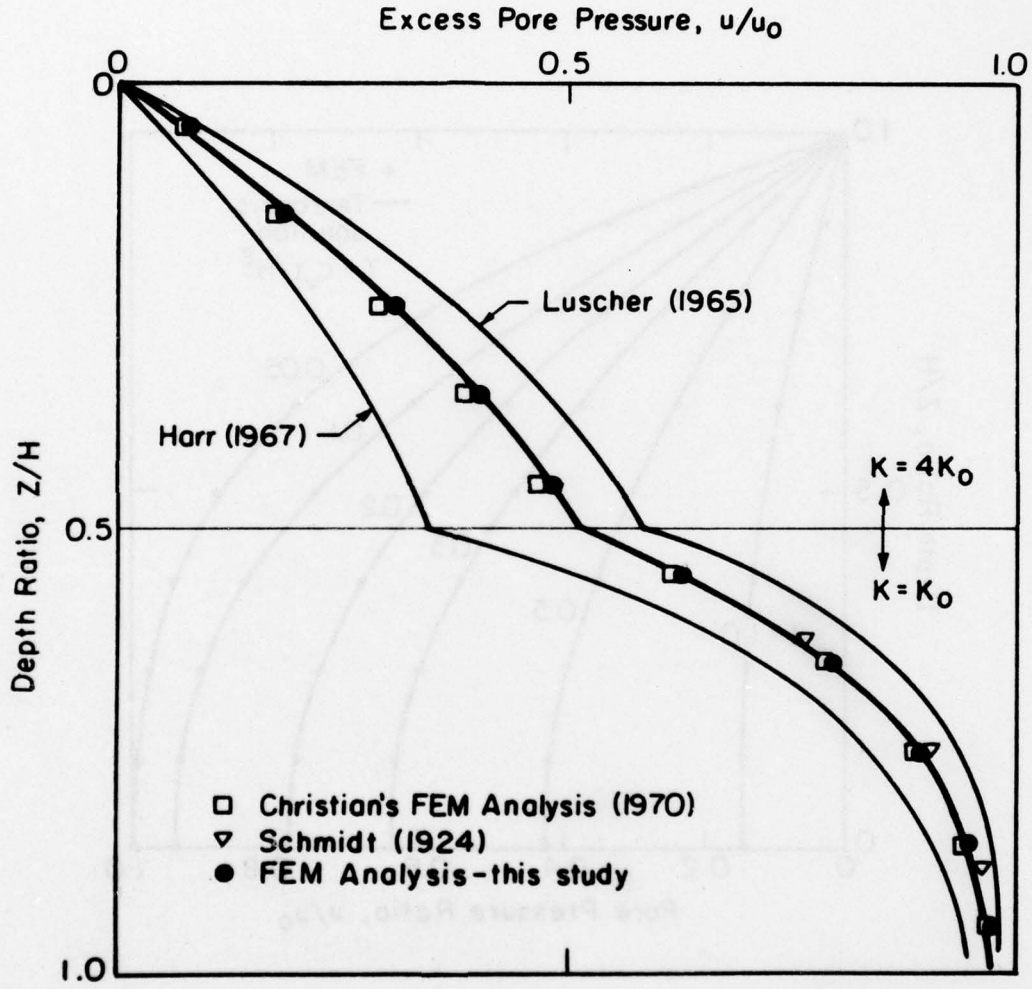

FIG. 5.2 CALCULATED PORE PRESSURE ISOCHRONES FOR CONTIGUOUS LAYERS WITH DIFFERENT PERMEABILITIES

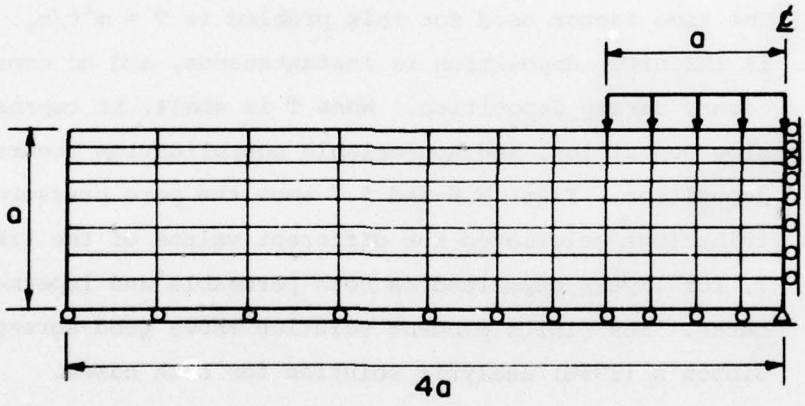

FIG. 5.3 FINITE ELEMENT MESH FOR A STRIP FOOTING ON A FINITE LAYER

solution developed by Gibson, et al. (1970). In Fig. 5.4, the displacement is plotted against time factor. It can be seen that the results of the finite element analysis are in good agreement with the closed form solution.

(4) One-dimensional incremental deposition to simulate the time-dependent deposition and simultaneous consolidation of a layer of material; elements are added to the mesh at intervals of time. As shown in Fig. 5.5 element no. 2 is placed on top of element no. 1 and element no. 3 is placed on top of element no. 2 to simulate the increase of the layer thickness with time. The rate of deposition is m (units of length/time). The time factor used for this problem is $T = m^2t/c_v$. When T is infinite, deposition is instantaneous, and no consolidation occurs during deposition. When T is small, it represents slow deposition, and appreciable consolidation occurs during deposition. Figs. 5.6 and 5.7 show the pore pressure distributions calculated for different values of the time factor, T, for layers deposited on both permeable and impermeable bases. The finite element solution shows good agreement with Gibson's (1958) analytic solution for both cases.

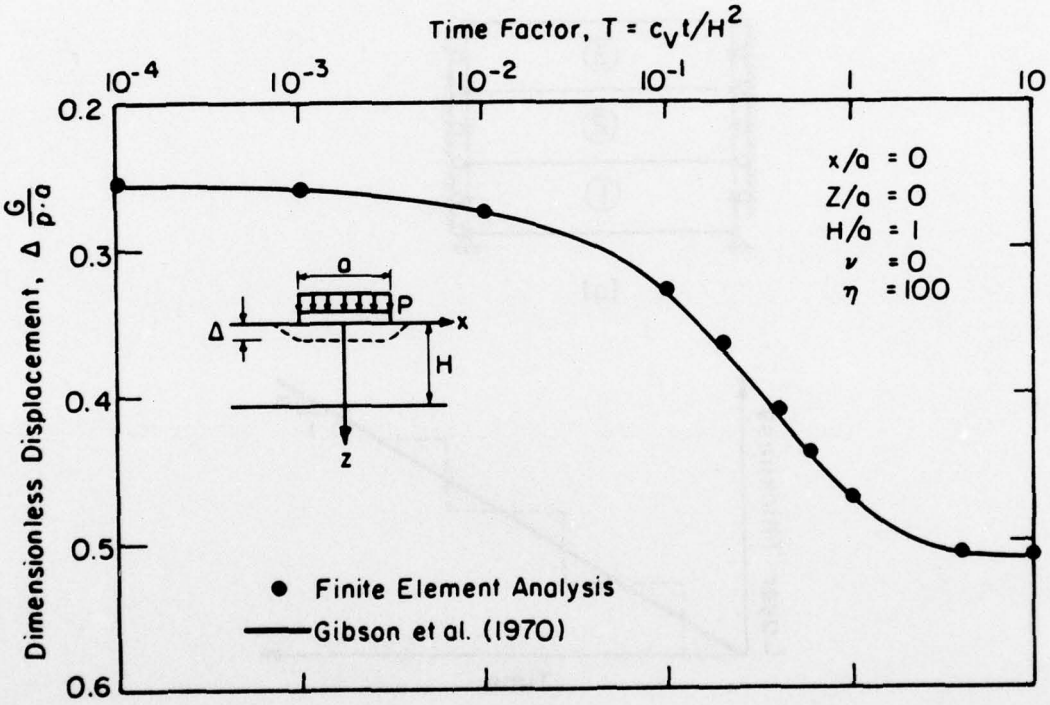

FIG. 5.4 SURFACE DISPLACEMENT OF A STRIP FOOTING ON A LAYER OF FINITE THICKNESS

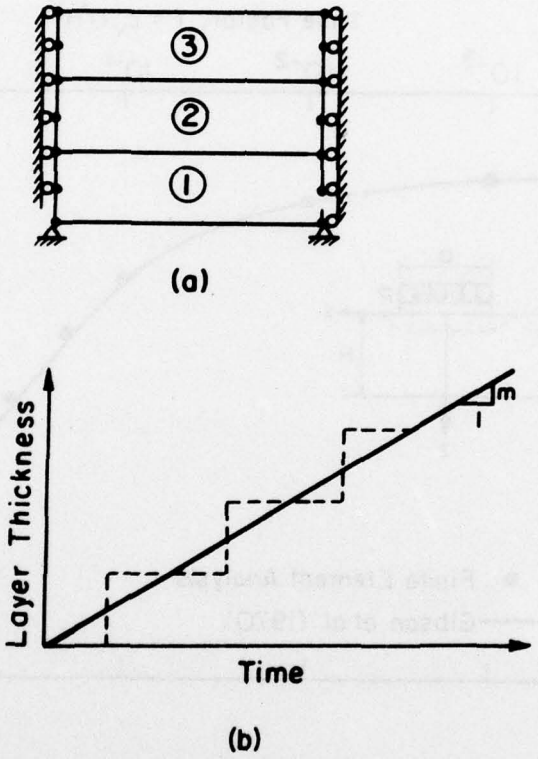

FIG. 5.5 ONE-DIMENSIONAL DEPOSITION OF A SOIL LAYER

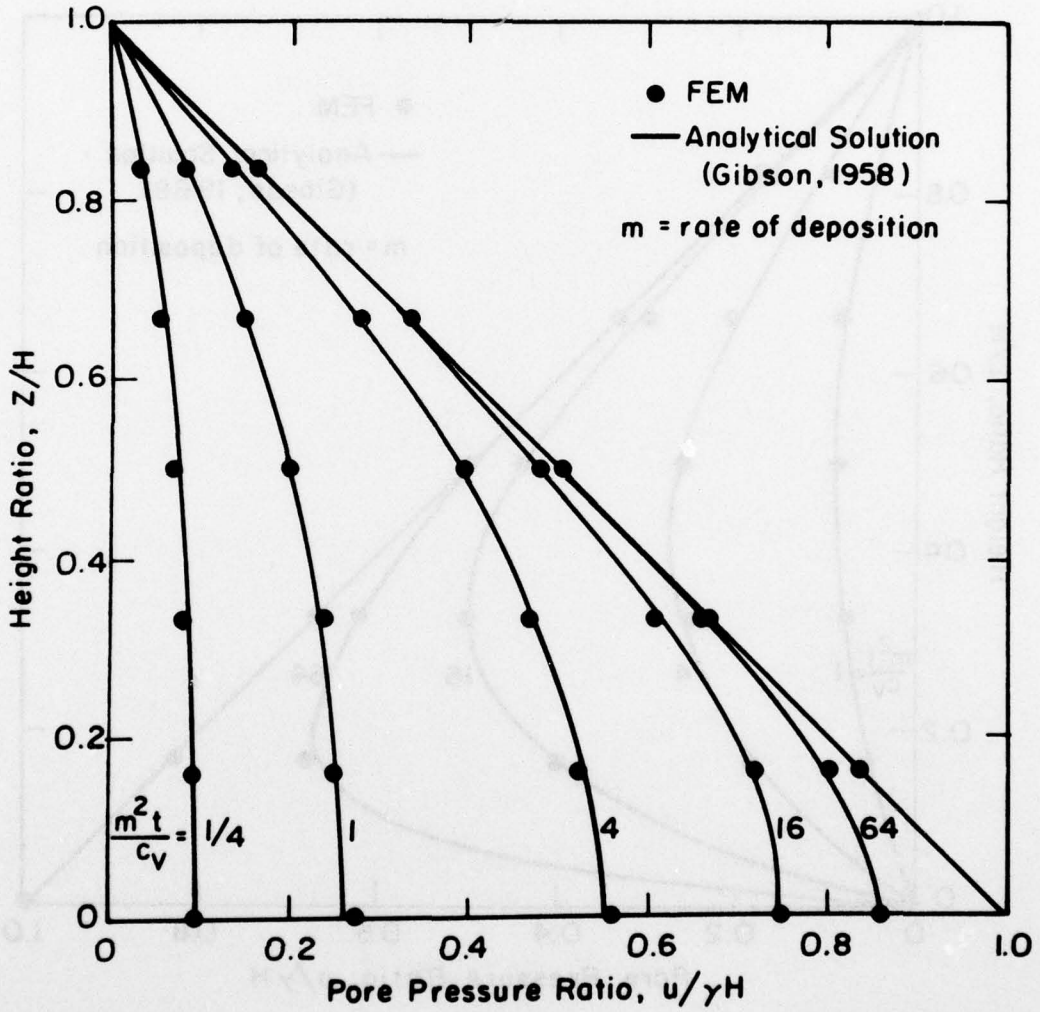

FIG. 5.6 PORE DISTRIBUTIONS FOR DEPOSITION ON AN IMPERMEABLE BASE

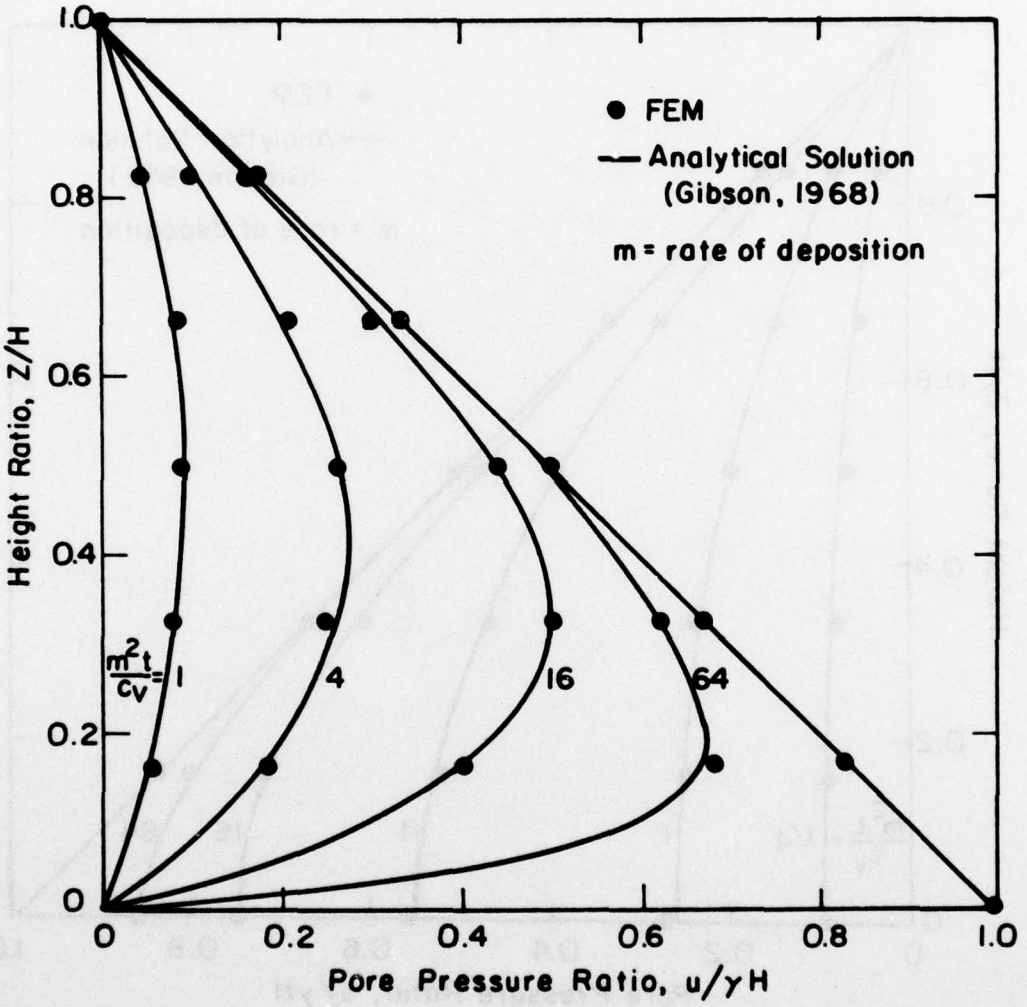

FIG. 5.7 PORE PRESSURE DISTRIBUTION FOR DEPOSITION ON A PERMEABLE BASE

CHAPTER 6

FINITE ELEMENT ANALYSIS OF CONSOLIDATION OF PARTLY SATURATED CLAY

INTRODUCTION

As discussed in Chapter 4, a three-phase unsaturated soil can be treated phenomenologically as a two-phase saturated material with a compressible pore fluid. This means that a partly saturated soil can be analyzed using the theory of consolidation developed in the pervious chapter, provided the correct values of permeability and compressibility are used. The permeability and compressibility of partly saturated clay were discussed in Chapters 3 and 4.

In this chapter, the finite element formulation is derived for an unsaturated soil with a pore fluid which contains occluded bubbles. This important practical case frequently occurs where the core of an earth dam is compacted to a water content in the neighborhood of optimum. A number of cases were analyzed to demonstrate the applicability of this theory.

FIELD EQUATION

The equations governing the consolidation of a saturated material with a homogenized compressible pore fluid are:

(1) the equilibrium equation,
(2) the effective stress equation,
(3) the continuity equation,
(4) Darcy's Law, and
(5) the effective stress-strain relationship

These equations have been derived in Chapter 5 for a material saturated with water. Partly saturated materials may be considered to be saturated with a homogenized compressible pore fluid, and the equations governing the consolidation behavior are the same as those developed in

Chapter 5, except that the pore water pressure is now replaced by the homogenized pore fluid pressure.

As discussed in Chapter 4 the homogenized pore fluid pressure is equal to the pore water pressure for clays compacted wet of optimum. Therefore, in this case, the equations governing the consolidation behavior are precisely those developed in Chapter 5.

FINITE ELEMENT FORMULATION

The derivation of finite element formulation is the same as that given in Chapter 5 and will not be repeated here.

The matrix is:

$$\begin{bmatrix} [K^t] & [L] \\ [L]^T & -[H]\theta\Delta t - [E] \end{bmatrix} \begin{Bmatrix} \Delta w \\ u_{t_1} \end{Bmatrix} =$$

$$\begin{Bmatrix} \Delta F + \Delta F_b \\ \theta\Delta t\{\Gamma\}_{t_1} + (1-\theta)\Delta t\{\Gamma\}_{t_0} \end{Bmatrix} + \begin{Bmatrix} [L]\{u\}_{t_0} \\ ([H](1-\theta)\Delta t - [E])\{u\}_{t_0} \end{Bmatrix} \tag{6.8}$$

where
$$[H] = \sum_{n=1}^{N} \int_v \frac{1}{\gamma_\omega} (N_u)^T \{\nabla\}^T [k] \{\nabla\} (N_u) \, dV \tag{6.9}$$

$$[E] = \sum_{n=1}^{N} \int_v \frac{1}{Q} (N_u)^T (N_u) \, dV \tag{6.10}$$

In Eq. 6.9 and Eq. 6.10, the permeability and compressibility are functions of both degree of saturation and void ratio. As described in Chapter 3 and Chapter 4, Eq. 3.2 and Eq. 4.26 can be employed to calculate the appropriate values of permeability and compressibility.

The computer program developed based on this theory is described in Appendix E. Isoparamatric elements with four to eight nodes (Bathe

and Wilson, 1973) are used in the computer program. The advantage of using this type of element for analyses of consolidation are:

(1) The numerical difficulties caused by sudden variations in pore pressure gradients are reduced considerably by using four point Gaussian integration. This method utilizes higher order elements capable of better approximating variations in pore pressure gradients.

(2) Any number of nodes from four to eight can be specified for each element. Triangular shaped elements can be formed by superimposing nodes. This allows considerable flexibility in mesh layout for the complicated geometry of a zoned dam.

EXAMPLES

Two examples are given in this chapter to demonstrate the application of this theory, to check the accuracy of numerical calculation, and to compare the consolidation behavior of saturated and partly saturated soil.

As a first example, the one-dimensional consolidation test for a linear elastic material with a constant permeability and a constant pore fluid compressibility was considered.

This problem gives some insight into the consolidation behavior of unsaturated soils and has the advantage that it was possible to deduce an analytic solution, so that the accuracy of the finite element approximation can be checked.

When the soil is saturated with water, the compressibility of pore fluid $(1/Q)$ is very small, and the equations reduce to the familiar one-dimensional consolidation equation. The solution is the well known Terzaghi's solution. When the soil is completely dry, the value of pore fluid compressibility is infinite, and no consolidation takes place. For partly saturated soils, the value of Q lies between zero and infinity, and some behavior intermediate between the extremes discussed above may be expected.

For the purpose of comparing the consolidation behavior of soils with different degrees of compressibility of pore fluid it is convenient to define a dimensionless parameter $\bar{\eta}$:

$$\bar{\eta} = \frac{Q}{D'} \tag{6.11}$$

where D' is the constrained modulus of the soil skeleton.

The one-dimensional consolidation behavior was calculated with a range of $\bar{\eta}$ from 1 to 20000 using the finite element method described previously. The time-settlement curves are shown in Fig. 6.1, and the pore pressure dissipation curves are shown in Fig. 6.2. It may be seen that the results obtained from the finite element analyses agree well with those obtained from a theoretical solution given in Appendix B.

The results indicate that a significant initial settlement occurs for materials with highly compressible pore fluid. As time goes on, the rate of settlement is retarded by the effect of the compressibility of the pore fluid. These characteristics are often observed in the field. The same tendency has been found in 10-in.-dia. oedometer tests on undisturbed samples of compacted clay fill from Derwent Dam (Barden, 1965).

The material properties used in the above example are an oversimplification of the properties of a real soil. For the second example, the one-dimensional consolidation behavior was studied using the properties of the soft core material from New Melones Dam.

It was assumed that the soil is an elastic-plastic material with stress-strain relationships of the type described in Chapter 2. The summary of parameters for the stiff core material of New Melones Dam is given in Table 6.1. The determination of these parameters is discussed in Appendix D.

The permeability of the pore fluid and the permeability of the soil vary with degree of saturation and void ratio, as discussed in Chapter 3 and Chapter 4.

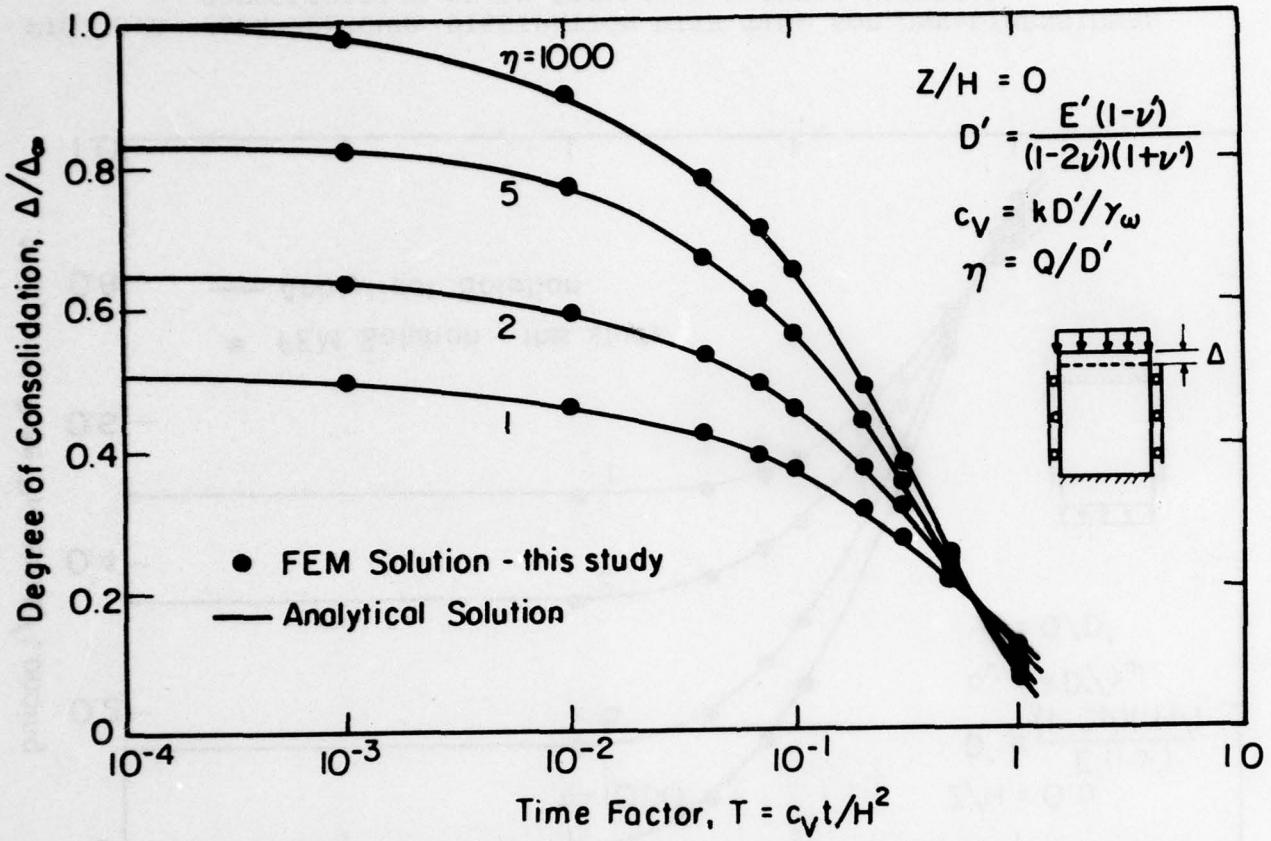

FIG. 6.1 VARIATION OF DEGREE OF CONSOLIDATION WITH TIME FOR ONE-DIMENSIONAL CONSOLIDATION OF AN IDEALIZED ELASTIC MATERIAL

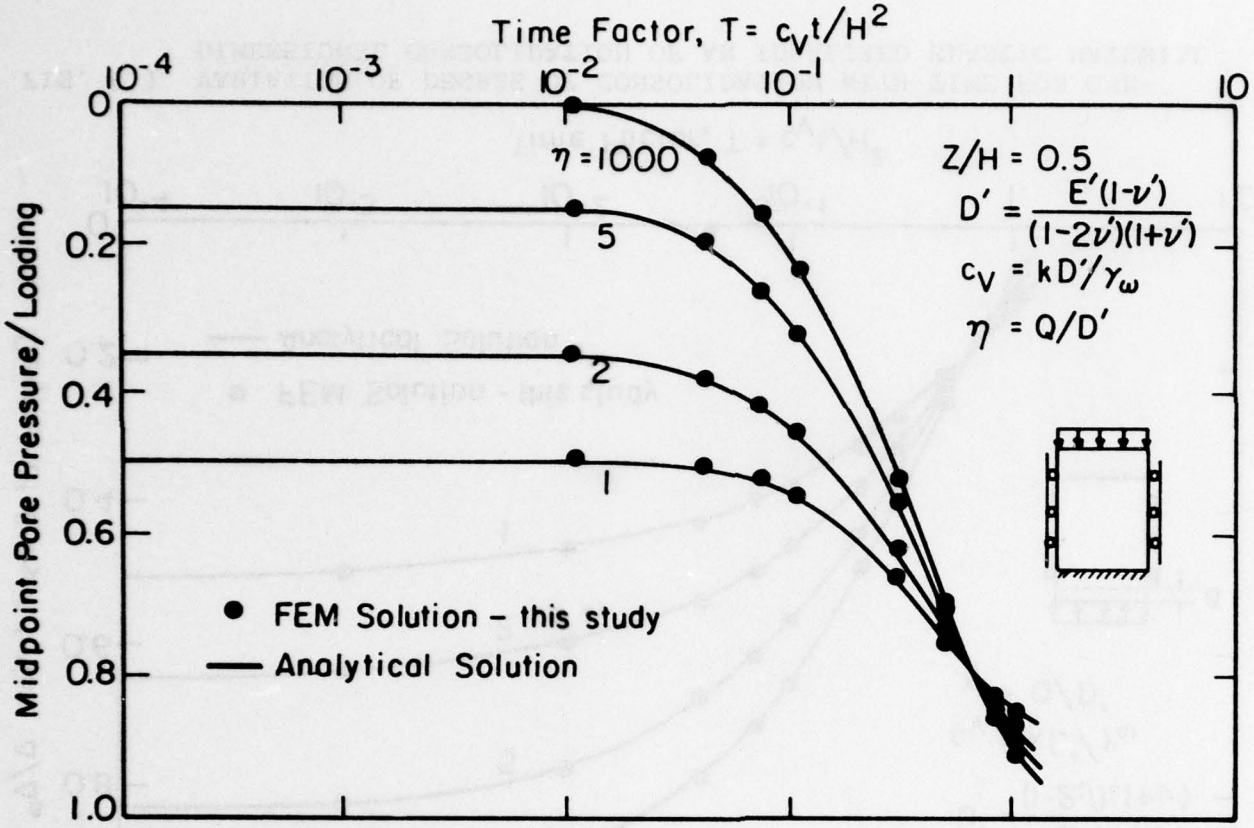

FIG. 6.2 PORE PRESSURE DISSIPATION WITH TIME FOR ONE-DIMENSIONAL CONSOLIDATION OF AN IDEALIZED ELASTIC MATERIAL

Table 6.1 Summary of Elastic Plastic Cam Clay in Parameters for Stiff Core in New Melones Dam

Relationship Between p and e

$P_{(tsf)}$	e
0	.52
10	.47
20	.42
30	.39

c	0
ϕ'	37°
B	2280 tsf
ν'	0.35
α	0.05
S_0	0.85
e_0	0.52
k_{hs}	4.0 ft/yr
k_{vs}	1.6 ft/yr
γ_d	0.075 tcf

The relationship between the degree of saturation, the void ratio and the permeability used for this example is

$$k = k_s S^3 \frac{e^3}{1 + e} \Big/ \frac{e_0^3}{1 + e_0} \tag{6.12}$$

where e_0 is the initial void ratio.

Eq. 4.26 was used in this example to calculate the compressibility of the pore fluid, and it was assumed that the surface tension term in Eq. 4.26 was negligible. Thus the compressibility of the pore fluid was expressed as

$$\frac{1}{Q} = \frac{\dfrac{1}{1 + e_0}}{\dfrac{(e_0 + HSe_0 - Se_0)}{(e + HSe - Se)^2} \; (u_{a0} + p_a)} \tag{6.13}$$

Two conditions were considered. The first was a one-dimensional consolidation test of a saturated sample, and the second was a one-dimensional consolidation test on a partly saturated sample compacted to a degree of saturation of 85%. The time-settlement curves of these two samples were calculated in three load increments. The results are shown in Fig. 6.3.

During the first load increment, from 1 tsf to 4 tsf, the compressibility of the pore fluid was high in the partly saturated sample, and the initial settlement was large compared to the subsequent consolidation settlement. During the load increment from 4 tsf to 16 tsf, the degree of saturation of the partly saturated sample increased, so that less difference between the shapes of the consolidation curves for the saturated and partly saturated samples was observed.

During the load increment from 16 tsf to 40 tsf, the unsaturated sample was sufficiently compressed to become saturated. Therefore, the time settlement curve is essentially identical to that of the saturated sample.

AD-A045 332 CALIFORNIA UNIV BERKELEY OFFICE OF RESEARCH SERVICES F/G 13/2
ANALYSIS OF CONSOLIDATION OF EARTH AND ROCKFILL DAMS. VOLUME I.--ETC(U)
SEP 77 C S CHANG, J M DUNCAN DACW39-74-C-0027
UNCLASSIFIED TE-77-3-VOL-1 WES-CR-S-77-4-VOL-1 NL

2 OF 2
AD
A045332

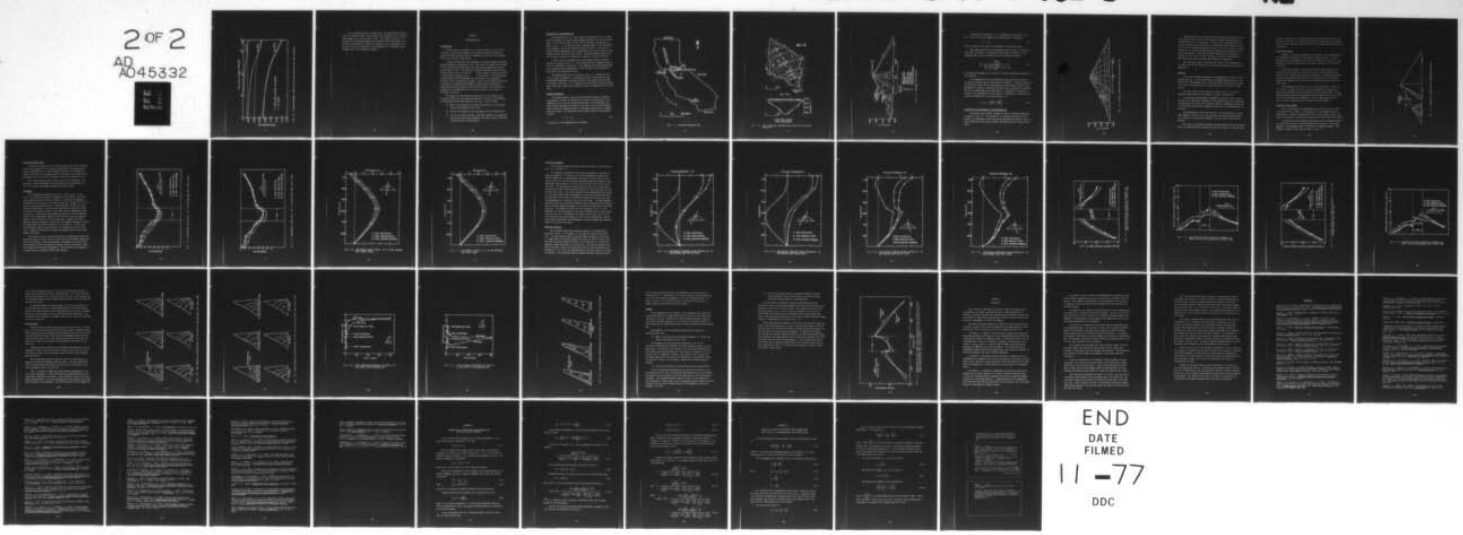

END
DATE
FILMED
11 -77
DDC

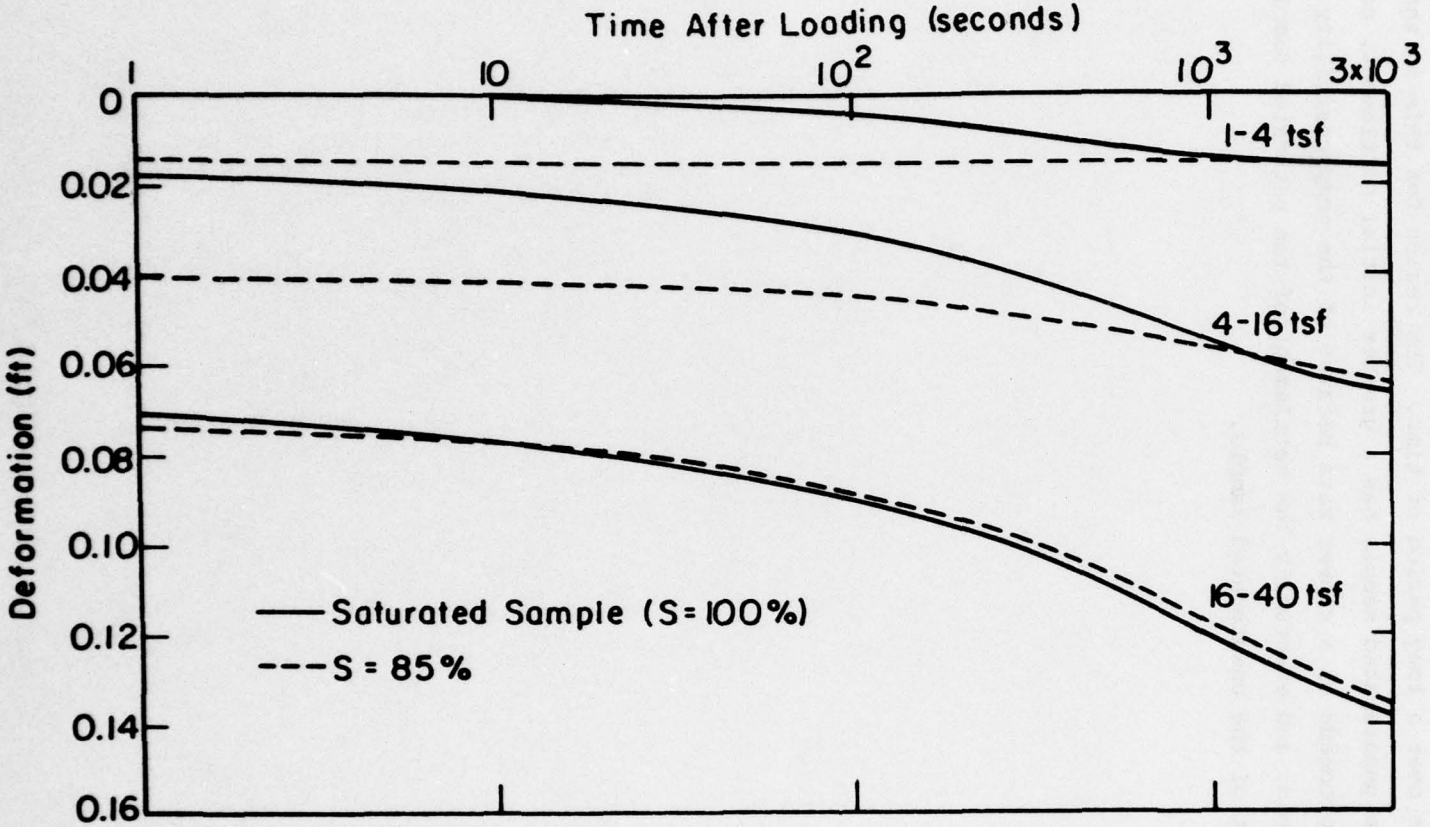

FIG. 6.3 TIME-SETTLEMENT CURVE FOR THE NEW MELONES DAM CORE MATERIAL

It is interesting that, for this soil, the calculations indicate that the saturated sample would undergo more settlement than the unsaturated sample over a long period of time. The reason for this is that although the unsaturated sample has a greater initial settlement, consolidation proceeds at a slower rate because of the compressibility of the pore fluid, and eventually the settlement of the saturated sample exceeds that of the unsaturated sample.

CHAPTER 7

NEW MELONES DAM

INTRODUCTION

The procedures for analysis of the consolidation of partly saturated soils which was described in the previous chapters was used to analyze the pore pressures and the movements in the core of New Melones Dam during and after construction.

A number of dams have been analyzed to determine probable movements during construction (Kulhawy, et al., 1969) and to calculate the stresses in the long term condition after all excess pore pressures have dissipated (Duncan, 1972). The analyses of long-term stresses have been performed assuming that the dams were built very slowly, and that there were no excess pore pressures at any stage of construction. Although Koppula and Morgenstern (1972) developed simple procedures for approximate analyses of the consolidation of dams, it has not been possible until now to analyze the stresses and movements in dams during consolidation, taking into account nonlinear stress-strain behavior and variations in permeability and compressibility of the pore fluid as the degree of saturation increases.

The analysis of New Melones Dam described in this chapter thus provides insight into some important questions relating to the behavior of zoned dams during consolidation of the core. These include:

(1) What is the nature of the expected movements in a zoned dam during consolidation of the core?

(2) How do the stresses in the dam change during consolidation?

(3) Are the long-term stresses, calculated assuming slow construction and no excess pore pressure, the same as these calculated taking account of consolidation?

DESCRIPTION OF NEW MELONES DAM

New Melones Dam is now (1976) being constructed by the U. S. Army Corps of Engineers to create a multi-purpose reservoir on the Stanislaus River. It is located about 40 miles east of Stockton, California, as shown in Fig. 7.1. The dam will have a maximum height of 625 feet above the stream-bed, and a crest length of about 1600 feet. It will be a rolled rockfill embankment with an impervious core, and will have a total volume of about 16 million cubic yards. The gross storage capacity of the reservoir created by the dam will be about 2.4 million acre-feet.

A plan view of the damsite and a longitudinal section along the dam axis are shown in Fig. 7.2. The valley walls have average slopes of 1.2 to 1 (horizontal to vertical). The abutments and stream bottom have been stripped of soil overburden, so that the dam will be founded on relatively hard metavolcanic rocks.

The maximum data section is shown in Fig. 7.3. The dam will be built in three increments - a construction dike to elevation 630 feet, an upstream cofferdam to elevation 808 feet, and finally the main dam to elevation 1135 feet. It is expected that the dam will be built within about three and a half years, and that it will be completed by the end of 1978.

ANALYSIS PROCEDURE

The elastic-plastic stress-strain theory described in Chapter 2 was employed to model the effective stress-strain relationship of the compacted clay in the core of New Melones Dam. The homogenized pore fluid concept described in Chapter 4 was used to treat the three-phase partly saturated compacted clay as a two-phase material with a compressible pore fluid. The effective stress equation used in this analysis is thus

$$\sigma' = \sigma - u_m \tag{7.1}$$

in which u_m is the homogenized pore pressure.

FIG. 7.1 PROJECT LOCATION MAP

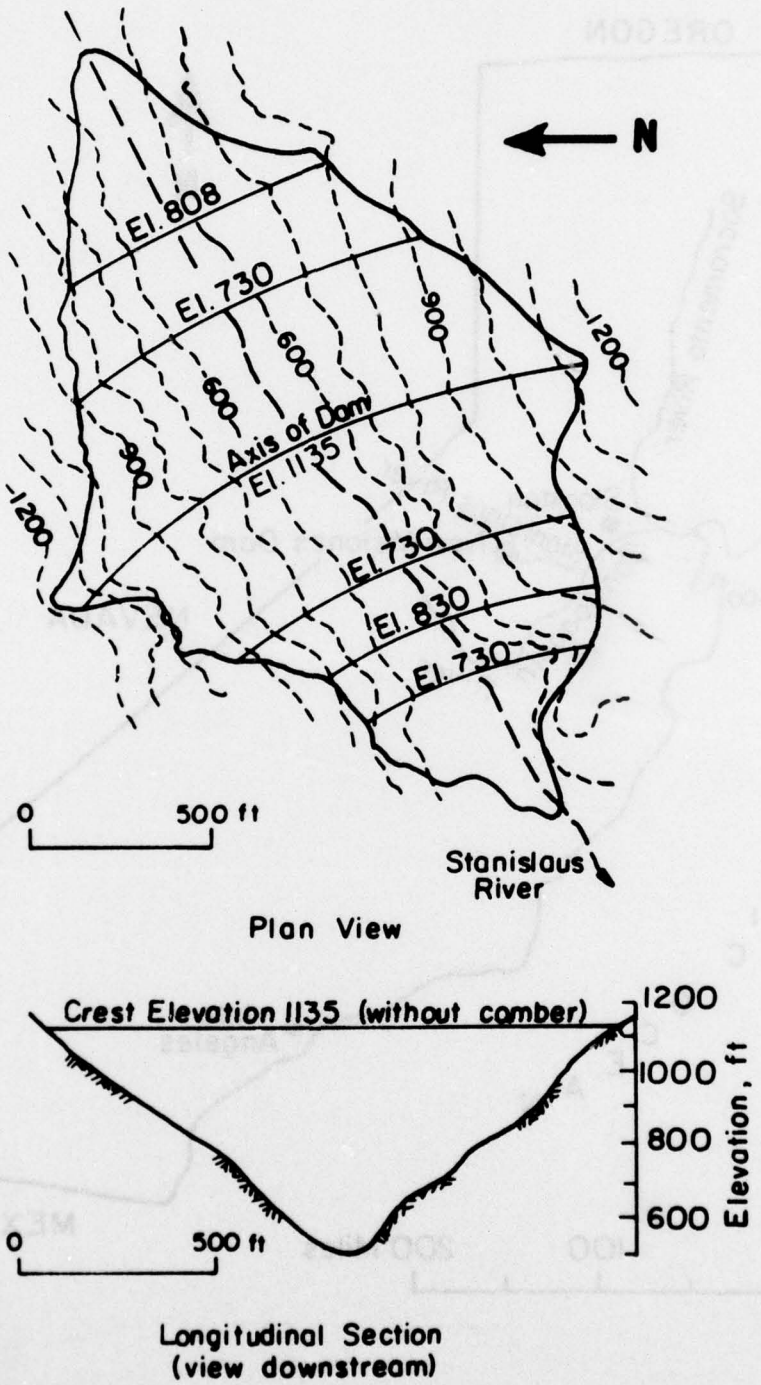

FIG. 7.2 PLAN VIEW AND LONGITUDINAL SECTION OF DAM AND ABUTMENTS

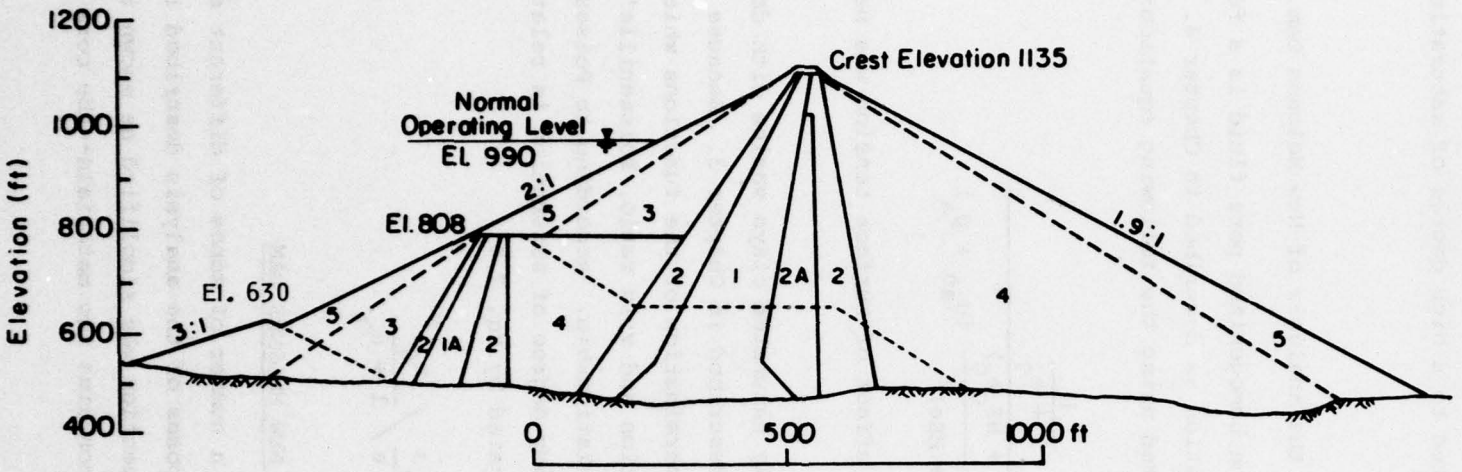

Zone No.	
1	Impervious Core
1A	Impervious Core
2	Transition
2A	Filter Transition
3	Processed Rock
4	Quarry Run Rock
5	Oversize Rock (optional)

FIG. 7.3 MAXIMUM DAM SECTION

As described in Chapter 4, it is reasonable to write Eq. 7.1 as Eq. 7.2 for a clay core compacted to a high degree of saturation

$$\sigma' = \sigma - u_w \tag{7.2}$$

and this equation was used for the analysis of New Melones Dam.

The compressibility of the homogenized pore fluid is a function of void ratio and degree of saturation as described in Chapter 4. This compressibility can be calculated using the following equation:

$$\frac{1}{Q} = \frac{\dfrac{1}{1 + e_0}}{\dfrac{(e_0 - Se_0 + HS_0e_0)}{(e - Se + HSe)^2}\,(u_{a0} + p_a)} \tag{7.3}$$

As explained in Chapter 4, the effect of surface tension was neglected in this analysis.

The permeability of partly saturated clays varies with degree of saturation and void ratio, as described in Chapter 3. Because there were not sufficient data for the determination of the functions which relate permeability, degree of saturation and void ratio, Poisseuille's equation was used to approximate this relationship. According to Poiseuille's equation, the permeability at any degree of saturation is related to the saturated permeability as indicated by Eq. 7.4.

$$k = k_s\, S^3\, \frac{(e)^3}{1 + e} \Big/ \frac{(e_0)^3}{1 + e_0} \tag{7.4}$$

PROPERTIES OF THE MATERIALS IN NEW MELONES DAM

New Melones Dam contains a number of zones of different materials, as shown in Fig. 7.3. For purposes of the analysis described in this chapter, the embankment cross-section was simplified as shown in Fig. 7.4. This simplified cross-section contains two materials--the core and the shell.

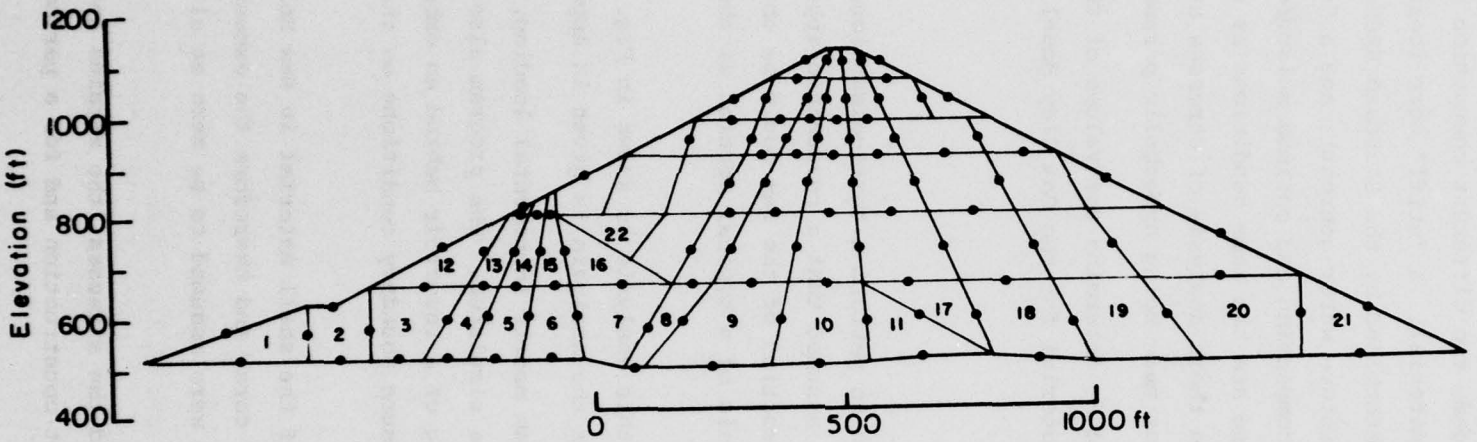

FIG. 7.4 FINITE ELEMENT MESH FOR NEW MELONES DAM

Because variations in water content and dry density may occur during construction of the dam, two different compaction conditions were considered for the core material: a "stiff" core (corresponding to 95% relative compaction as determined by the Standard AASHO compaction test, and 1% dry of optimum moisture water content), and a "soft" core (corresponding to 90% relative compaction and optimum moisture content at the time of placement). These are the same conditions as considered by Quigley, et al. (1976) in their analysis of stresses and movements in New Melones Dam, which was made using hyperbolic parameters.

The procedures used to determine the values of the parameters of the shell and the core material for the Cam Clay Model are described in Appendix D.

ANALYSIS

It was not feasible to perform a three-dimensional analysis of the New Melones Dam. It was assumed that a reasonable approximation to the behavior at the maximum section of the dam could be obtained by performing a plane strain analysis of a typical section at the center of the valley.

The mesh used for this analysis is shown in Fig. 7.4, and the computer program used for the analysis is given in Appendix E.

The computer program models incremental loading, so that the construction of a dam can be simulated. The program also has the capability of simulating the filling of a reservoir behind an embankment by specifying the proper pore pressure boundary conditions on the upstream face of the core.

The permeability of the shell material in New Melones Dam is very high compared to that of core, and therefore the excess pore pressures in the shells of the dam were assumed to be zero at all stages of the analysis.

The analysis traced the stresses, the strains and the pore pressures within the dam throughout construction and for a period of 80 years after

the end of construction. Three principal stages were considered in the analysis. They are: the construction stage, the reservoir filling stage, and the stage following reservoir filling, when long-term seepage will be established.

Construction Stage

Elements 1 through 16 represent the cofferdam. The construction of the cofferdam was simulated in two layers in this analysis. The construction of the remainder of the dam, to an elevation of 1135 ft., was simulated by adding an additional six layers, consisting of elements 17 through 62.

Dissipation of excess pore pressure during construction was not considered in the analysis, although the finite element developed in Chapter 6 can be used to analyze this phenomenon. Dissipation of excess pore pressures during construction was not considered in the analysis because the expected length of time for construction of the dam is only three years.

The permeability of the core is in the range from 10^{-7} cm/sec to 10^{-8} cm/sec. Because the core is large, the amount of dissipation of excess pore pressure during construction will be insignificant. The undrained condition during construction was simulated by using a zero time step in this portion of the analysis. Using a time step of three or even six years would have given virtually identical results.

Reservoir Filling Stage

After the dam has been constructed, the reservoir will be filled to elevation 990 ft (MSL). In the analysis, it was assumed that the water will be raised to elevation 990 ft in a short period of time, and that no dissipation of excess pore pressure will occur during this period.

The reservoir water pressure was applied on the interface between the core and the shell, at the upstream side of the dam. Forces were applied to the submerged part of the shell to simulate buoyancy. The changes in load at this stage are shown in Fig. 7.5.

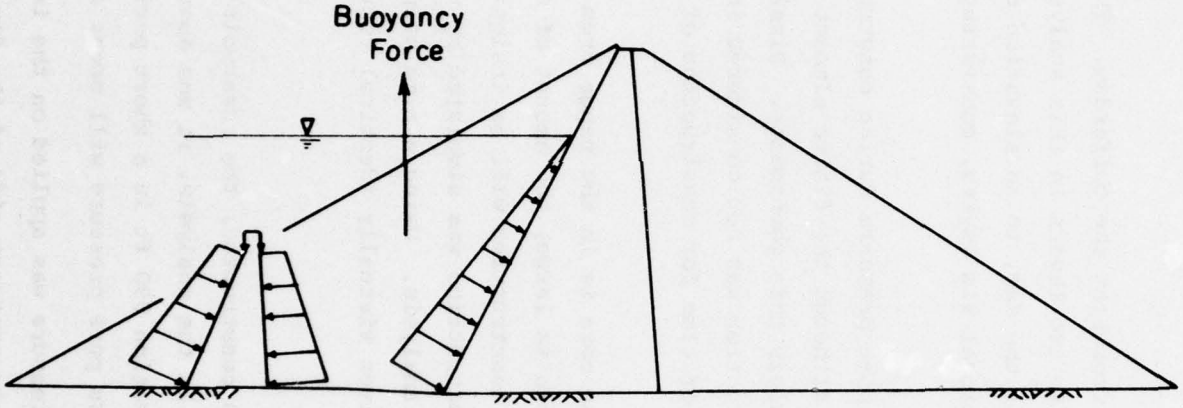

FIG. 7.5 CHANGES IN LOAD DUE TO RESERVOIR FILLING

Long Term Seepage Stage

Possible fluctuations in the reservoir water level were neglected, and it was assumed that the reservoir would remain at elevation 990 ft. During establishment of a steady seepage condition, the deformations within the dam will be influenced by the dissipation of the excess pore pressures in the core, and the seepage of the water through the core.

Five time steps were used in this portion of the analysis. The stresses, strains, movements, and pore pressures were calculated at 5, 15, 30, 50 and 80 years after raising of the water level.

Settlement

The settlement at elevation 803 ft are shown in Fig. 7.6 and Fig. 7.7 for the two conditions considered in the analysis--the stiff core condition and the soft core condition. Initially, the maximum settlement, which occurs at the center of the core, is about 11.5 ft for both the stiff and the soft core. During reservoir filling, the core deflects upward about 1 ft for both the stiff and the soft core condition due to the buoyancy forces in the shell and the submerged portion of the core. During long term seepage, the analysis indicates approximately 1 ft of additional rebound in the stiff core case, and approximately 1 inch of rebound in the soft core case. Because the initial effective stress is greater in stiff core, the rebound capacity is higher. The same effect can also be noted in Fig. 7.8 and Fig. 7.9 which show the settlement along a nearly vertical line through the center of the core. It may be noted that the largest settlement occurs near the mid-height of the dam.

The fact that these analyses indicate some rebound during reservoir filling and after is due to the fact that creep and secondary compression were not considered. Some time-dependent settlements will result from these effects, and the resulting settlements would be expected to affect the rebound resulting from submergence. The net effect will probably be a small amount of settlement rather than rebound.

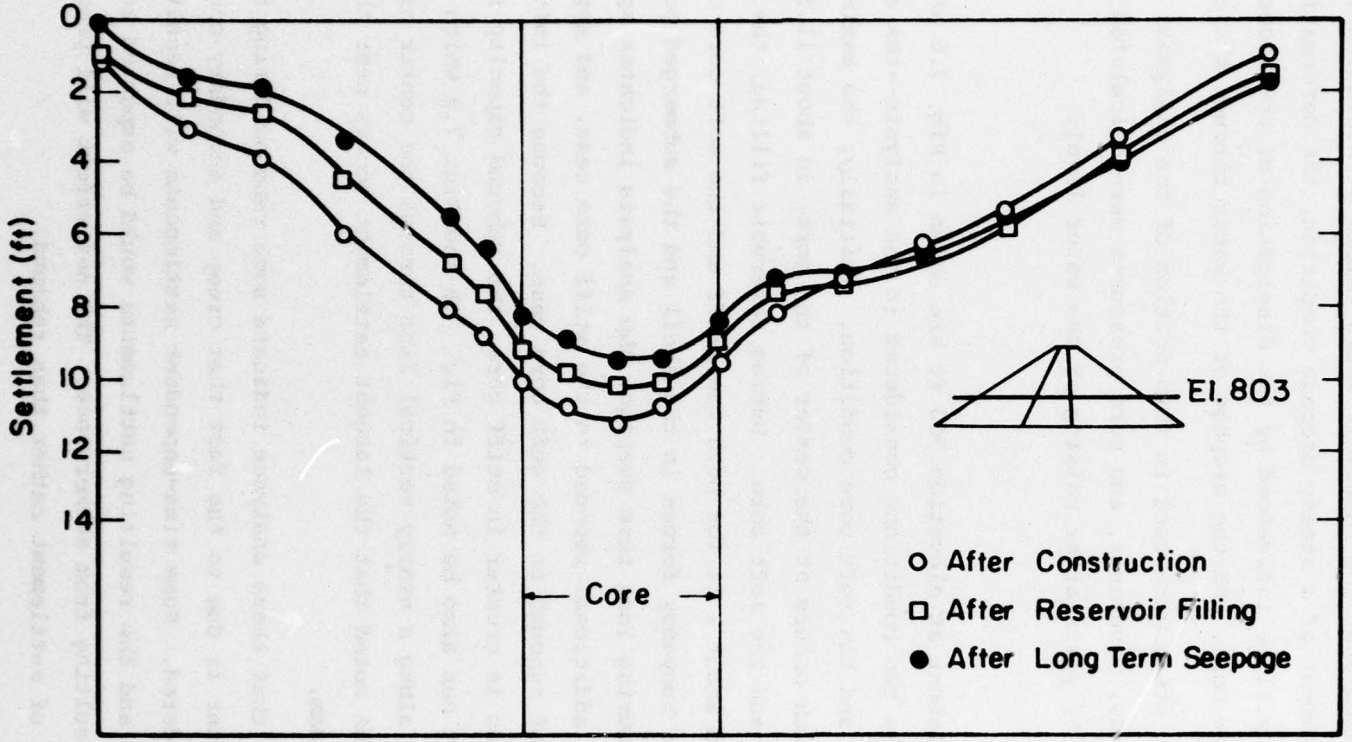

FIG. 7.6 SETTLEMENT ALONG ELEV. 803 IN NEW MELONES DAM (STIFF CORE)

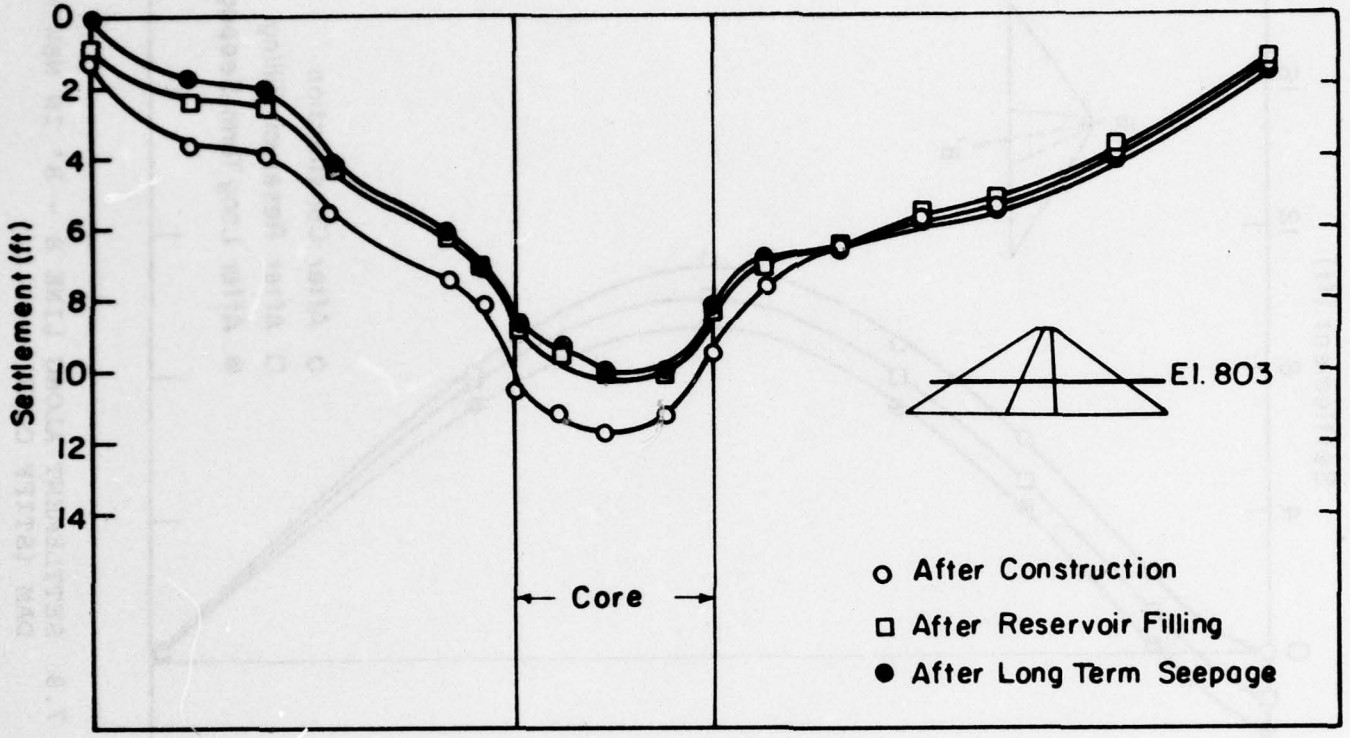

FIG. 7.7 SETTLEMENT ALONG ELEV. 803 IN NEW MELONES DAM (SOFT CORE)

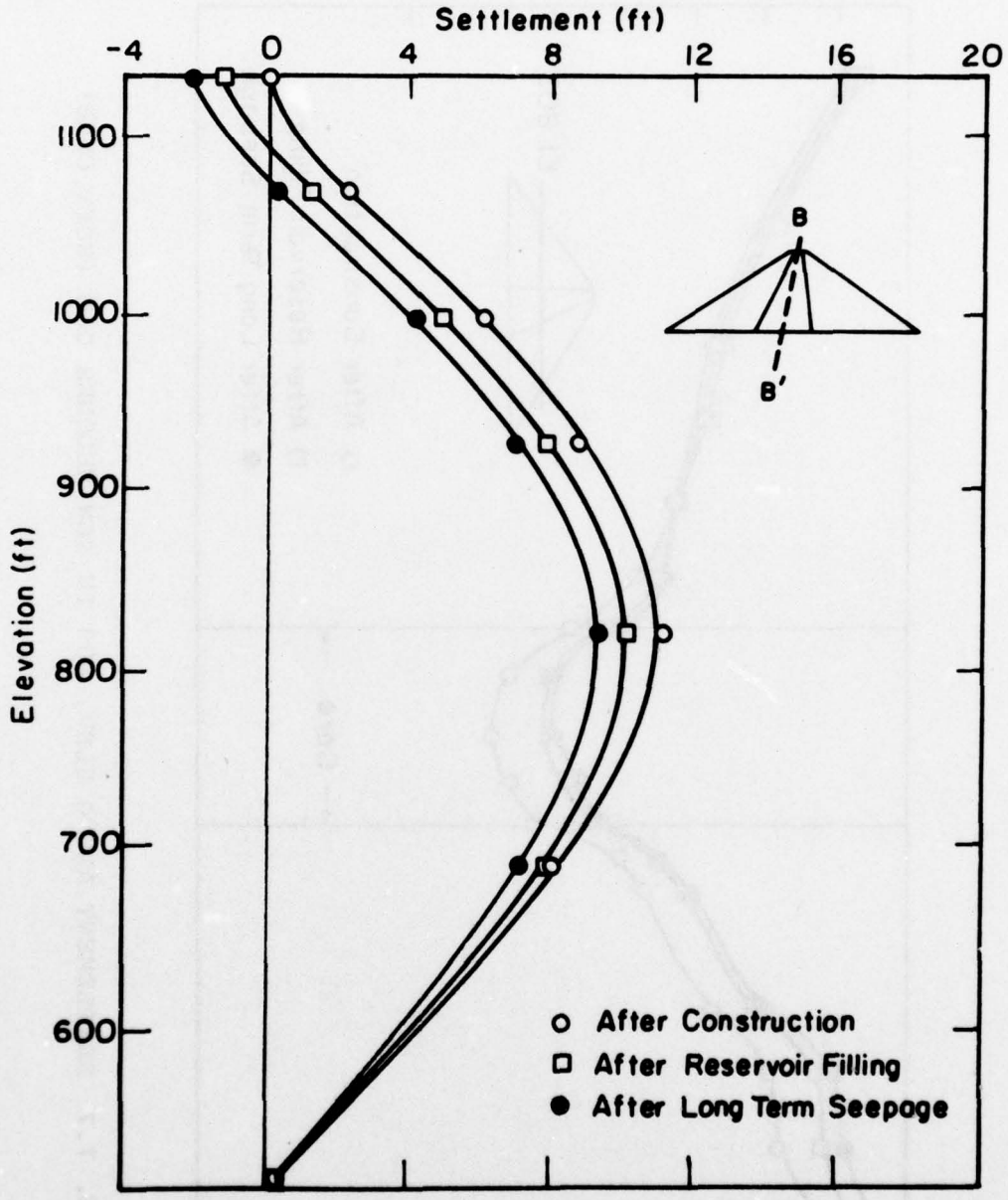

FIG. 7.8 SETTLEMENT ALONG LINE B - B' IN NEW MELONES DAM (STIFF CORE)

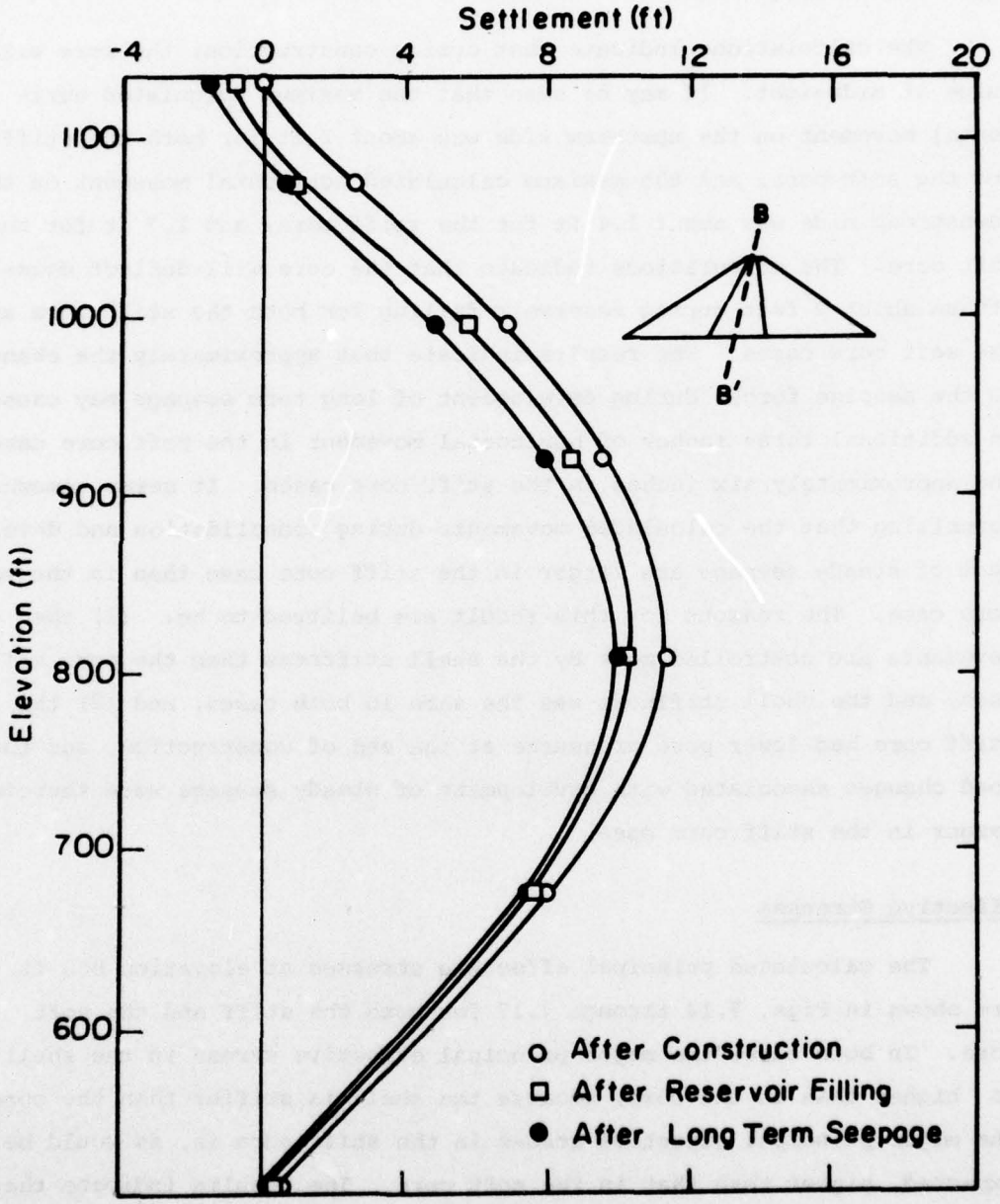

FIG. 7.9 SETTLEMENT ALONG B - B' IN NEW MELONES DAM (SOFT CORE)

Horizontal Movement

The horizontal movements along sections AA' and CC' are plotted in Figs. 7.10 through 7.13.

The calculations indicate that during construction, the core will bulge at midheight. It may be seen that the maximum calculated horizontal movement on the upstream side was about 2 ft for both the stiff and the soft core, and the maximum calculated horizontal movement on the downstream side was about 1.4 ft for the stiff core, and 1.7 ft for the soft core. The calculations indicate that the core will deflect downstream about 2 feet during reservoir filling for both the stiff core and the soft core cases. The results indicate that approximately the changes in the seepage forces during development of long term seepage may cause an additional three inches of horizontal movement in the soft core case, and approximately six inches in the stiff core cases. It seems somewhat surprising that the calculated movements during consolidation and development of steady seepage are larger in the stiff core case than in the soft core case. The reasons for this result are believed to be: (1) the movements are controlled more by the shell stiffness than the core stiffness, and the shell stiffness was the same in both cases, and (2) the stiff core had lower pore pressures at the end of construction, and the load changes associated with development of steady seepage were therefore larger in the stiff core case.

Effective Stresses

The calculated principal effective stresses at elevation 860 ft are shown in Figs. 7.14 through 7.17 for both the stiff and the soft core. In both cases the major principal effective stress in the shell is higher than in the core, because the shell is stiffer than the core. The major principal effective stress in the stiff core is, as would be expected, higher than that in the soft core. The results indicate that during reservoir filling, both the major and the minor stresses will be reduced by 1.5 - 2 tsf in the upstream side of the shell due to the effect of buoyancy. The calculated values of major principal effective stress

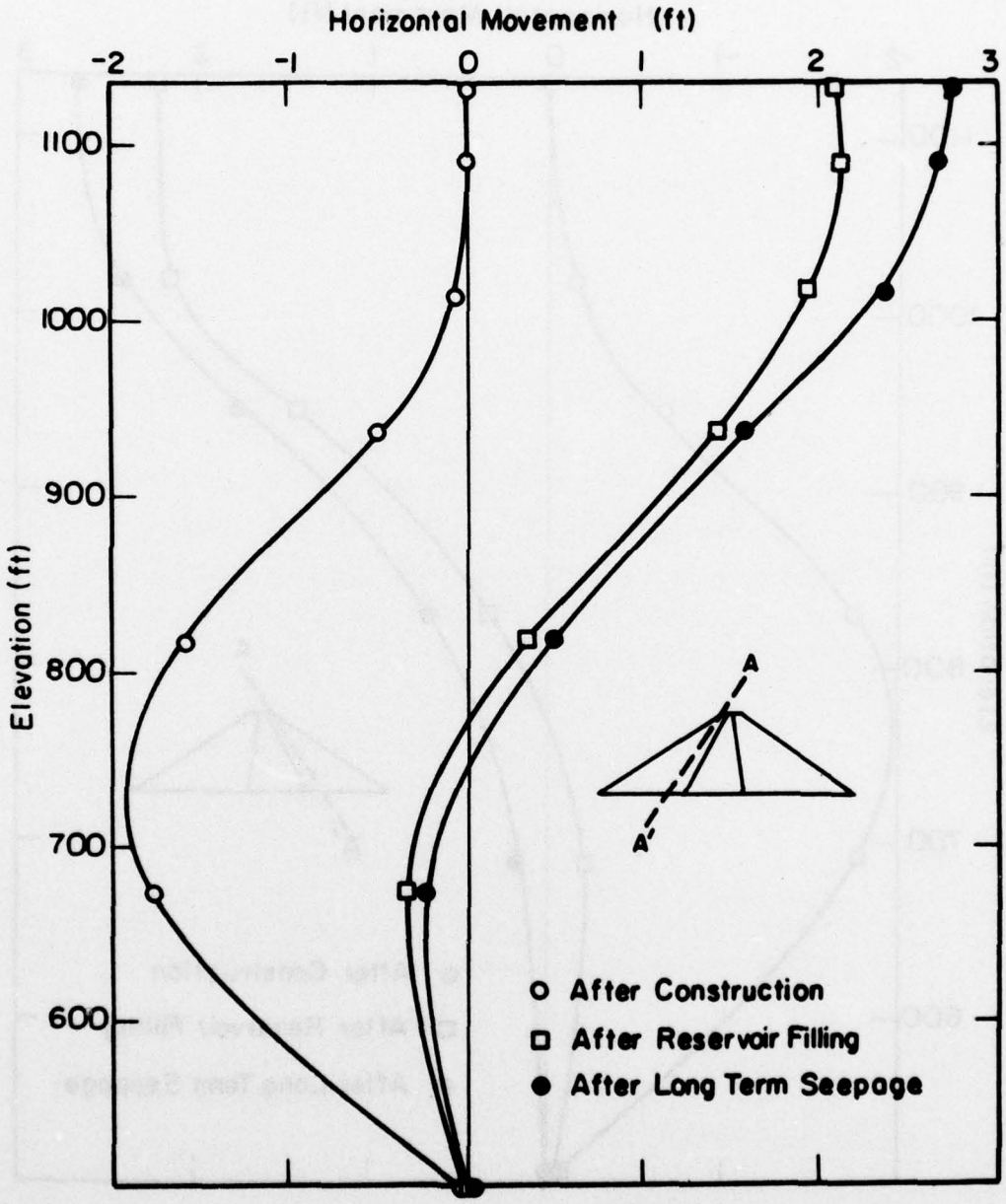

FIG. 7.10 HORIZONTAL MOVEMENT ALONG SECTION AA' IN NEW MELONES DAM (STIFF CORE)

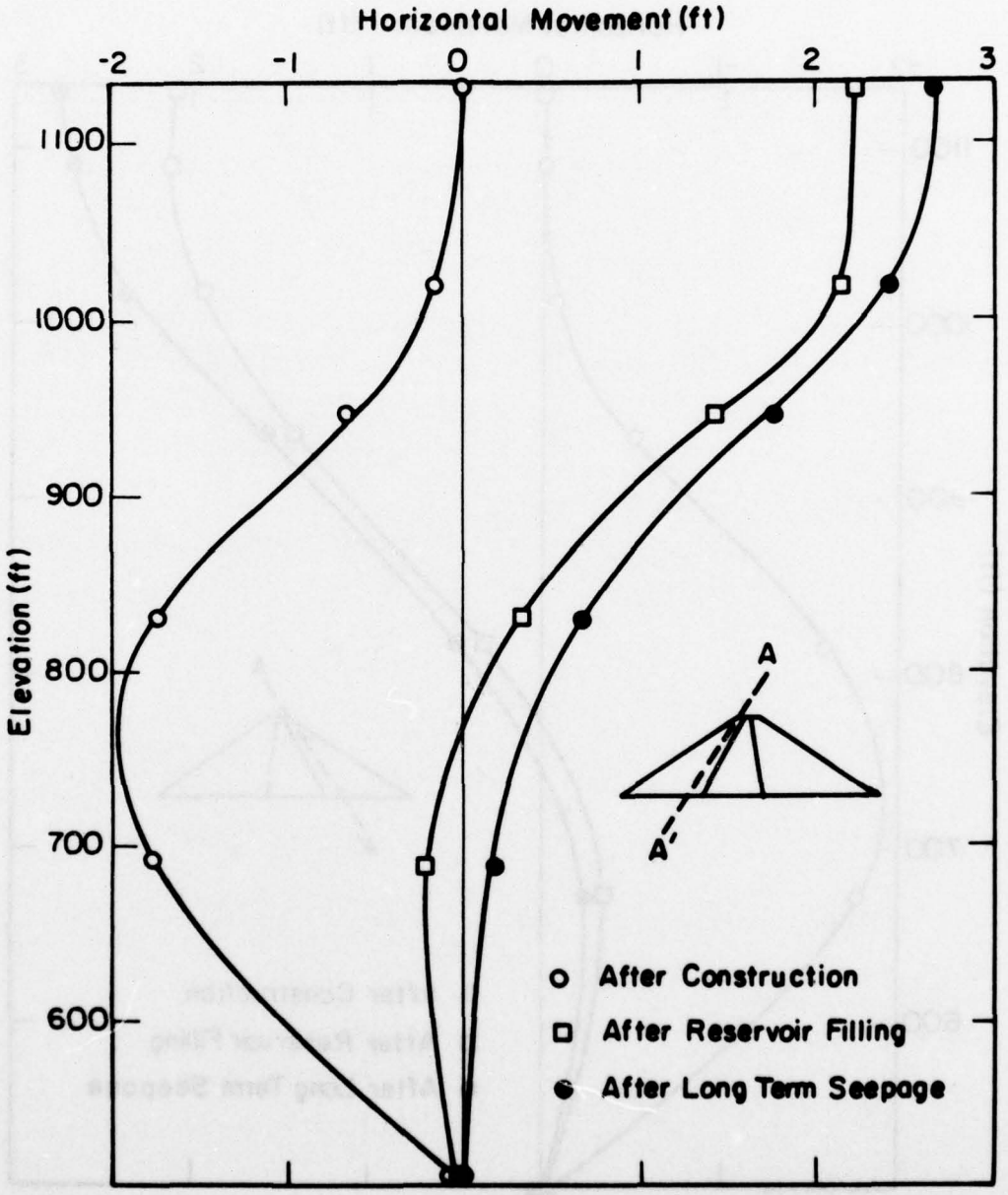

FIG. 7.11 HORIZONTAL MOVEMENT ALONG SECTION AA' IN NEW MELONES DAM (SOFT CORE)

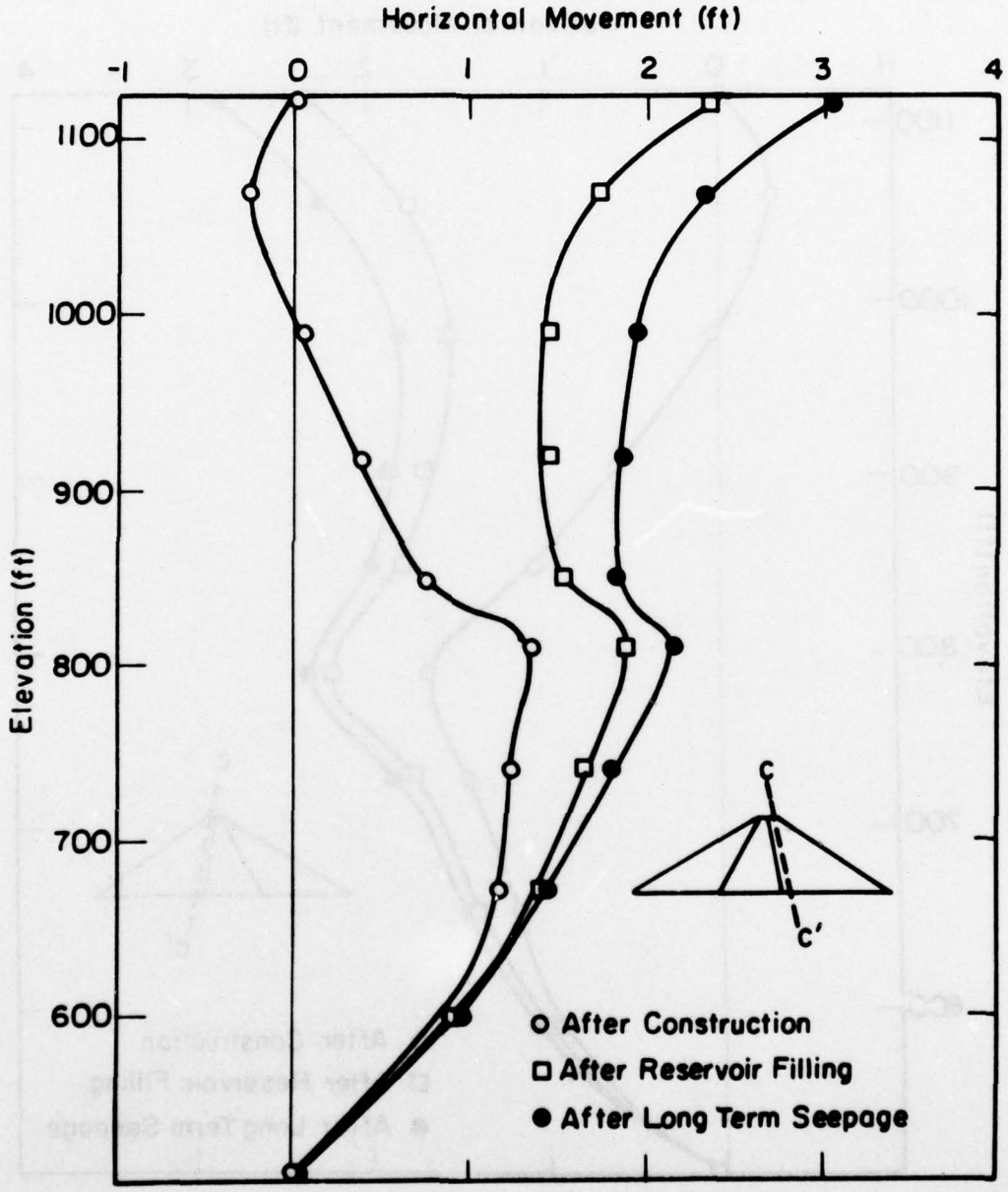

FIG. 7.12 HORIZONTAL MOVEMENT ALONG SECTION CC' IN NEW MELONES DAM (STIFF CORE)

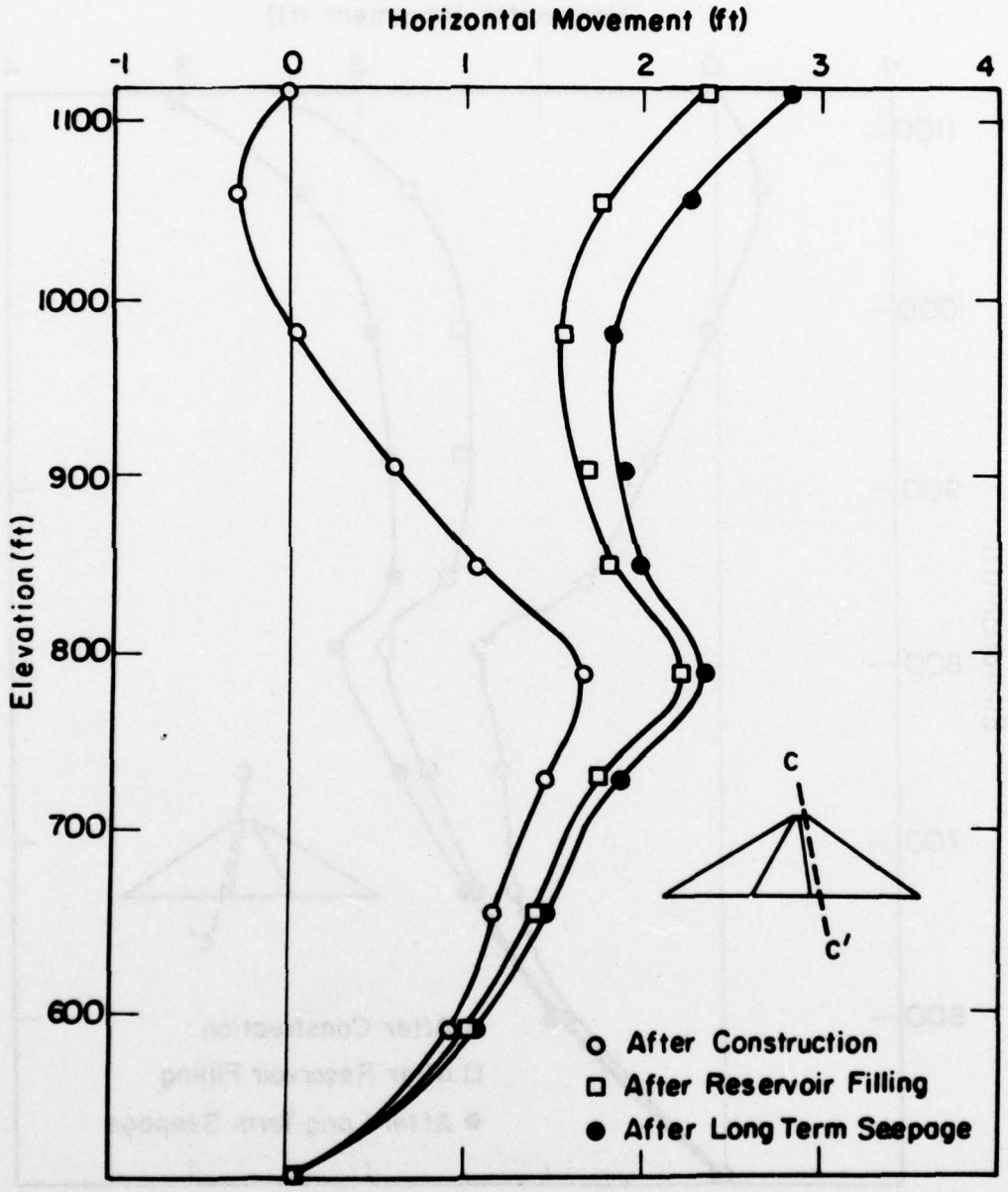

FIG. 7.13 HORIZONTAL MOVEMENTS ALONG SECTION CC' IN NEW MELONES DAM (SOFT CORE)

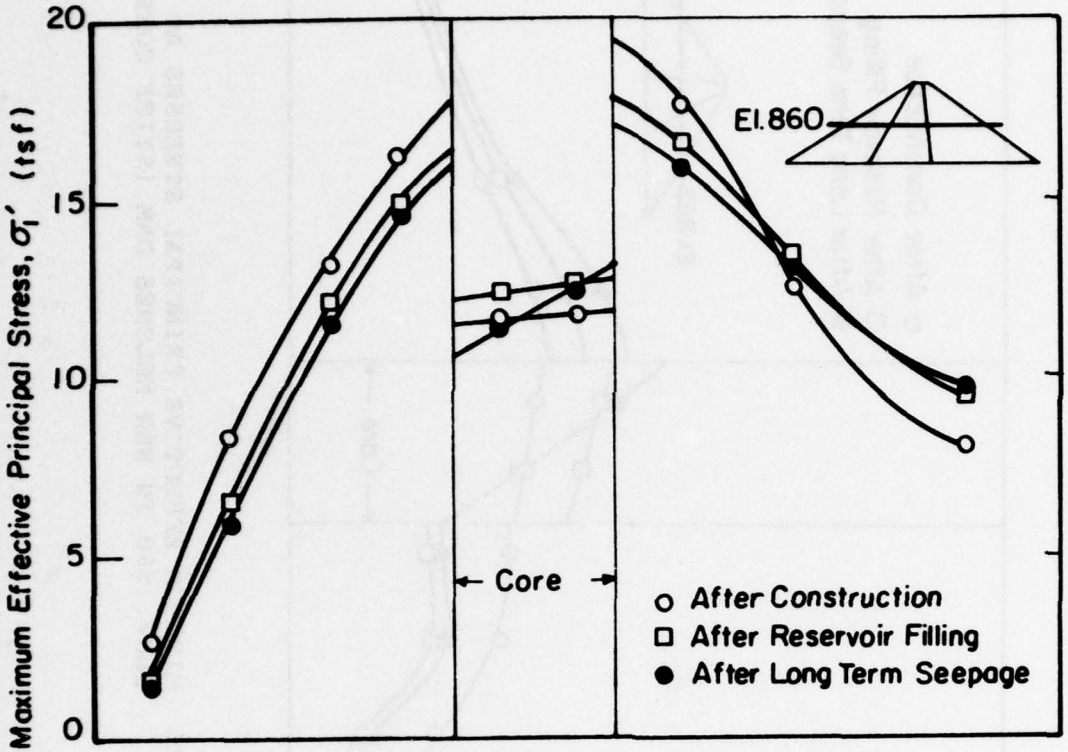

FIG. 7.14 MAXIMUM EFFECTIVE PRINCIPAL STRESSES AT ELEV. 860 IN NEW MELONES DAM (STIFF CORE)

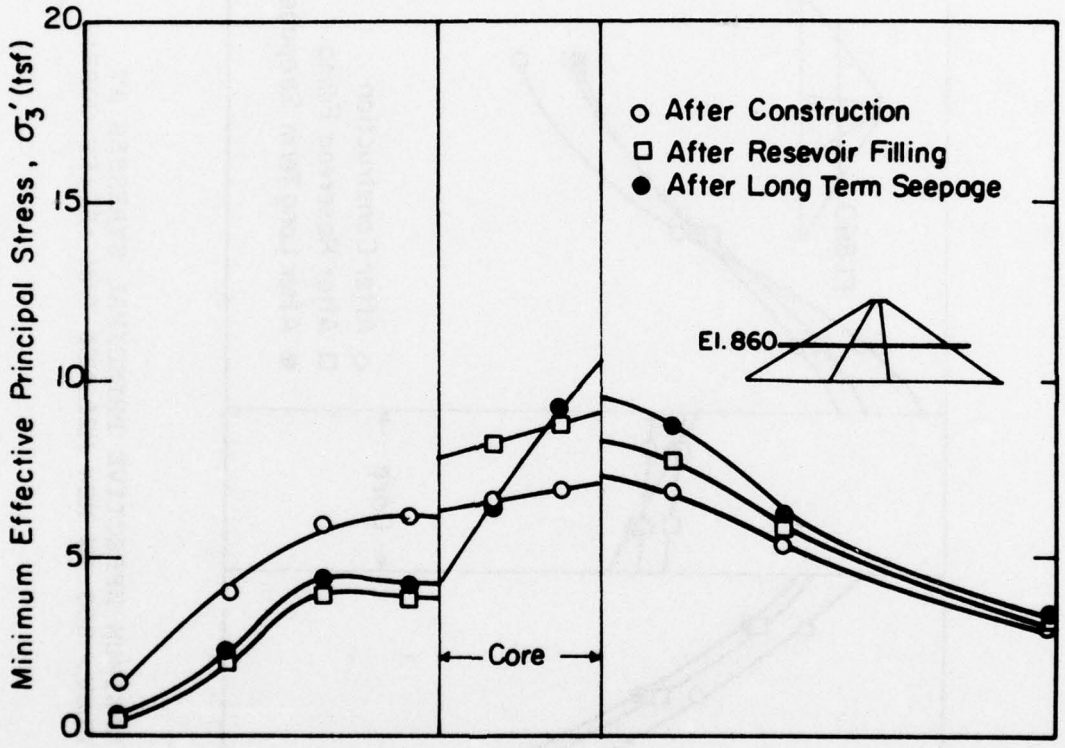

FIG. 7.15 MINIMUM EFFECTIVE PRINCIPAL STRESSES AT ELEV. 860 IN NEW MELONES DAM (STIFF CORE)

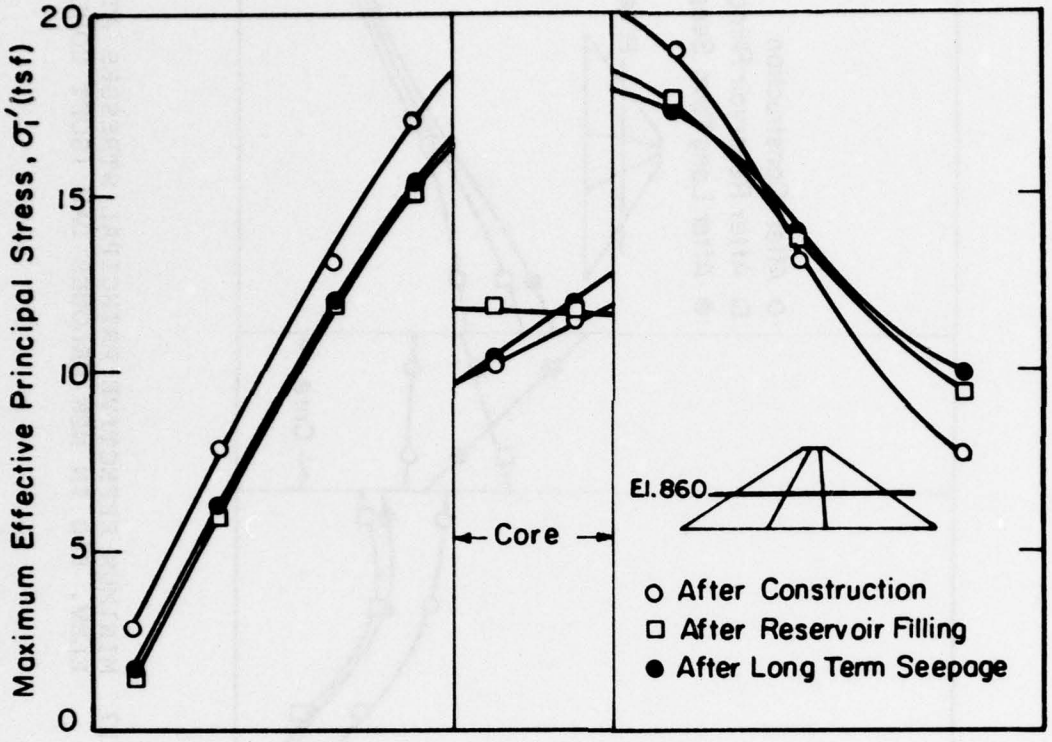

FIG. 7.16 MAXIMUM EFFECTIVE PRINCIPAL STRESSES AT ELEV. 860 IN NEW MELONES DAM (SOFT CORE)

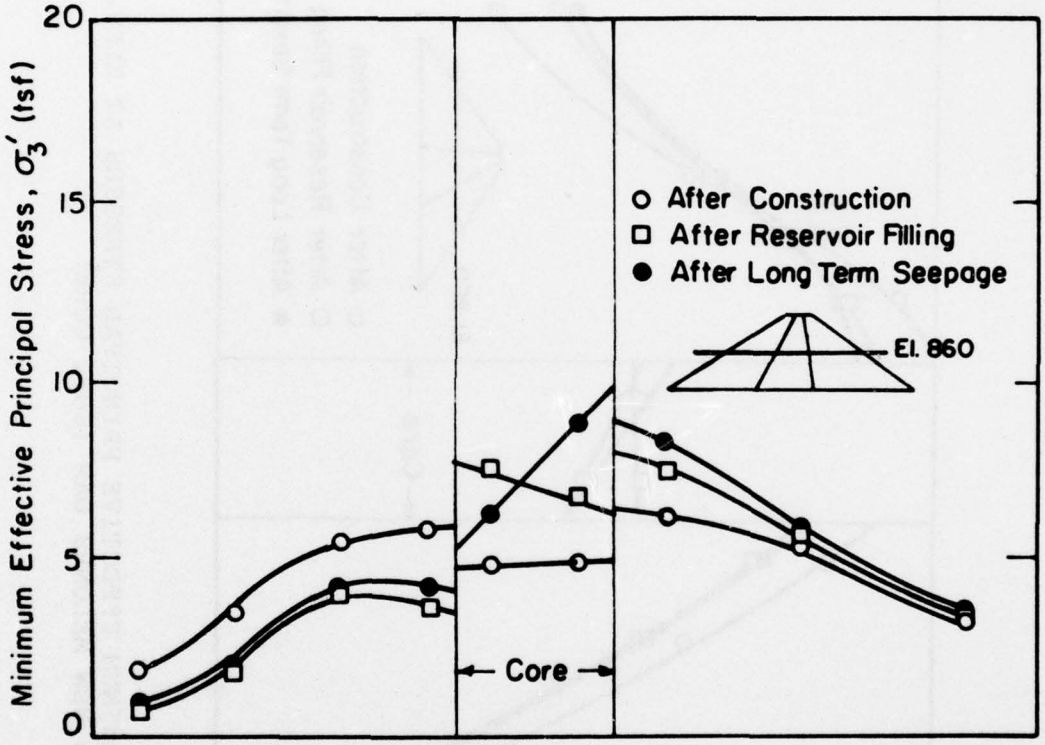

FIG. 7.17 MINIMUM EFFECTIVE PRINCIPAL STRESSES AT ELEV. 860 IN NEW MELONES DAM (SOFT CORE)

in the core increased by about 0.5 tsf, and the calculated values of minor principal effective stress increased about 2.5 tsf when the water pressure was applied to the upstream side of the core. The increases in the calculated stresses were slightly higher for the stiff core case than for soft core case.

During development of steady seepage, the calculated stresses on the upstream side of the core decreased because of the seepage forces and the calculated stresses on the downstream side of the core increased because of the dissipation of the initial excess pore pressures. The calculated stress changes are somewhat larger in the stiff core case than in the soft core case.

Pore Pressures

Calculated pore pressure distributions are shown in Fig. 7.18 and Fig. 7.19 for the stiff core and the soft core cases at different stages. After construction, the calculated pore pressure at the base of the soft core was found to be about 8 tsf, and the corresponding value for the stiff core was about 3 tsf. The larger pore pressure in the soft core occurs as a result of its higher initial degree of saturation in the soft core.

During reservoir filling, the calculated pore pressure at the base increased to about 10 tsf in the soft core case, and to about 8 tsf in the stiff core case, due to the water pressure forces on the upstream face of the core.

The calculations indicate that both cores will reach about the same pore pressure distribution after 80 years. The calculated variations of pore pressure with time at points A and B at the base of the core are shown in Figs. 7.20 and 7.21.

Fig. 7.22 shows the calculated pore pressure distribution in the core of the cofferdam. It may be seen that the anticipated pore pressures after construction are small. After reservoir filling, the calculated pore pressures in the core increase due to the weight of the loads from the water in the reservoir. The pore pressures at the boundary of

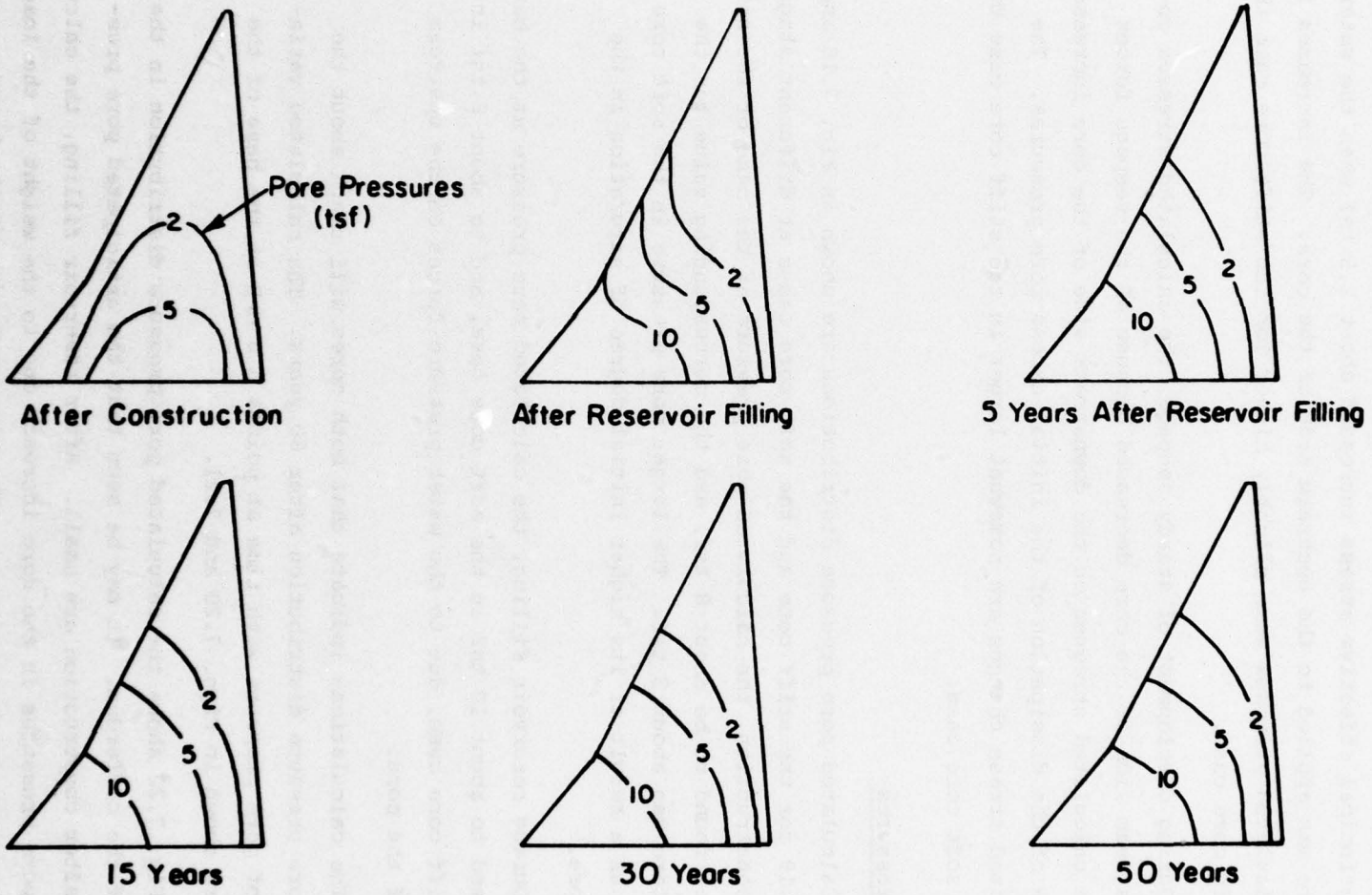

FIG. 7.18 PORE PRESSURE DISTRIBUTIONS IN THE CORE OF NEW MELONES DAM (SOFT CORE)

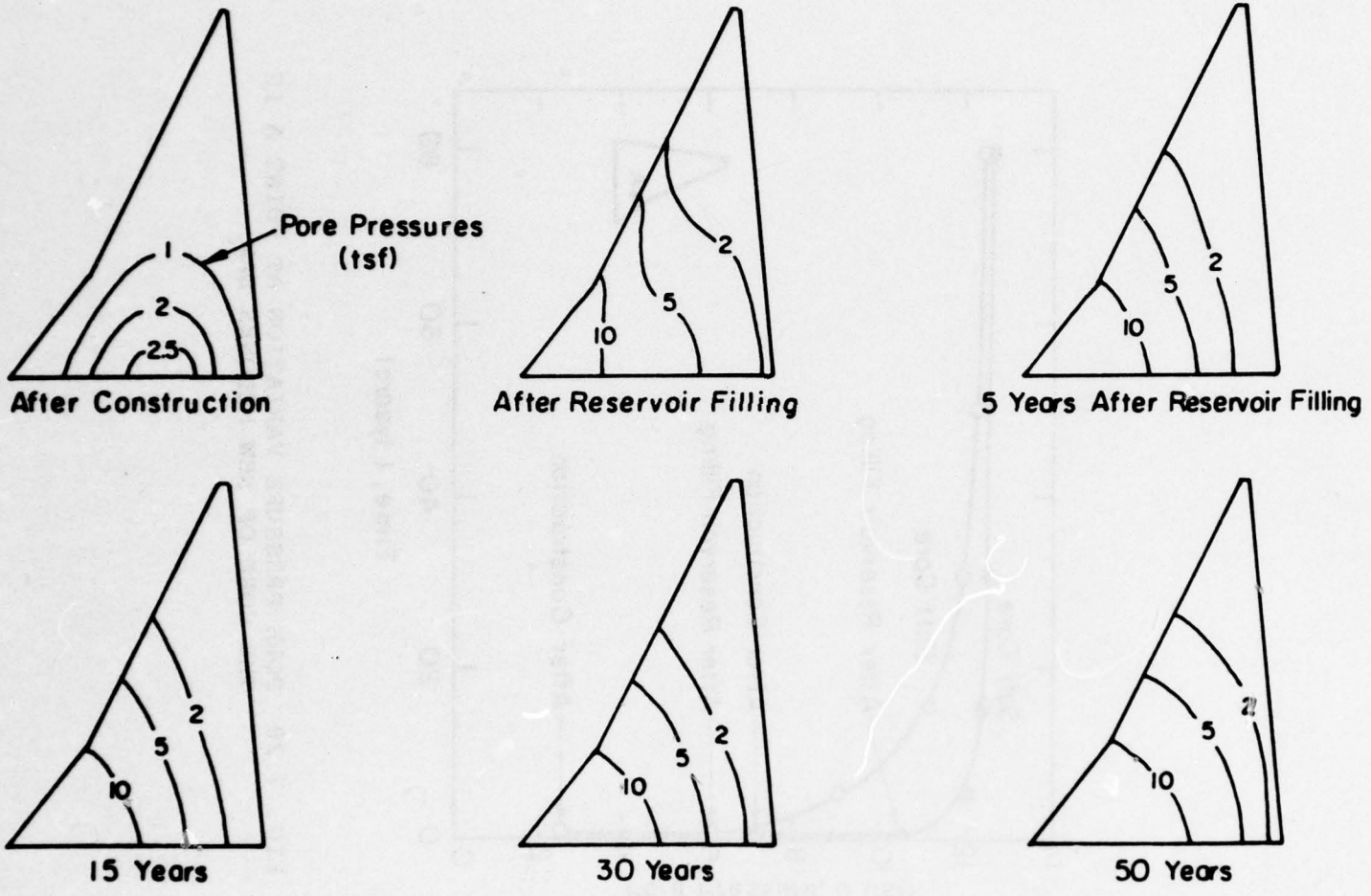

FIG. 7.19 PORE PRESSURE DISTRIBUTIONS IN THE CORE OF NEW MELONES DAM (STIFF CORE)

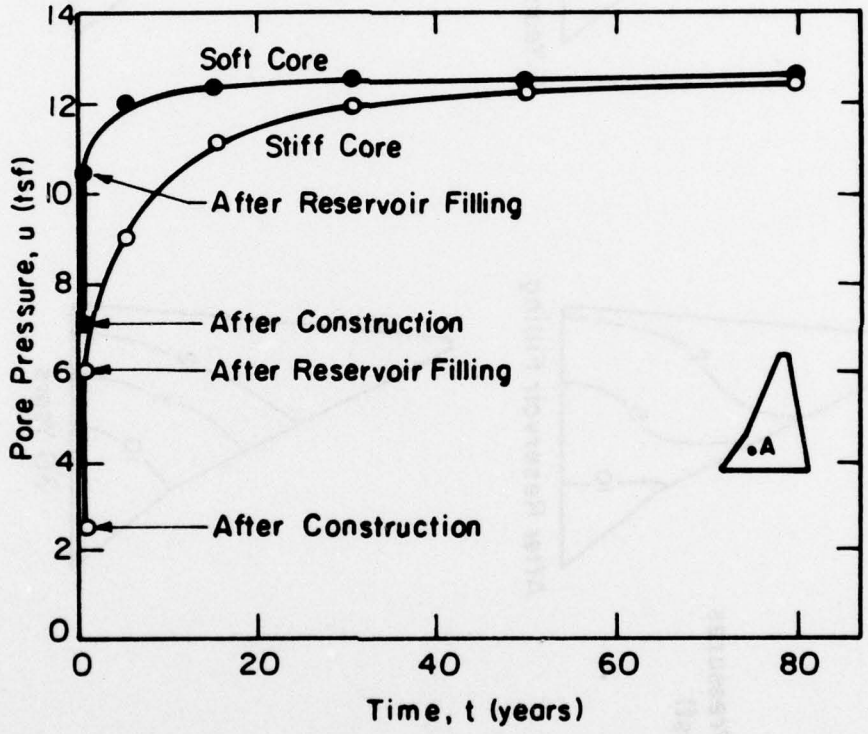

FIG. 7.20 PORE PRESSURE VARIATION AT POINT A IN THE CORE OF NEW MELONES DAM

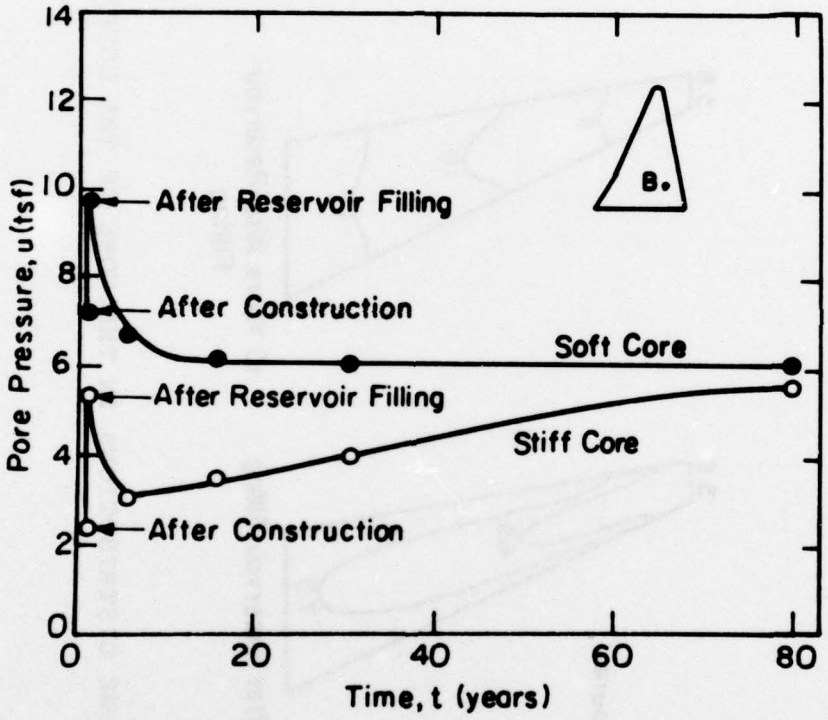

FIG. 7.21 PORE PRESSURE VARIATION AT POINT B IN THE CORE OF NEW MELONES DAM

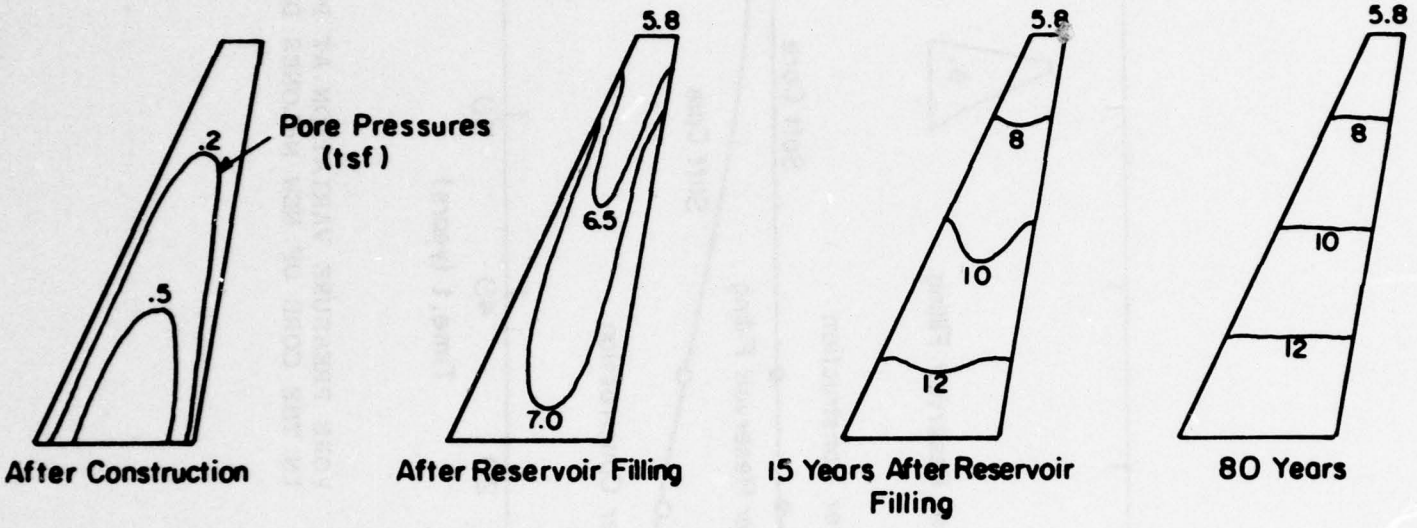

FIG. 7.22 PORE PRESSURE DISTRIBUTIONS IN THE CORE OF THE COFFERDAM (STIFF CORE)

the core and the shell increase, corresponding to the water level at elevation 990 ft. Subsequently, as the water begins to seep through the core, the calculated pore pressures in the core increase further. As shown in the Fig. 7.20, after 80 years, the results indicate that a nearly steady state condition will be reached.

SUMMARY

At the beginning of this chapter, three questions were posed concerning the behavior of zoned dams during the time when the excess pore pressures in the core dissipate and steady seepage develops. Based on the result discussed previously, it is possible to provide answers to these questions for conditions similar to these considered for New Melones Dam.

The questions, and the answers indicated by the analyses of New Melones Dam, are:

(1) What is the nature of the expected movements in a zoned dam during consolidation of the core?

The maximum calculated horizontal movement of the core of New Melones Dam during development of steady seepage was about 0.6 feet downstream. The analysis also indicates that some upward movement may occur during long term seepage due to the effects of buoyancy as the upstream shell is submerged. However, other effects such as creep and secondary compression, which were not considered in the analysis, would be expected to cause a net settlement rather than an upward movement rebound.

(2) How do the stresses in the dam change during consolidation?

Both the maximum and minimum principle effective stresses in the upstream side of the core of New Melones Dam decreased due to the effects of buoyancy when the upstream shell was submerged and long term seepage developed. The maximum principal effective stress in the downstream shell decreased a small amount, and the minimum principal effective stress increased a little during consolidation and development of long term seepage in the core.

(3) Are the long term stresses, calculated assuming slow construction and no excess pore pressure, the same as these calculated taking account of consolidation?

For the range of compaction condition considered likely for New Melones Dam, the calculated movements and stress changes during consolidation of the core were quite small. The long-term stresses calculated by Quigley, et al. (1976), using the hyperbolic stress-strain relationship and assuming slow construction with no excess pore pressures at any stage, were found to be very close to those calculated taking account of consolidation, as shown in Fig. 7.23.

Had a condition been analyzed in which the core was much wetter and softer than was considered to be likely for New Melones Dam, it might be expected that the settlements and stress changes during consolidation of the core would be larger and more important. It might also be found there would be a greater difference between the long-term stresses calculated assuming slow construction with no excess pore pressures, and those calculated taking account of consolidation. Thus, although the hyperbolic model and the Cam Clay Model produce very similar results for the case illustrated in Fig. 7.23, this conclusion might not apply to dams with softer, wetter cores.

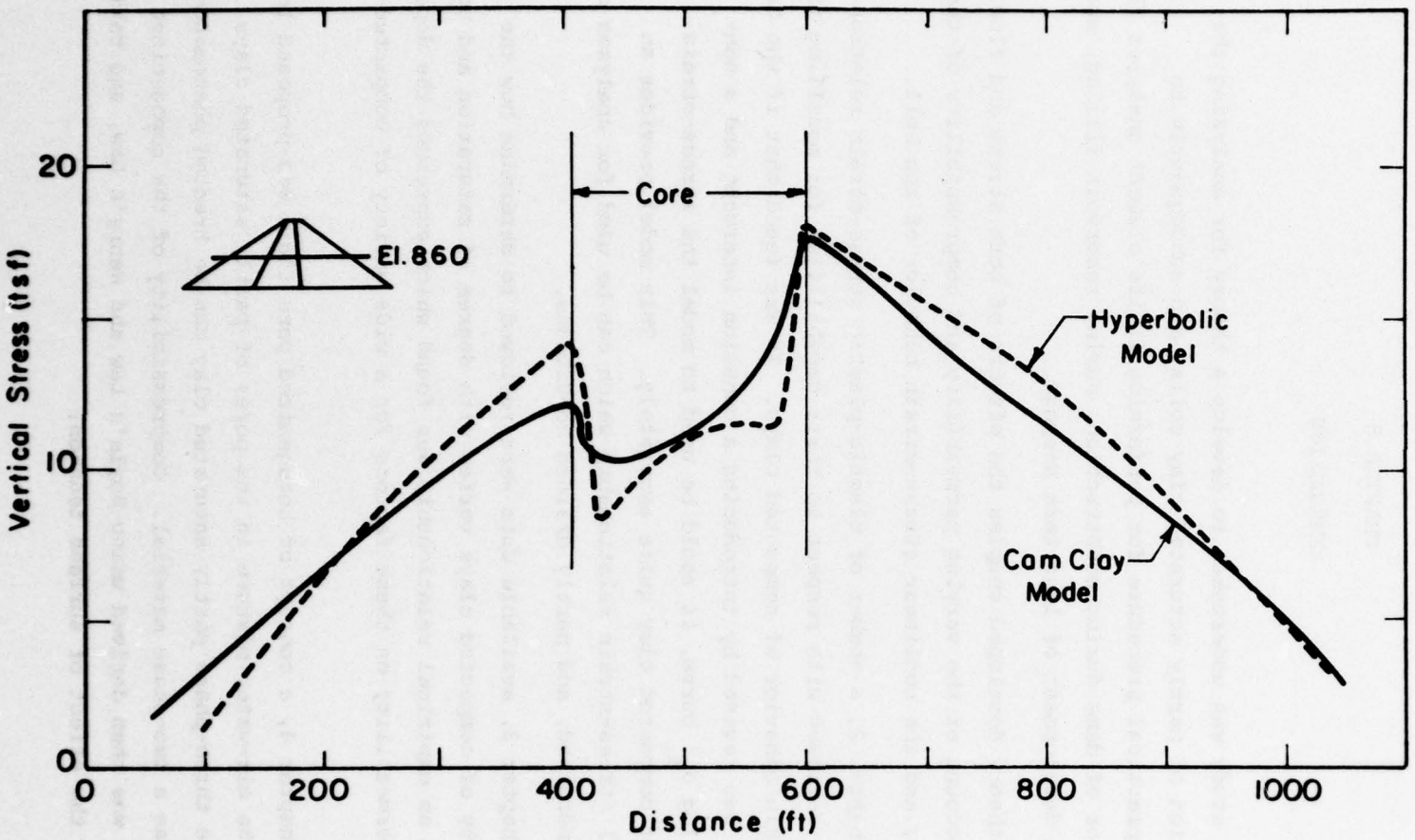

FIG. 7.23 COMPARISON OF LONG TERM STRESS CALCULATED USING HYPERBOLIC STRESS-STRAIN RELATIONSHIP WITH SLOW CONSTRUCTION AND CAM CLAY STRESS-STRAIN RELATIONSHIP WITH CONSOLIDATION

CHAPTER 8

CONCLUSION

This study was undertaken to develop a theory for analyzing the consolidation of partly saturated clay soils, and subsequently to develop a practical procedure for performing finite element analyses for the behavior of dams during construction, during reservoir filling, and during the development of long term seepage.

The theory developed couples the effects of both stress and flow. It takes account of the varying permeability and compressibility of the pore fluid, and the nonlinear stress-strain behavior of the soil.

In Chapter 2, a number of elastic-plastic stress-strain relationships were reviewed with respect to their capabilities for modelling the stress-strain behavior of compacted clays. It was found that if the Cam Clay Model was revised by introducing a cohesion intercept and a nonlinear $e - \log \sigma_m'$ curve, it could be used to model the stress-strain behavior of compacted clay quite accurately. This model provides an incremental stress-strain relationship which can be used for analyses of drained, undrained, and partly drained conditions.

In Chapter 3, available data were reviewed to determine how the permeability of compacted clays varies with degree of saturation and void ratio, and an empirical relationship was found which expresses the dependence of permeability on these factors for a wide variety of compacted clays.

In Chapter 4, a concept of homogenized pore fluid was proposed to simulate the air-water mixture in the pores of partly saturated clays so that the three-phase partly saturated clay can be treated phenomenologically as a two-phase material. Compressibility of the homogenized pore fluid was then derived using Boyle's Law and Henry's Law, and taking account of the effect of surface tension.

In Chapter 5, Biot's theory of consolidation was reviewed, and the finite element formulation for the consolidation of saturated soils was derived. The computer program based on this formulation was verified by comparing results derived from the program with known solutions for several problems.

In Chapter 6, the theory of consolidation for partly saturated soil was derived and a computer program was developed. To check the utility and effectiveness of the theory and the computer program developed, two examples of one-dimensional consolidation with compressible pore fluid and varying permeability were analyzed.

In Chapter 7, an analyses of New Melones Dam was performed using the program developed. The stresses, strains, pore pressures and movements in the dam were calculated during construction and at various times during a period of 80 years following construction. To account for possible variations in the field compaction conditions in New Melones Dam, two different conditions of water content and compacted density of the core were considered in the analyses.

The analyses were performed for three different stages; the construction stage, the reservoir filling stage, and the stage after reservoir filling when long term seepage had developed. The construction and reservoir filling stage were assumed to occur under undrained conditions.

During the construction and reservoir filling stages, the pore pressures in the soft core case were found to be significantly higher than those in the stiff core case. After a period of about 80 years, when a nearly steady state seepage condition had developed, the pore pressure distributions were found to be about the same for both cases.

More undrained deformation was found in the soft core case during construction and reservoir filling stages than in the stiff core case, and higher stresses were found in the stiff core case than in the soft core case. After reservoir filling, the settlement and stress changes during consolidation of the core were small for both the stiff core and the soft core cases.

Had a condition been analyzed in which the core was much wetter and softer than either of the cases analyzed, it might be expected that the settlements and stress changes during consolidation of the core would be larger and more important than either case considered possible for New Melones Dam. It is interesting that within a practical range of conditions near optimum water content, the calculations indicate that the movements and stress changes during consolidation can be expected to be quite small.

The studies conducted during this investigation have shown that an incremental finite element analysis procedure, coupled with the non-linear stress-strain behavior, and flow behavior with variable permeability and compressibility of the pore fluid, is simple enough for practical use, and gives results which appear reasonable when compared to field experience and the results of other analyses. The procedure is well suited for practical use because the required stress-strain parameters may be determined from the results of isotropic compression tests and drained triaxial tests. The other required parameters may be readily determined from compaction data and permeability test results.

Based on the results of the analyses performed, it seems likely that these analysis procedures may be used to predict pore pressures, stresses, strains and movements in dams during any stage after the beginning of construction of the dam and may be useful for selecting desirable instrument locations in dams, and to help in interpreting the results of instrumentation studies

Perhaps the greatest value of these procedures is in connection with instrumentation studies. Piezometers are sometimes used to control the rate of construction, and this procedure could be even more effective if the rate of pore pressure development and dissipation could be predicted accurately. The analyses would also be useful for interpreting the significance of movements measured during and after construction.

REFERENCES

Aitchison, G. D. (1960), "Relationships of Moisture Stress and Effective Stress Functions in Unsaturated Soils," Proceedings of the Conference on Pore Pressure and Suction in Soils, London: Butterworth, 1960, pp. 47-52.

Barden, L. (1965), "Consolidation of Compacted and Unsaturated Clays," Geotechnique, 1965, p. 267.

Bathe, K. J. and Wilson, E. L. (1973), "NONSAP - A General Finite Element Program for Nonlinear Dynamic Analysis of Complex Structures," Paper M3/1, Proceedings of the 2nd International Conference on Structural Mechanics in Reactor Technology, Berlin, September, 1973.

Beek. W. J. (1963), Physische Transportverschijnselen, Collegedictaat, (in Dutch).

Biot, M. A. (1941a), "General Theory of Three-Dimensional Consolidation," Journal of Applied Physics, Vol. 12, pp. 155-164.

Biot, M. A. (1941b),"Consolidation Settlement Under a Rectangular Load Distribution," Journal of Applied Physics, Vol. 12, pp. 426-430.

Biot, M. A. (1955), "Theory of Elasticity and Consolidation for a Porous Anisotropic Solid," Journal of Applied Physics, Vol. 26, pp. 182-185.

Biot, M. A. (1956a), "Theory of Deformation of a Porous Viscoelastic Anisotropic Solid," Journal of Applied Physics, Vol. 27, p. 459.

Biot, M. A. (1956b), "General Solutions of the Equations of Elasticity and Consolidation for a Porous Material," Transactions, Journal of Applied Mechanics, ASME, Vol. 78, pp. 91-96.

Bishop, A. W. (1959), "The Principle of Effective Stress," Tek. Ukebladk, Norway, No. 39.

Blight, G. E. (1965), "A Study of Effective Stress for Volume Change," Symposium on Moisture Equilibrium and Moisture Changes in Soils Beneath Covered Areas, Butterworths, Australia, 1965, pp. 259-269.

Booker, J. R. (1973), "A Numerical Method for the Solution of Biot's Consolidation Theory," Quarterly Journal of Mechanics and Applied Mathematics, Vol. 26, p. 457.

Booker, J. R., Carter, J. P., and Small, J. C. (1975), "An Effective Method of Analysis for the Drained and Undrained Behavior of an Elastic Soil," Research Report No. R267, Civil Engineering Laboratories, The University of Sydney, July, 1975.

Booker, J. R., and Small, J. C. (1974), "An Investigation of the Stability of Numerical Solutions of Biot's Equations of Consolidation," International Journal on Solids Structures, 1975, Vol. 11, pp. 907-917.

Burland, J. B. (1967), "Deformation of Soft Clay," Ph.D. thesis, Cambridge University.

Carillo (1942), "Simple Two and Three Dimensional Cases in the Theory of Consolidation of Soils," Journal of Mathematics and Physics, Vol. 21, p. 1.

Carman, P. C. (1956), Flow of Gases Through Porous Media, Academic, New York.

Carslaw and Jaeger (1959), Conduction of Heat in Soils, Oxford Press.

Casagrande, A., and Hirschfeld, R. C. (1962), "Second Progress Report on Investigation of Stress-Deformation and Strength Characteristics of Compacted Clays," Soil Mechanics Series, No. 65, Harvard University, April, 1962.

Christian, J. T. (1966), "Plane Strain Deformation Analysis of Soils," Contract Report No. 3-129, Contract DA-22-079-eng-471, U. S. Army Engineers Waterways Experiment Station, Corps of Engineers, Vicksburg, Mississippi, Dept. of Civil Engineering, Massachusetts Institute of Technology, December, 1966.

Christian, J. T., and Boehmer, J. W. (1970), "Plane Strain Consolidation by Finite Elements," Journal of the Soil Mechanics and Foundations Division, ASCE, Vol. 96, pp. 1435-1457.

Clough, R. W., and Woodward, R. J., III (1967), "Analysis of Embankment Stresses and Deformations," Journal of the Soil Mechanics and Foundations Division, ASCE, Vol. 93, No. SM4, July, pp. 529-549.

DiMaggio, F. L., and Sandler, I. S. (1971), "Material Model for Granular Soils," Journal of the Engineering Mechanics Division, ASCE, Vol. 97, No. EM3, Proc. Paper 8212, June, pp. 935-950.

Drucker, D. C., Gibson, R. E., and Henkel, D. (1957), "Soil Mechanics and Work-Hardening Theories of Plasticity," ASCE Transactions, Vol. 122, Paper No. 2864.

Duncan, J. M. (1972), "Finite Element Analyses of Stresses and Movements in Dams, Excavations, and Slopes," State-of-the-Art Report, Symposium on Applications of the Finite Element Method in Geotechnical Engineering, U. S. Army Engineer Waterways Experiment Station, Vicksburg, Mississippi, May, 1972.

Gibson, R. E. (1958), "The Process of Consolidation in a Clay Layer Increasing in Thickness with Time," Geotechnique, Vol. VIII, p. 171.

Gibson, R. E., and Lumb, P. (1953), "Numerical Solution of Some Problems in the Consolidation of Clay," Journal of Inst. Civil Engineers 1, Part 1, p. 182.

Gibson, R. E., Schiffman, R. L., and Pu, S. L. (1970), "Plane Strain and Axially Symmetric Consolidation of a Clay Layer on a Smooth Impervious Base," Quarterly Journal of Mechanics and Applied Mathematics, Vol. 16, pp. 34-50.

Gurtin, M. (1964), "Variational Principles for Linear Elasto-Dynamics," Arch. Rat. Mech. and Anal., Vol. 16, pp. 34-50.

Hagmann, A. J. (1971), "Prediction of Stress and Strain Under Drained Loading Conditions," D.Sc. Thesis, Massachusetts Institute of Technology.

Harr, M. S. (1967), Foundations of Theoretical Soil Mechanics, McGraw-Hill Book Company, New York.

Hilf, J. W. (1948), "Estimating Construction Pore Pressure in Rolled Earth Dams," Proceedings of the 2nd International Conference on Soil Mechanics and Foundation Engineering, Rotterdam, Vol. III, p. 234.

Hwang, C. T., Morgenstern, N. R., and Murray, D. W. (1971), "On Solutions of Plane Strain Consolidation Problems by Finite Element Method," Canada Geotechnical Journal, Vol. 8, No. 1, February, p. 109.

Jenike, A. W., and Shield, R. T. (1959), "On the Plastic Flow of Coulomb Solids Beyond Original Failure," Journal of Applied Mechanics, December, pp. 599-602.

Josselin De Jong, G. De. (1957), "Application of Stress Functions to Consolidation Problems," Proceedings of the 4th International Conference on Soil Mechanics and Foundation Engineering, Vol. 1, pp. 320-323.

Josselin De Jong, G. De. (1963), "Consolidation in Drie Dimensies," L.G.M. Medelingen, Delft, The Netherlands, Vol. 7, No. 3, pp. 57-73.

Koiter, W. T. (1953), "Stress-Strain Relations, Uniqueness and Variational Theorems for Elastic-Plastic Material with a Singular Yield Surface," Quarterly Applied Mathematics, Vol. 11, No. 3.

Koppula, S. D., and Morgenstern, N. R. (1972), "Consolidation of Clay Layer in Two Dimensions," Journal of the Soil Mechanics and Foundations Division, ASCE, Vol. 98, No. SM1, January, p. 79.

Kozeny, J. (1927), "Ueber Kapillare Leitung des Wassers im Boden," Wein, Akad, Wiss., Vol. 136, Part 2a, p. 271.

Kulhawy, F. H., Duncan, J. M., and Seed, H. B. (1969), "Finite Element Analyses of Stresses and Movements in Embankments During Construction," Geotechnical Engineering Report No. TE 69-4, Department of Civil Engineering, University of California, Berkeley.

Lambe, T. W. (1958), "The Engineering Behavior of Compacted Clay," Journal of the Soil Mechanics and Foundations Division, ASCE, Vol. 84, No. SM2, Proc. Paper 1655, May.

Lambe, T. W. and Whitman, R. V. (1969), Soil Mechanics, John Wiley & Sons, Inc.

Luscher, Ulrich (1965), "Discussion of 'Elastic Analogs in Time-Settlement Problem' by Patrick Domenico and Glen Clark," Journal of the Soil Mechanics and Foundations Division, ASCE, Vol. 91, No. SM1, Proc. Paper 4197, January, pp. 190-195.

McNamee, J. and Gibson, R. E. (1960a), "Displacement Functions and Linear Transforms Applied to Diffusion Through Porous Elastic Media," Quarterly Journal of Mechanics and Applied Mathematics, Vol. 13, pp. 98-111.

McNamee, J. and Gibson, R. E. (1960b), "Plane Strain and Axially Symmetric Problems of Consolidation of a Semi-Infinite Clay Stratum," Quarterly Journal of Mechanics and Applied Mathematics, Vol. 13, pp. 210-227.

Mitchell, J. K., Hooper, D. R., and Campanella, R. J. (1965), "Permeability of Compacted Clay," Journal of the Soil Mechanics and Foundations Division, ASCE, Vol. 91, No. SM4, Proc. Paper 4392, July, pp. 41-65.

Olsen, H. W. (1961), "Hydraulic Flow Through Saturated Clays," Sc.D. Thesis, Massachusetts Institute of Technology, Cambridge, Massachusetts.

Prevost, J. H., and Höeg, K. (1975), "Effective Stress-Strain-Strength Model for Soils," Journal of the Geotechnical Engineering Division, ASCE, Vol. 101, No. GT3, Proc. Paper 11157, March.

Quigley, D. W., Duncan, J. M., Caronna, S., Moroux, P. J., and Chang, C. S. (1976), "Three-Dimensional Finite Element Analysis of New Melones Dam," Geotechnical Engineering Report, Department of Civil Engineering, University of California, Berkeley.

Rendulic, L. (1936), "Porenziffer und Porenwassendruck in Tonen," Der Bauingenieur, Vol. 17, Berlin, West Germany, p. 559.

Roscoe, K. H., and Schofield, A. N. (1963), "Mechanical Behavior of an Idealized 'Wet Clay'", Proceedings of the 2nd European Conference on Soil Mechanics, Wiesbaden, Vol. I, pp. 47-54.

Roscoe, K. H., Schofield, A. N., and Thurairajah, A. (1963), "Yielding of Clays in States Wetter than Critical," Geotechnique, Vol. 13, No. 3, 1963, pp. 211-240.

Roscoe, K. H., and Burland, J. B. (1968), "On the Generalized Stress-Strain Behavior of 'Wet' Clay," Engineering Plasticity, edited by J. Heyman and F. A. Leckie, Cambridge University Press, pp. 535-609.

Sandhu, R. S., and Wilson, E. L. (1969), "Finite Element Analysis of Flow in Saturated Porous Elastic Media," Journal of Engineering Mechanics Division, ASCE, Vol. 95, pp. 641-652.

Schmidt, E. (1924), "Uber die Andwendung de Differenzen Rechnung auf Technische Anheiz-und-Abkuhlungsprobleme," A. Foppl Festschrift. Springer-Verlag OHG, Berlin, pp. 179-189.

Schuurman, Ir. E. (1966), "The Compressibility of an Air/Water Mixture and a Theoretical Relation Between the Air and Water Pressures," Geotechnique, Vol. 16, pp. 269-281.

Scott, R. F. (1963), Principles of Soil Mechanics.

Seed, H. B., and Chan, C. K. (1959), "Structure and Strength Characteristics of Compacted Clay," Journal of the Soil Mechanics and Foundations Division, ASCE, Vol. 85, No. SM5, Proc. Paper 2216, pp. 87-109.

Singh, Rameshwar (1965), "Unsteady and Unsaturated Flow in Soils in Two-Dimensions," Technical Report No. 54, Department of Civil Engineering, Stanford University, July.

Skempton, A. W., and Bishop, A. W. (1954), "Building Materials, their Elasticity and Inelasticity," Soils, Chapter 10, North Holland Publishing Company, Amsterdam.

Small, J. C., Booker, J. R., and Davis, E. H. (1976), "Elasto-Plastic Consolidation of Soil," International Journal of Solids Structures, Vol. 12, pp. 431-448.

Sparks, A. D. W. (1963), "Theoretical Considerations of Stress Equations for Partly Saturated Soils," 3rd Regular Conference for Africa on Soil Mechanics and Foundation Engineering, Salisburg.

Subrahmanyam, G. and Venkata, R. (1971), "Analytical Solution for the Consolidation of an Anisotropic Soil under Three-Dimensional Drainage," Indian Journal of Technology, Vol. 9, No. 3, p. 103.

Taylor, D. W. (1948), Fundamentals of Soil Mechanics, John Wiley & Sons, Inc.

Terzaghi, Karl (1924), "Die Theorie der Hydrodynamischen Spannungserscheinungen undihr Erdbautechnisches Anwendungsgebiet," Proceedings of the 1st Insternational Congress on Applied Mechanics, Delft, The Netherlands.

Wong, K. S., and Duncan, J. M. (1974), "Hyperbolic Stress-Strain Parameters for Nonlinear Finite Element Analyses of Stresses and Movements in Soil Masses," Geotechnical Engineering Report No. TE 74-3, Department of Civil Engineering, University of California, Berkeley.

Yokoo, Yamagata, and Nagaoka (1971a), "Finite Element Method Applied to Biot's Consolidation Theory," Soils and Foundations, Vol. 11, No. 1, March.

Yokoo, Yamagata, and Nagaoka (1971b), "Finite Element Analysis of Consolidation Following Undrained Deformations," Soils and Foundations, Vol. 11, No. 4, December.

Yokoo, Yamagata, and Nagaoka (1971c), "Variational Principle for Consolidation," Soils and Foundations, Vol. 11, No. 4, December.

Zienkiewicz, O. C., and Naylor, D. J. (1971), "The Finite Element Method Applied to Soils and Other Porous Media," Lecture presented to the N.A.T.O. Symposium on Continuum Mechanics, Lisbon, Portugal, September.

Zienkiewicz, O. C., and Naylor, D. J. (1972), "Adaption of Critical State Soil Mechanics for Use in Finite Elements," Stress-Strain Behavior of Soils, edited by R. H. G. Parry, G. T. Poulos, and Co., Ltd., pp. 537-547.

APPENDIX A

DERIVATIONS OF STRESS-STRAIN RELATIONSHIP FOR AN ELASTIC PLASTIC MATERIAL

For an elasto-plastic material with hardening parameter h, the yield surface may be expressed in the form

$$f(\{\sigma_c'\}, h) = 0 \tag{A.1}$$

For the elasto-plastic model used in this study, the hardening parameter is a function of plastic strain only. $\{\sigma_c'\}$ is the vector of current effective stresses. It is related to the changes in stress, discussed in Chapter 5, as follows:

$$\{\sigma_c'\} = \{\sigma_0'\} + \{\sigma'\}$$

where $\{\sigma_0'\}$ is the vector of initial effective stresses.

The strain increment $\{\dot{\varepsilon}\}$ can be thought of as being composed of an elastic component $\{\dot{\varepsilon}_E\}$ and a plastic component $\{\dot{\varepsilon}_p\}$, which are related as follows:

$$\{\dot{\varepsilon}\} = \{\dot{\varepsilon}_E\} + \{\dot{\varepsilon}_p\} \tag{A.2}$$

where
$$\{\dot{\varepsilon}_E\} = [C^E]^{-1}\{\dot{\sigma}'\} \tag{A.3}$$

and $[C^E]$ is the matrix of elastic constants defined previously.

Suppose that the soil skeleton has an associated flow rule

$$\{\dot{\varepsilon}_p\} = \lambda \frac{\partial f}{\partial \{\sigma_c'\}} \tag{A.4}$$

where λ is a positive parameter, f is the plastic potential function. For an associated flow rule, the plastic potential function is identical to the yield surface.

For an associated flow rule, substituting Eqs. A.4 and A.3 into Eq. A.2, may be shown that

$$\{\dot{\varepsilon}\} = [C^E]^{-1}\{\dot{\sigma}'\} + \lambda \frac{\partial f}{\partial \{\sigma_c'\}} \tag{A.5}$$

During plastic deformation, the stress state remains on the yield surface so that

$$df = \frac{\partial f}{\partial \{\sigma_c'\}} d\{\dot{\sigma}'\} + \frac{\partial f}{\partial h}\left(\frac{\partial h}{\partial \{\varepsilon_p\}}^T\right) d\{\dot{\varepsilon}_p\} = 0 \tag{A.6}$$

Using Eq. A.5 and Eq. A.6, λ can be expressed in terms of $\{\dot{\varepsilon}\}$ as follows:

$$\lambda = \frac{\left(\frac{\partial f}{\partial \{\sigma_c'\}}\right)^T [C^E]\{\dot{\varepsilon}\}}{\left(\frac{\partial f}{\partial \{\sigma_c'\}}\right)^T [C^E] \left(\frac{\partial f}{\partial \{\sigma_c'\}}\right) - \frac{\partial f}{\partial h}\left(\frac{\partial h}{\partial \{\varepsilon_p\}}\right)^T \frac{\partial f}{\partial \{\sigma_c'\}}} \tag{A.7}$$

The stress-strain relationship now can be written as:

$$\{\dot{\sigma}\} = [C^E](\{\dot{\varepsilon}\} - \{\dot{\varepsilon}_p\}) \tag{A.8}$$

Substituting Eqs. A.4 and A.7 into Eq. A.8, it may be shown that

$$\{\dot{\sigma}\} = [C^{Ep}]\{\dot{\varepsilon}\} \tag{A.9}$$

where $[C^{Ep}]$ is the elasto-plastic stress-strain matrix defined by

$$[C^{Ep}] = [C^E] - \frac{[C^E] \frac{\partial f}{\partial \{\sigma_c'\}} \left(\frac{\partial f}{\partial \{\sigma_c'\}}\right)^T [C^E]^T}{\left(\frac{\partial f}{\partial \{\sigma_c'\}}\right)^T [C^E] \frac{\partial f}{\partial \{\sigma_c'\}} - \frac{\partial f}{\partial h}\left(\frac{\partial h}{\partial \{\varepsilon_p\}}\right)^T \frac{\partial f}{\partial \{\sigma_c'\}}} \tag{A.10}$$

$[C^{Ep}]$ is a symmetric matrix because an associated flow rule has been assumed in the development.

For the Cam Clay elasto-plastic model described in Chapter 2, the yield surface is described in two parts,

$$f_1(\{\sigma_c'\}, h_1) = 0 \tag{A.11}$$

$$f_2(\{\sigma_c'\}, h_2) = 0 \tag{A.12}$$

Each of the yield functions depends on a different hardening parameter. Within the region defined by either of these two functions, equation A.10 applies. However, at the junction of two surfaces, it is assumed the total plastic strain is the sum of the contributions from both of them (Koiter, 1953).

$$\{\dot{\varepsilon}_p\} = \lambda_1 \frac{\partial f_1}{\partial \{\sigma_c'\}} + \lambda_2 \frac{\partial f_2}{\partial \{\sigma_c'\}} \tag{A.13}$$

Koiter has further shown that the constants λ_1 and λ_2 may be determined from $f_1 = 0$, and $f_2 = 0$ in a manner similar to that for in Eq. A.7. It follows that

$$\lambda_1 = \frac{\left(\frac{\partial f_1}{\partial \{\sigma_c'\}}\right)^T [C^E]\{\dot{\varepsilon}\}}{\left(\frac{\partial f_1}{\partial \{\sigma_c'\}}\right)^T [C^E] \frac{\partial f_1}{\partial \{\sigma_c'\}} - \frac{\partial f_1}{\partial h_1}\left(\frac{\partial h_1}{\partial \{\varepsilon_p\}}\right)^T \frac{\partial f_1}{\partial \{\sigma_c'\}}} \tag{A.14}$$

and

$$\lambda_2 = \frac{\left(\frac{\partial f_2}{\partial \{\sigma_c'\}}\right)^T [C^E]\{\dot{\varepsilon}\}}{\left(\frac{\partial f_2}{\partial \{\sigma_c'\}}\right)^T [C^E] \frac{\partial f_2}{\partial \{\sigma_c'\}} - \frac{\partial f_2}{\partial h_2}\left(\frac{\partial h_2}{\partial \{\varepsilon_p\}}\right)^T \frac{\partial f_2}{\partial \{\sigma_c'\}}} \tag{A.15}$$

Hence

$$[C^{Ep}] = [C^E] - \frac{[C^E] \frac{\partial f_1}{\partial \{\sigma_c'\}} \left(\frac{\partial f_1}{\partial \{\sigma_c'\}}\right)^T [C^E]}{\left(\frac{\partial f_1}{\partial \{\sigma_c'\}}\right)^T [C^E] \frac{\partial f_1}{\partial \{\sigma_c'\}} - \frac{\partial f_1}{\partial h_1}\left(\frac{\partial h_1}{\partial \{\varepsilon_p\}}\right)^T \frac{\partial f_1}{\partial \{\sigma_c'\}}}$$

$$- \frac{[C^E] \frac{\partial f_2}{\partial \{\sigma_c'\}} \left(\frac{\partial f_2}{\partial \{\sigma_c'\}}\right)^T [C^E]}{\left(\frac{\partial f_2}{\partial \{\sigma_c'\}}\right)^T [C^E] \frac{\partial f_2}{\partial \{\sigma_c'\}} - \frac{\partial f_2}{\partial h_2}\left(\frac{\partial h_2}{\partial \{\varepsilon_p\}}\right)^T \frac{\partial f_2}{\partial \{\sigma_c'\}}} \tag{A.16}$$

APPENDIX B

ANALYTICAL SOLUTION FOR MATERIAL WITH COMPRESSIBLE PORE FLUID IN A ONE-DIMENSIONAL CONSOLIDATION CASE

In the one-dimensional consolidation case, Biot's equations reduce to

$$\frac{\partial}{\partial z}\frac{k}{\gamma_\omega}\frac{\partial u}{\partial z} = \frac{1}{D'} + \frac{1}{Q}\frac{\partial u}{\partial t} \tag{B.1}$$

where D' is the drained constrained modulus of the material, Q is the compressibility of the pore fluid and p is pore pressure.

If the permeability is constant, Eq. B.1 can also be expressed as

$$\bar{c}_v \frac{\partial^2 u}{\partial z^2} = \frac{\partial u}{\partial t} \tag{B.2}$$

where

$$\bar{c}_v = c_v \Big/ \left(1 + \frac{1}{\bar{\eta}}\right) \tag{B.3}$$

$$c_v = \frac{kD'}{\gamma_\omega} \tag{B.4}$$

$$\bar{\eta} = \frac{Q}{D'} \tag{B.5}$$

For a material with a compressible pore fluid, a change in load is carried by both the soil skeleton and the pore fluid. Therefore, there is an initial settlement due to the portion of the load carried by the soil skeleton, and there is an initial excess pore pressure due to the portion of the load carried by the pore fluid.

The initial pore fluid is:

$$u_0 = \sigma_z \Big/ \left(1 + \frac{1}{\bar{\eta}}\right) \tag{B.6}$$

Eq. B.2 can be solved for both two way or one way drainage boundary conditions. It is found that

$$\frac{u(z,t)}{u_0} = F\left(\frac{z}{H}, \frac{\bar{c}_v t}{H^2}\right) \tag{B.7}$$

where $F\left(\frac{z}{H}, \frac{\bar{c}_v t}{H^2}\right)$ is the same function as given by Terzaghi's solution except that c_v in Terzaghi's solution is replaced by another parameter $\bar{c}_v$, which is defined by Equation B.3. Thus Terzaghi's solution can be used to calculate the dissipation of excess pore pressures for materials with compressible pore fluids.

The total settlement, w_∞, at infinite time is:

$$w_\infty = \frac{\sigma_z}{D'} H \tag{B.8}$$

The initial settlement, w_0, at zero time is:

$$w_0 = w_\infty \frac{1}{1 + \bar{\eta}} \tag{B.9}$$

The degree of settlement can be expressed as:

$$\frac{w(t) - w_0}{w_\infty - w_0} = U\left(\frac{\bar{c}_v t}{H^2}\right) \tag{B.10}$$

where $U\left(\frac{\bar{c}_v t}{H^2}\right)$ is the same function as given by Terzaghi (1924). Therefore, Terzaghi's solution can be used to calculate the one-dimensional settlement of a material with compressible pore fluid.

In accordance with letter from DAEN-RDC, DAEN-ASI dated 22 July 1977, Subject: Facsimile Catalog Cards for Laboratory Technical Publications, a facsimile catalog card in Library of Congress MARC format is reproduced below.

Chang, S Ching
Analysis of consolidation of earth and rockfill dams / by Ching S. Chang and James M. Duncan, College of Engineering, Office of Research Services, University of California, Berkeley, Calif. Vicksburg, Miss. : U. S. Waterways Experiment Station, 1977.
2 v. : ill. ; 27 cm. (Contract report - U. S. Army Engineer Waterways Experiment Station ; S-77-4)
Prepared for Office, Chief of Engineers, U. S. Army, Washington, D. C., under Contract No. DACW39-74-C-0027.
Includes bibliography.
Contents: v.1. Main text and Appendices A and B.--v.2. Appendices C-E: User's manual for computer program CON2D for the finite element analysis of consolidation in zoned dams.

1. Clay soils. 2. Consolidation (Soils). 3. Dam instrumentation. 4. Earth dams. 5. Finite element method. 6. Rockfill dams. 7. Saturated soils. 8. Stress-strain relations (Soils).

(Continued on next card)

Chang, S Ching
Analysis of consolidation of earth and rockfill dams ... 1977. (Card 2)

I. Duncan, James Michael, joint author. II. California. University. College of Engineering. Office of Research Services. III. United States. Army. Corps of Engineers. IV. Series: United States. Waterways Experiment Station, Vicksburg, Miss. Contract report ; S-77-4.
TA7.W34c no.S-77-4